‖‖‖ **1.0**	4.5 5.0 5.6	**2.8**	**2.5**		
		3.2	**2.2**		
		3.6			
		4.0	**2.0**		
‖‖‖ **1.1**					
			‖ **1.8**		
‖‖ **1.25**	‖‖ **1.4**	‖ **1.6**			

MICROCOPY RESOLUTION TEST CHART

NATIONAL BUREAU OF STANDARDS-1963-A

②

MECHANISMS OF EXHAUST POLLUTANTS AND PLUME
FORMATION IN CONTINUOUS COMBUSTION

AFOSR 78-3586

FINAL REPORT

G.S. Samuelsen

UCI-ARTR-84-7

June 1984

DTIC
ELECTE
MAY 2 2 1985
B

COMBUSTION LABORATORY

Mechanical Engineering

University of California

Irvine 92717

REPORT DOCUMENTATION PAGE

1a. REPORT SECURITY CLASSIFICATION	1b. RESTRICTIVE MARKINGS
Unclassified	

2a. SECURITY CLASSIFICATION AUTHORITY	3. DISTRIBUTION/AVAILABILITY OF REPORT
-	Approved for public release;
2b. DECLASSIFICATION/DOWNGRADING SCHEDULE	distribution unlimited

4. PERFORMING ORGANIZATION REPORT NUMBER(S)	5. MONITORING ORGANIZATION REPORT NUMBER(S)
ARTR-84-7	AFOSR·TR· 85-0387

6a. NAME OF PERFORMING ORGANIZATION	6b. OFFICE SYMBOL (If applicable)	7a. NAME OF MONITORING ORGANIZATION
University of California UCI Combustion Laboratory		Air Force Offic of Scientific Research

6c. ADDRESS (City, State and ZIP Code)	7b. ADDRESS (City, State and ZIP Code)
Mechanical Engineering University of California Irvine, California 92717	Bolling AFB DC 20332-6448

8a. NAME OF FUNDING/SPONSORING ORGANIZATION	8b. OFFICE SYMBOL (If applicable)	9. PROCUREMENT INSTRUMENT IDENTIFICATION NUMBER
Air Force Office of Scientific Research	NA	AFOSR 78-3586

8c. ADDRESS (City, State and ZIP Code)	10. SOURCE OF FUNDING NOS.			
Bolling AFB DC 20332-6448	PROGRAM ELEMENT NO.	PROJECT NO.	TASK NO.	WORK UNIT NO.
	61102F	2308	A2	

11. TITLE (Include Security Classification) Mechanisms of Exhaust Pollutants and Plume Formation in Continuous Combustion

12. PERSONAL AUTHOR(S)
G.S. Samuelsen

13a. TYPE OF REPORT	13b. TIME COVERED	14. DATE OF REPORT (Yr., Mo., Day)	15. PAGE COUNT
Final	FROM 01APR81 TO 31MAR82	1984, JUNE	

16. SUPPLEMENTARY NOTATION

17. COSATI CODES			18. SUBJECT TERMS (Continue on reverse if necessary and identify by block number)
FIELD	GROUP	SUB. GR	Combustion and Ignition, Sampling, Jet and Gas Turbine,
21	01		Pollutants Formation, Complex Flows, Engines,
21	02		Modeling, Air Breathing Engines)

19. ABSTRACT (Continue on reverse if necessary and identify by block number)

The development of combustors that are both fuel efficient and fuel flexible requires spatially resolved measurements of velocity, temperature, and concentration in complex flows representative of both premixed and non-premixed systems. Such data are needed to provide the physical insight necessary to understand the basic processes of turbulent mixing and transport, and support the evolution of modeling. The goals of the AFOSR program at the UCI Combustion Laboratory was to develop laboratory model combustors and experimental methodology suitable for the acquisition of the desired information. The objectives of the program were (1) to establish and evaluate laboratory model combustors for both premixed and non-premixed fuel air injection suitable for studies of the complex flows; (2) to acquire spatially resolved flowfield data using state-of-the-art diagnostics for the purposes of model verification and providing insight into the transport of mass, momentum, and energy in complex flows; and (3) to conduct supplementary studies to support the development of methodologies required for measurements in complex flows.

20. DISTRIBUTION/AVAILABILITY OF ABSTRACT	21. ABSTRACT SECURITY CLASSIFICATION
UNCLASSIFIED/UNLIMITED ☒ SAME AS RPT ☐ DTIC USERS ☐	UNCLASSIFIED

22a. NAME OF RESPONSIBLE INDIVIDUAL	22b. TELEPHONE NUMBER (Include Area Code)	22c. OFFICE SYMBOL
JULIAN M TISHKOFF	(202) 767-4935	AFOSR/NA

Four combustion modules were considered: the Opposed Jet Combustor (OJC) for premixed injection and, for non-premixed injection, the Centerbody Combustor (CBC), the Centerbody Combustor with swirl, and the Dilute Swirl Combustor (DSC). An evaluation of combustor performance and compatability with a list of criteria for laboratory complex flow combustors established the DSC as a viable configuration for non-premixed, complex flow combustor studies in which swirl was a major aerodynamic feature. Originator Supplied Keywords(?)

Spatially resolved flowfield data were obtained in each of the premixed and non-premixed modules. Although laser anemometry and flow visualization were the principal diagnostic tools employed, flow mapping of species concentration and temperature were acquired in the OJC for a wide range of operating conditions. Studies in a hydrodynamic (water-channel) facility were also completed for both the OJC and CBC geometries. Extensive two-component laser anemometry data were obtained as well in the DSC including measurement of the Reynolds stress. In a complementary program with the National Science Foundation (NSF), the two-color measurements were combined with a fine-wire thermocouple probe to yield direct measurement of both axial and azimuthal heat flux in the DSC.

Three supplemental studies were completed: LA Seeder, Dump Combustor, and NO Sampling. The LA Seeder study addressed the development and evaluation of a seed generator for laser anemometer measurements in a reacting flow with two or more separate streams of fuel and air. Such flows require refractory particles injected uniformly in each of the individual streams to avoid biasing. The dump combustor study was directed to the acquisition of single component laser anemometry data in a dump combustor configuration with two area ratios for both non-reacting and reacting flows. The NO Sampling study explored the chemical transformations of nitrogen oxides that can occur while sampling combustion products. The present effort expanded previous work conducted for AFOSR to (1) conduct experiments with more accurate temperature control, (2) consider the presence of water vapor in the simulated combustion products as well as dry samples, and (3) evaluate combustion product composition representative of gas turbine exhausts.

Table of Contents

References

Accession For

A-1

LIST OF TABLES

LIST OF FIGURES

SECTION 1

INTRODUCTION

Continuous flow combustion systems are both turbulent and strongly backmixed. Such flows are classified as <u>complex</u> because of the complicated fluid dynamics in contrast to simple flows which, while turbulent as well as laminar, do not have zones of recirculation (Launder, 1978). Examples of practical continuous flow combustion systems of direct interest to the Air Force are gas turbine and ramjet combustors.

An increased understanding of complex flows is required as gas turbine and ramjet combustors are pushed to higher levels of performance, and as the fuel available for gas turbine engines decreases in quality. This need, somewhat fortuitously, coincides with the advances in laser diagnostics and modeling that will be necessary to provide the needed insight.

Experiments are required in laboratory systems that provide spatially resolved measurements of velocity, temperature, and concentration in complex flows representative of both premixed and non-premixed systems. Mathematical modeling is required in order to plan and interpret experimental research and, ultimately, to design hardware.

The goal of the present AFOSR grant at the UCI Combustion Laboratory was to develop laboratory model combustors and experimental methodology suitable for the acquisition of the desired information. The objectives of the program were as follows:

(1) To <u>establish</u> and <u>evaluate</u> laboratory model combustors for both premixed and non-premixed fuel/air injection suitable for studies of complex flows,

(2) To <u>acquire</u> spatially-resolved flowfield data, using state-of-the-art

1

diagnostics for the purposes of model verification and providing insight into the transport of mass, momentum, and energy in complex flows,

(3) To conduct supplementary studies to support the development of methodologies required for measurements in complex flows.

To meet these objectives, the program was divided in a task organization combusting of three elements:

- Element A: Model Laboratory Combustor Development and Evaluation
- Element B: Physical and Chemical Processes in Complex Flows
- Element C: Supplemental Studies

The experimental facilities developed to support the research are described in the following section. In Section 3.0, the modeling procedure used in the present program is described. The results are presented in Section 4.0 for each of the elements delineated above. Finally, a summary is provided in Section 5.0.

SECTION 2

EXPERIMENTAL FACILITIES

2.1 Laboratory Combustor Facility

The Laboratory Combustor Facility (LCF) provides air flow sufficient to produce a reference velocity of 15.24 mps (50 ft/sec) in a 80 mm (3-inch) duct, and flow rates of gaseous fuels to yield overall equivalence ratios exceeding 2.0. A separate fuel and air supply system, independent of the main flow, is available for operating the jet flow in the opposed-jet combustor module. Details of the test stand are available (Peterson and Himes, 1978).

The facility is designed to accommodate a variety of combustor configurations. In the present research program, the following four combustor modules were evaluated:

Combustor Module	Fuel/Air Injection
Opposed-Jet	Premixed
Centerbody	Non-Premixed
Centerbody with Swirl	Non-Premixed
Dilute Swirl	Non-Premixed

A schematic of each module is presented in Figure 1.

Opposed Jet Combustor Module. The opposed jet combustor (OJC) module consists of a 51 mm (2-inch) inside diameter cylindrical Vycor duct containing an opposing axisymmetric jet (Figure 1a). The inner diameter of the tube from which the jet issues is 1.3 mm (0.052-inch). The outer diameter of the tube is 6.4 mm (0.25-inch). The space between the inner and outer walls is hollow except for one partitioning barrier to provide for two-pass water cooling (in the case of HOT, reacting flow studies) or water heating (in the case of

3

a) 51 mm Opposed Jet Combustor (OJC)
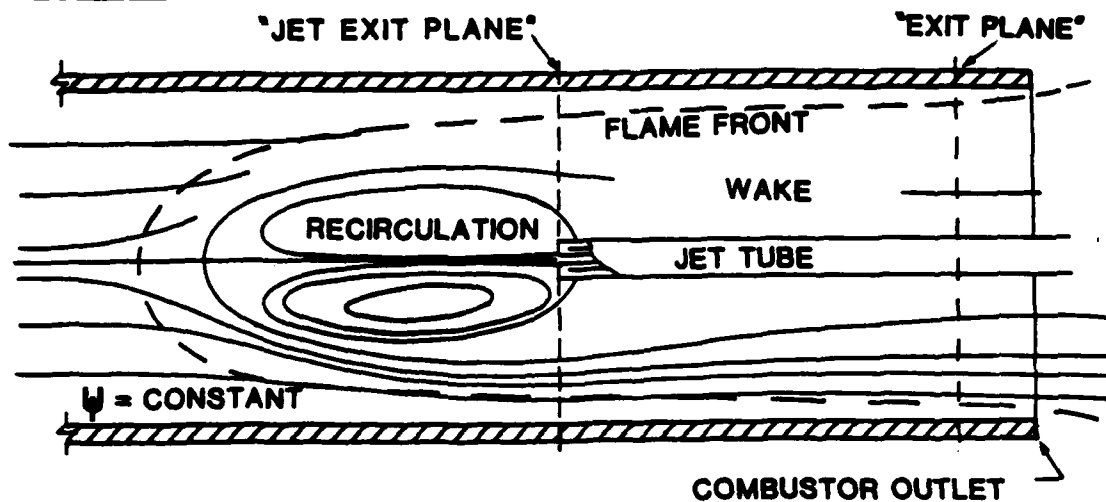
b) 51 mm Centerbody Combustor (CBC)
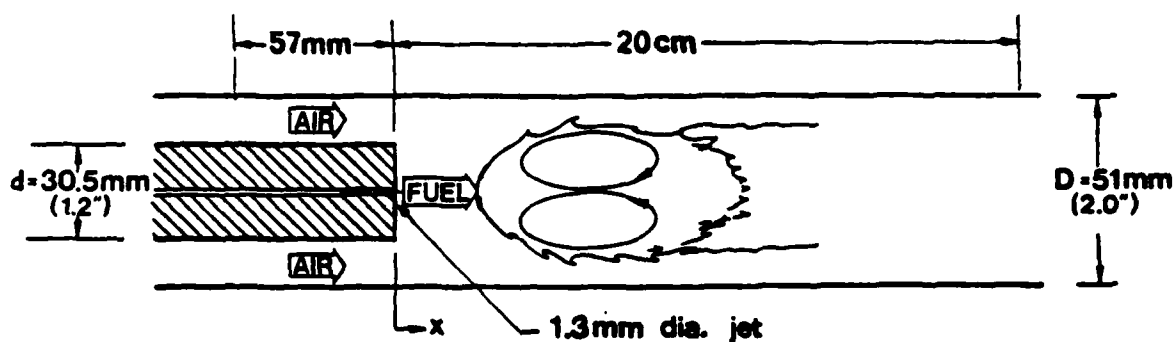
c) 51 mm Centerbody Combustor with Swirl (CBC)
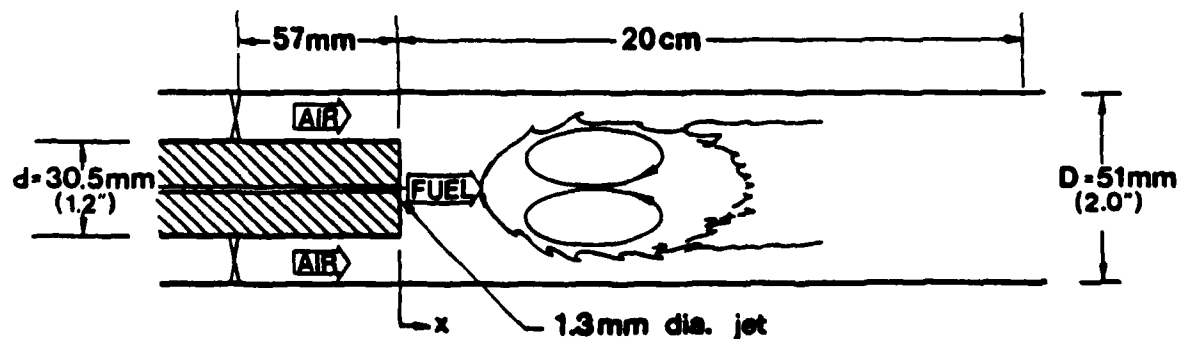
Figure 1. Combustor Modules

d) 80 mm Dilute Swirl Combustor
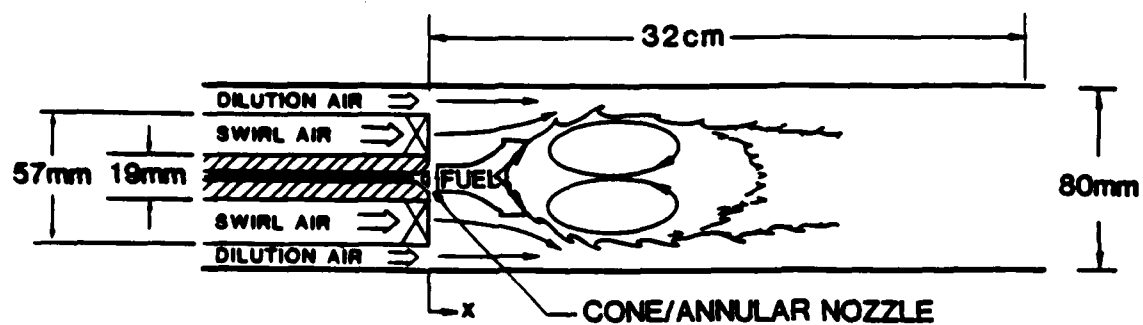
Figure 1. (concluded)

HEATED jet, non-reacting flow studies).

The Vycor duct is butted against and attached to an equal diameter stainless steel duct 18 duct diameters (i.e., 92 cm) in length. The purpose of the stainless steel duct is to provide some relaxation of the flow before entering the Vycor duct. The Vycor duct is nominally 9 duct diameters in length (46 cm). For purposes of measurement, the inlet plane (i.e., $x/d = 0$) is arbitrarily assigned an axial location 4.25 duct diameters downstream of the joining point of the Vycor and stainless steel duct. This places the exit plane of the duct at $x/d = 4.71$ (i.e., 240 mm from the inlet plane). The inlet plane of the opposing jet is arbitrarily selected to be $x/d = 3.54$ (180 mm from the inlet plane).

Details of the experimental setup are described by Peterson and Himes (1978), and Wuerer (1978).

Centerbody (Non-Swirl) Module. The centerbody combustor (CBC) module is a 1/5th scaled version of the combustor developed and used at the Air Force Wright Aeronautical Laboratory (Roquemore, et al., 1980). The CBC consists of a 51 mm (2-inch) ID cylindrical pyrex tube (3 mm wall) that houses an internal centerbody of 30.5 mm (1.2-inch) OD around which the annular air can be swirled (Figure 1b). Fuel (Propane for reacting HOT cases; CO_2 for non-reacting COLD and HEATED cases) is introduced through a jet of 1.3 mm (0.052-inch) diameter centrally located in the centerbody. The test section is arbitrarily selected to be at 20 cm (7.87-inch) as measured from the centerbody face. The overall length of the tube is 70 cm (27.55-inch).

Details of the experimental setup are available (Ikioka, 1982).

Centerbody (Swirl) Module. Swirl was added to the CBC in the present study to evaluate the performance of the module with a swirl-induced recirculation zone (Figure 1c). The swirl was induced in the annular air by

placement of 45 degree straight swirl vanes at a location 57 mm (2.24-inch) upstream of the centerbody face.

Details of the experimental setup are available in Ikioka (1982).

Dilute Swirl Module. The Dilute Swirl Combustor (DSC) module consists of a 80 mm (3-inch) ID duct (Figure 1d) within which is located a small central body just sufficient to house a small fuel nozzle. Immediately surrounding the central body is a set of swirl vanes. Surrounding the swirl vanes is non-swirled dilution air. Dilution and swirl air are metered separately. The dilution (i.e., non-swirling) air is introduced through a flow straightener in the outer annulus. The swirl air passes through a set of swirl vanes which impart a solid body angle of turn to the flow, 60° in the present case. Either liquid or gaseous fuels may be introduced through a nozzle at the end of the central tube. The exit plane of the fuel injector is set at the same axial location as the exit plane of the swirl air to provide a clean, well defined boundary condition for modeling. The overall combustor tube length may be varied.

Details of the experimental setup are available (Brum, 1983).

2.2 Hydrodynamic Facility

The Hydrodynamic Facility (HDF) is a continuous flow, closed-loop system with water circulated by a centrifugal pump. The test section consists of two 76 mm (3-inch) ID tubes, 380 cm (12.5-foot) and 61 cm (24-inch) in length respectively, mounted horizontally. Combustor modules, such as the opposed jet and centerbody combustor modules, are installed between the two lengths of pipe. In the case of the OJC, the 380 cm long tube serves as the test section. In the case of the CBC, the 61 cm long tube serves as the test section.

The opposed jet configuration adopted for the present study (Figure 2a)

a) Opposed Jet Combustor Module

DUCT WALL (PYREX GLASS)

0.952 cm OD

0.198 cm ID

7.62 cm

AXIS OF SYMMETRY

JET TUBE
(TYPE 316 STAINLESS STEEL)

18 cm

b) Centerbody Combustor Module

DUCT WALL (PYREX GLASS)

CENTERBODY
(PVC)

JET
0.198 cm ID

4.41 cm

7.62 cm

AXIS OF SYMMETRY

18 cm
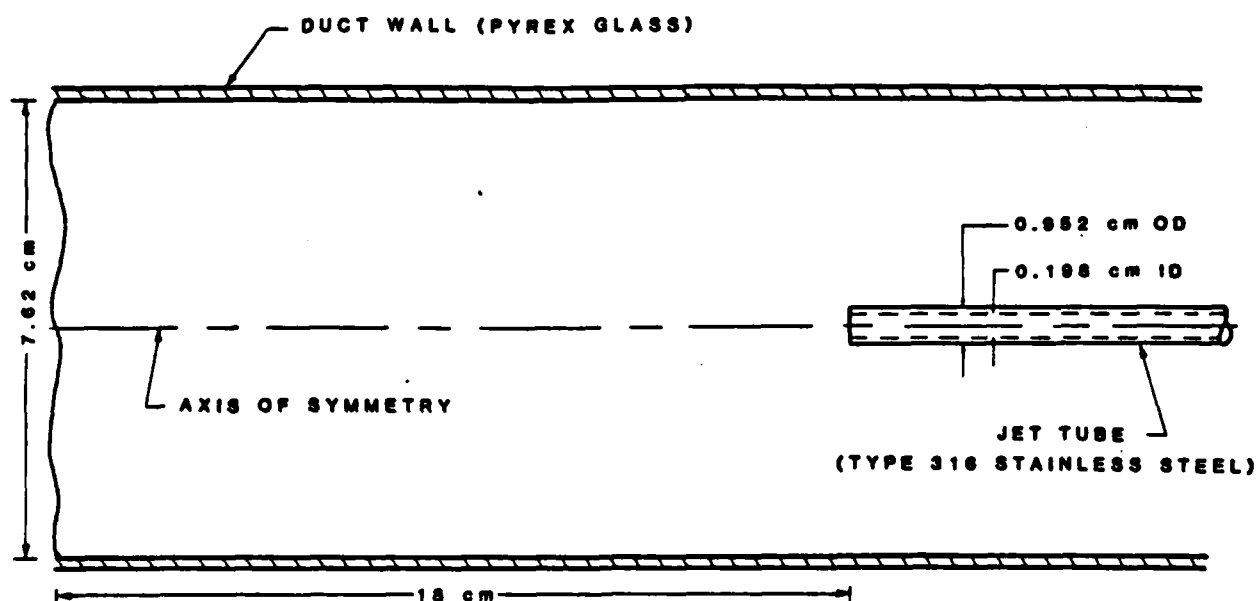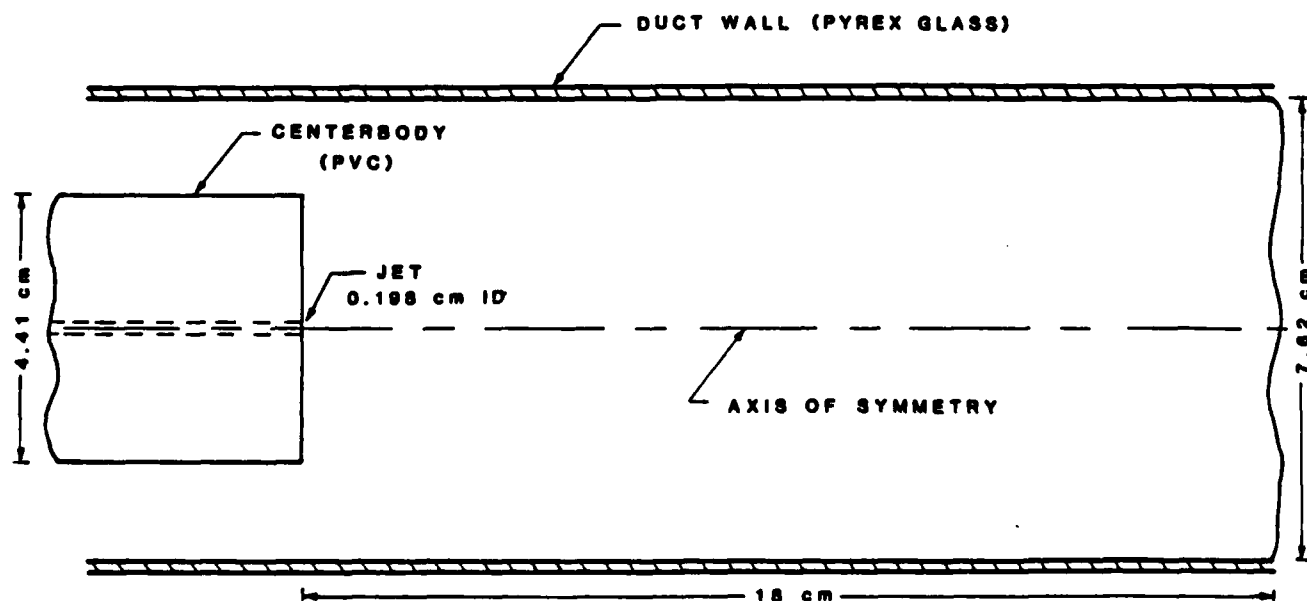
Figure 2. Hydrodynamic Facility (HDF)

8

employs an 0.198 cm (0.078-inch) inner diameter (ID) jet tube, having an 0.952 cm (0.375-inch) outer diameter (OD), and made of type 316 stainless steel. The jet tube is positioned concentrically in a 76 mm (3-inch) ID Pyrex glass duct which comprises the test section of the HDF. The jet tube extends 23.5 cm (9.25-inch) into the test field. The opposed jet has a mass flow rate of approximately 1 ℓ/m and opposes mainstream flows of 87 ℓ/m and 174 ℓ/m in two different test cases.

The centerbody configuration (Figure 2b) consists of a 4.41 cm (1.74-inch) OD cylindrical PVC bluff body, 12.7 cm (5-inch) in length, with a flat end face. The centerbody is situated concentrically in the 76 mm (3-inch) ID glass duct of the HDF. An axisymmetric jet issues from an 0.198 cm (0.078-inch) diameter opening in the center of the bluff body face and has a flow rate equal to 0.64 percent of the total flow (46.3 gpm) of the system.

Details of the experimental setup are available in Arcoumanis (1980) and Grudovich (1983).

2.3 Laser Anemometer (LA)

Two laser anemometers were developed and employed in the present program: a single component and a two component. The former is used exclusively on the HDF whereas the latter supports the LCF.

Single Component LA. The single component LA, shown in Figure 3a, is a dual beam anemometer. The laser beam is split into two equal intensity parts which are made to intersect by means of a system of plano-convex lenses. As a laser source, a 5mW Helium-Neon laser (Spectra-Physics model #120) is used which operates in the TEM_{oo} mode, the lowest order transverse mode. The 0.8 mm beam diameter is focused by means of lens L_1 (f_1 = 124 mm), which is mounted on the laser head, onto a radial diffraction grating. The Technisch Physische Dienst (TPD) rotating grating functions both as a beam splitter and as a

9

a) Single-Component
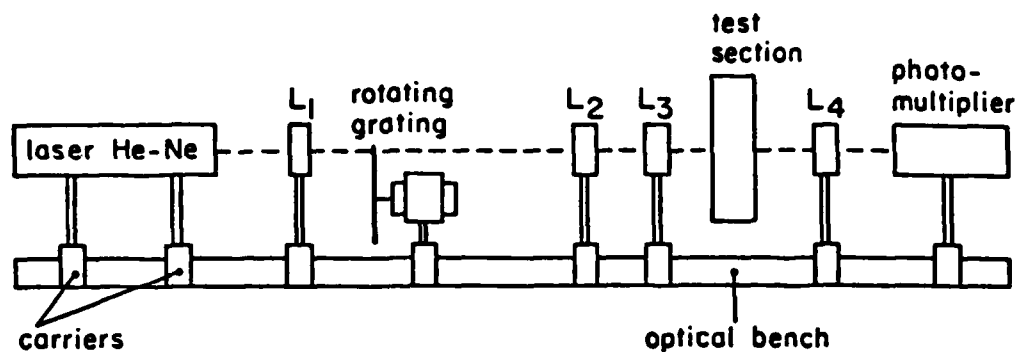
b) Two-Component
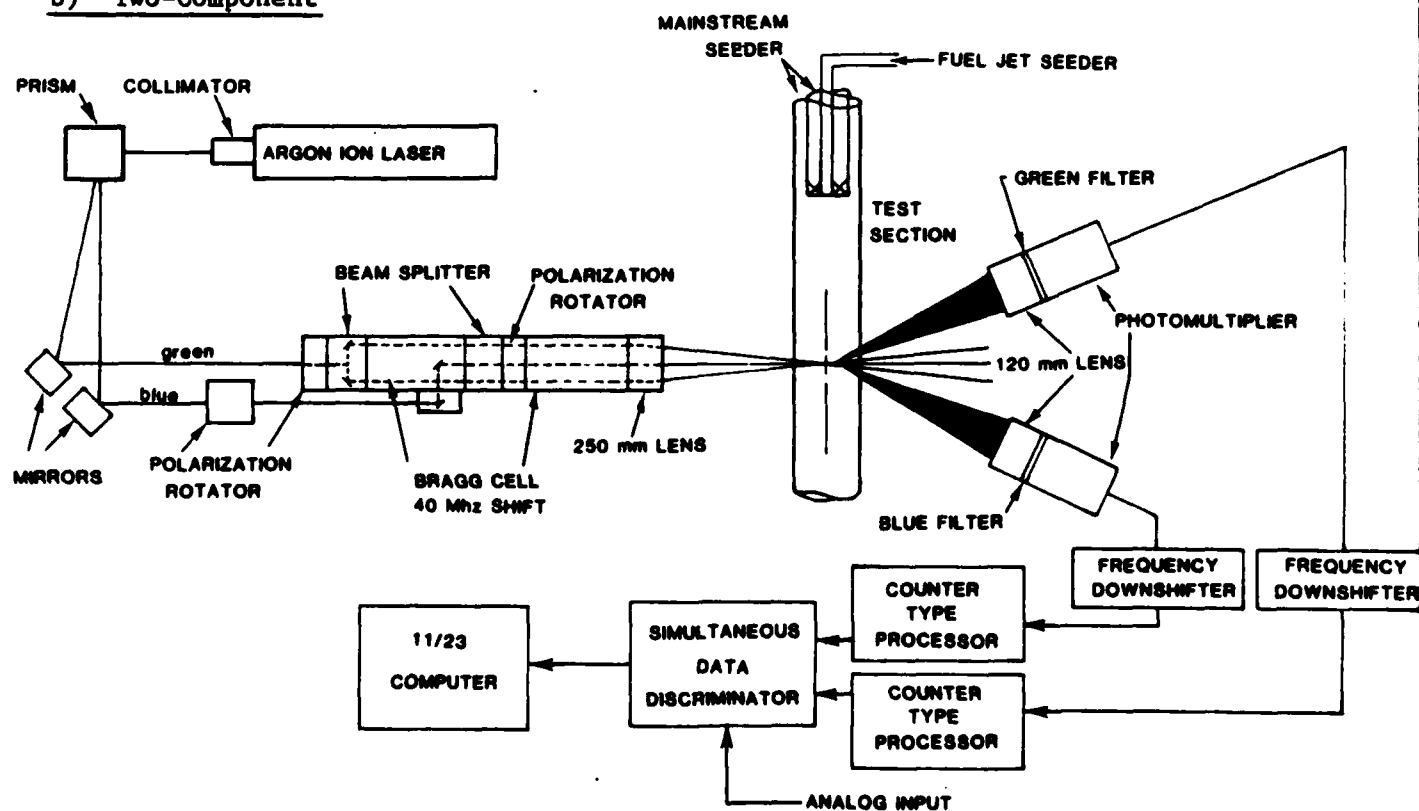
Figure 3. Laser Anemometer (LA)

10

frequency shifter. As a beam splitter, it diffracts the incident laser beam into two equal-intensity beams independent of the state of polarization of the incident light. On the other hand, as a frequency shifter, it provides a frequency shift in the two diffracted beams, thus causing a moving fringe pattern in a direction which depends on the direction of the disc rotation.

The laser anemometer setup is mounted on an optical bench and the whole system is traversed in the horizontal plane along the axis of the test section and perpendicular to this axis. The optical arrangement results in a fringe volume diameter of 0.76 mm and length of 0.58 mm. The scattered light from the particles which are traversing the fringes is detected by a DISA photomultiplier (Model #55L10).

The signal is processed by either a DISA Model 55L20 Frequency Tracker or a SDL Model VP 1001 Counter Processor. Details of the experimental setup are provided in Acroumanis (1980) and Grudovich (1983).

Two-Component LA. The two-color laser anemometry (LA) system is shown in Figure 3b. The beam from a 200 mW Argon-ion laser (Lexel Model 75) is collimated and passed through a prism to separate the various wavelengths. The two most intense beams, green (514 nm) and blue (488 nm) are each passed through a series of optics in which they are polarized and split into two beams of equal intensity 50 mm apart. An upstream 40 MHz frequency shift (TSI model 915 Bragg Cell) is applied to one of each pair of beams in order to avoid directional ambiguity that would otherwise result from the highly turbulent recirculating flow. The four beams (blue pair in the vertical plane and green pair in the horizontal plane) are then focused through a 250 mm lens to a common point within the test section. This results in set of perpendicular interference fringes spaced at 2.6 μm for the green beams (vertical fringes) and 2.5 μm for the blue beams (horizontal fringes) which

11

are responsive to the axial and tangential velocity components respectively.

Receiving optics consist of a 120 mm lens focused onto a 0.25 mm diameter photomultiplier tube aperture (via an appropriate dichromate filter to selectively pass either the blue or green light). These optics are placed at an angle of 20° off direct forward scatter which results in a probe volume of 0.022 mm^3 and cross-sectional area perpendicular to the axis of measurement of 0.10 mm^2. However, due to the requirement imposed by the processing electronics that both axial (u) and tangential (w) velocity components be obtained simultaneously, the effective probe cross-section is much less (approximately 0.03 mm^2). The transmitting and receiving optics are mounted on an optical bench capable of placing the measurement volume at points throughout the stationary combustor test section.

A special electronic interface was built to interface the output of the two counter process channels (u,w) directly to a DEC PDP 11/23 computer system. This interface identifies whether or not the u and w events occur within a certain aperature time of each other (normally $\leq$ 50 μs). If so, they are considered simultaneous, stored, and then multiplexed into the 11/23 via a parallel interface. Once the interface verifies that the 11/23 has read the data, it simultaneously resets both processor channels. The key feature of this system is that it permits a direct and instantaneous measurement of correlations such as $\overline{u'w'}$. An aperature time of 50 μs was selected since, at the maximum bulk velocity measured (15 m/s), an equivalent spatial resolution of less than 0.75 mm is obtained.

The 11/23 computer is equipped with an internal clock having a resolution of 100 μs which is initiated at the beginning of each run cycle. As the u, w data are received, the time of event t is combined with the raw data (u,w,t), and the data are permanently stored in an archival fashion for future

reference and analysis.

Details of the system are provided in Brum (1983).

Seeding. Natural seeding is used in the HDF. In the LCF, the main and fuel jet flows are seeded independently, but to the same levels of concentration, with 1 μm alumina particles. A liquid suspension atomization seeding technique is employed. Signal validation was obtained using two counter processors (Macrodyne Model 2098). This seeding technique, developed under the present program, is described in Section 4.3.1.

2.4 Temperature Measurements

Mean temperatures were obtained with a robust thermocouple probe and, under limited combustor operating conditions, fluctuating and mean temperatures were obtained with a fine-wire thermocouple probe.

Robust Thermocouple Probe. The robust probe consists of an unshielded, fine wire, platinum/platinum 13% rhodium thermocouple mounted on a micrometer traverse jig. A Doric digital pyrometer (Model DS-500) is used to record the thermocouple output.

Details of the probe are provided in McDannel (1979).

Fine-Wire Thermocouple Probe. A fine-wire probe was built under a complementary National Science Foundation (NSF) Grant (CPE-8013742) and used in conjunction with the two-component LA to acquire measurements of axial and azimuthal heat flux. Platinum/platinum 10% rhodium thermocouple wire of three diameters (25 μm, 50 μm, and 125 μm) are used in this work. The thermocouple junction is formed by overlapping and spotwelding the two small wires which yields a junction with a characteristic length less than 40 μm when 25 μm wire is used. The small diameter wire is then gas welded to larger support wires (of 250 μm and 500 μm diameter) of the same material. The support wires are cemented in a 0.159 cm (0.063-inch) or 0.318 cm (0.125-inch)

13

OD alumina tube which is in turn placed in Inconel tubing of various diameters and shapes. The various probe configurations are tested and the one that minimizes perturbation effects at a specific measurement location is used. Figure 4a shows the dimensions of the probe configurations used during these experiments. The probe is held in a mechanical traverse which moves with the LA optical table and is inserted into the flow through the exhaust plane of the combustor.

The thermocouple frequency response necessary to make accurate time-resolved measurements can be estimated from the physical dimensions of the combustor and the bulk mean velocity. If the length scale of the energy-containing structure is taken to be one-half the combustor radius, the corresponding frequency for a mean velocity of 15 m/s is about 750 Hz. Therefore, in order to accurately measure the root-mean-square temperature, the sensor frequency response must extend to at least two or three times the frequency of the energy-containing structures or to approximately 2 kHz. The uncompensated frequency response of the 25 μm sensor at this mean velocity is about 15 Hz. Thus, the frequency response must be increased by a factor of 130 and is accomplished using electronic compensation.

The compensation method used in this study is similar to the one used by Lockwood and Moneib (1981). A block diagram of the thermocouple signal processing electronics, shown in Figure 4b, can be divided into the following subcircuits: 1) a relay, a source of heating current, and a square wave generator to control the relay, 2) a low noise, low drift, differential input preamplified (AD 521; gain of 100), 3) a compensation circuit, and 4) a gain and bias amplifier to match the dynamic range of the temperature signal with that of the analog to digital converter.

The compensation subcircuit consists of a differentiator, an amplifier,

a) Probe Configurations

PROBE 1

PROBE 4

PROBE 4C
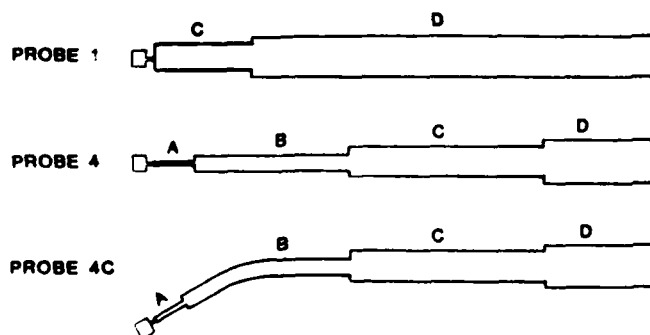
PROBE	DIMENSIONS, L(cm)/d(mm)			
	A	B	C	D
1	——	——	10.2/6.4	45.7/9.53
4	2.54/3.2	15.2/4.7	15.2/6.4	12.7/9.53
4C	2.54/3.2	20.3/4.7	15.2/6.4	12.7/9.53

SYMBOL	PROBE	ORIENTATION PLANE
○	1	—
○	4	—
△	4C	0°
□	4C	45°
○	4C	90°
○	4C	135°

END VIEW OF COMBUSTOR WITH PROBE 4C ON CENTERLINE

b) Electronics

TRIGGERING CIRCUIT

RELAY

HEATING CIRCUIT

TIME CONSTANT DETERMINATION

PREAMP

COMPENSATION STAGE

DIFFEREN-TIATOR

BIAS & GAIN AMP

SUMMER

LOW PASS FILTER

BIAS & GAIN AMP 1

BIAS & GAIN AMP 2

SAMPLE & HOLD

LINE DRIVER

SCOPE

FILTER

SCOPE

PDP 11/23
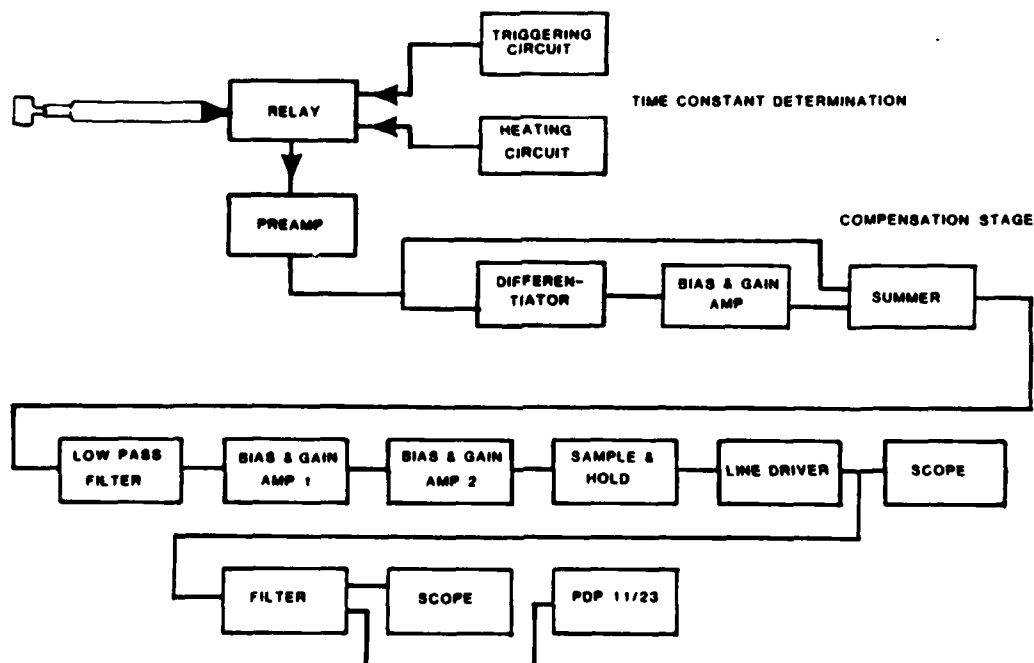
Figure 4. Fine-Wire Thermocouple

15

and a summing amplifier. The operation $[1 + \bar{\tau} (d/dt)]E$, where $\bar{\tau}$ is the mean time constant, is performed on the thermocouple voltage, E, to increase the inherently low ($\sim$ 15 Hz) frequency response of the sensor.

Details of the experimental setup are available (Seiler, 1983a).

2.5 Emissions Measurement

Combustion gases are sampled continuously using a hot (60°C/140°F) watercooled, 6.35 mm (0.25-inch) OD by 1.32 mm (0.052-inch) ID, stainless probe with a constant area inlet bounded by a cooled, streamlined tip. The sample probe is mounted on a micrometer traverse jig for sampling. The gas sample flows to the analysis instruments through heated (65°C/150°F), 6.35 mm (0.25-inch) OD Teflon tubing.

Analysis of the sample gas is performed using a packaged emission analysis system (Scott Research, Model 113). Passage of the gas through an ice bath allows all concentration measurements to be taken on a dry basis. Nitrogen oxides (NO, NO_x) concentrations are measured using a chemiluminescence analyzer (Scott Research, Model 125). Nondispersive infrared analyzers (Beckman, Models 315B and 315BL respectively) are used to measure carbon dioxide (CO_2) and carbon monoxide (CO) concentrations. Total hydrocarbon (HC) concentration is measured by a flame ionization detector (Scott Research, Model 215). Oxygen (O_2) concentration is measured by a paramagnetic analyzer (Scott Research, Model 150).

Details of the experiment setup are provided in McDannel (1979).

SECTION 3

MODELING

3.1 General Methodology

The computational procedure used to obtain the simultaneous solution of the governing elliptic partial differential equations is the TEACH method (Gosman and Pun, 1974) which has been expanded (1) for the opposed jet, centerbody, and dilute swirl configurations, and (2) to include species conservation, swirl, and reaction.

The governing equations are cast into a generalized equation of the form:

$$\frac{\partial}{\partial x}(\rho u \phi) + \frac{1}{r}\frac{\partial}{\partial r}r(\rho v \phi) = \frac{\partial}{\partial x}\left(\Gamma_{\phi,eff}\frac{\partial \phi}{\partial x}\right)$$

$$+ \frac{1}{r}\frac{\partial}{\partial r}\left(r\Gamma_{\phi,eff}\frac{\partial \phi}{\partial r}\right) + S_\phi \tag{1}$$

where:

ϕ = dependent variable

$\Gamma_{\phi,eff}$ = effective exchange coefficient

S_ϕ = source and/or sink terms

The boundary conditions are specified along the four boundaries of the solution domain. Where applicable, experimental data are used to specify the boundary conditions.

3.2 Turbulence Models

The form of the governing equations is based upon the gradient transport hypothesis. Closure of the equations requires the development of time mean of "effective" transport coefficients. The effective viscosity (μ_{eff}) is defined as follows:

17

$$\mu_{eff} = \mu_\ell + \mu_t \qquad (2)$$

where:

μ_ℓ = absolute viscosity of fluid

μ_t = eddy (or apparent) viscosity due to turbulent exchange

The turbulent transport of scalar quantities is related to the eddy viscosity through the appropriate Schmidt numbers as follows,

$$\Gamma_{\phi,eff} = \frac{\mu_\ell}{\sigma_{\phi,\ell}} + \frac{\mu_t}{\sigma_{\phi,t}} \qquad (3)$$

where:

$\sigma_{\phi,\ell}$ = laminar Schmidt Number

$\sigma_{\phi,t}$ = turbulent Schmidt Number

Two models were employed for the turbulent viscosity (μ_t) , an algebraic model and a two-equation k-ε model.

Algebraic Model. The employment of an algebraic model simplifies the closure of the governing equations be eliminating the need for the equations for k and ε. The use of algebraic models for recirculating flowfields has shown little evidence of success. However, their application is useful in revealing solution sensitivities to viscosity distribution. The algebraic model utilized in the present investigation was one proposed for the preliminary demonstration of numerical combustion models,

$$\mu_t = KD^{2/3} L^{-1/3} \rho^{2/3} (mU^2)^{1/3} \qquad (4)$$

18

where:

K = empirical coefficient

D = diameter of combustor

L = length of combustor

ρ = local density

mU^2 = inlet kinetic energy

As can be seen, the variation in μ_t is dependent only upon local density for a given geometry and inlet flow rate. For the isothermal flow of a mixture of two gases with assumed identical density and laminar transport properties, the case of the algebraic viscosity model becomes extremely simple (i.e., the effective viscosity, μ_{eff}, is constant through the flowfield).

Two-Equation k-ϵ Model. The two-equation k-ϵ model is the most commonly employed viscosity model for combustor flow analyses. The two-equation model accounts for the transport effects of two turbulence characteristics which may be taken as typical time scales and length scales of the energy containing motions. This is accomplished by calculating the local levels of turbulence kinetic energy (k) and the kinetic energy dissipation rate (ϵ). The representative length and time scales are:

$$\ell = \frac{k^{3/2}}{\epsilon} \tag{5}$$

and

$$t = \frac{k}{\epsilon} \tag{6}$$

The eddy viscosity is then calculated from the algebraic Prandtl-Kolmogorov formulation, i.e.

19

$$\mu_t = C_\mu \, \rho \, \frac{k^{1/2}}{\ell} = C_\mu \, \rho \, \frac{k^{3/2}}{\epsilon} \qquad (7)$$

where C_μ is an empirical coefficient.

Detailed information on the modeling in general is provided elsewhere (Wuerer, 1978; Brum, 1983, and Grudovich, 1983).

SECTION 4

RESULTS

A summary of the results are provided in this section for each of the
Elements, A, B, and C. Details are provided in papers presented,
publications, and both Master of Science Theses and Doctor of Philosophy
Dissertations completed under the present grant.

4.1 Element A: Model Laboratory Combustor Developments and Evaluation

The Opposed Jet Combustor (OJC) module was developed under a previous
AFOSR grant (74-2710) as a candidate configuration for a premixed model
complex flow laboratory combustor. In the present program, attention was
directed to candidate configurations for a non-premixed model complex flow
laboratory combustor using the following criteria for the purposes of
evaluation:

- allow good optical access for advanced laser diagnostics,

- be stabilized by a zone of strong backmixing,

- be capable of swirl inlet conditions,

- be axisymmetric to simplify modeling,

- have clean, well defined boundary conditions,

- be capable of reacting and non-reacting, non-premixed (multiple
  inlet stream) operation,

- allow sampling probe.

As a point of departure, a 1/5 scale model (Figure 1b) of a geometry
introduced for diagnostics and modeling development at the Air Force Wright
Aeronautical Laboratory (Roquemore, et al., 1980) was evaluated. The scaled
version of the Centerbody Combustor (CBC) consists of a 51 mm ID cylindrical
pyrex tube (3 mm wall) that houses an internal centerbody of 30.5 mm O.D.

21

around which the air is injected in an annular, non-swirling jet.

The CBC was evaluated in the present study, not only for the nominal operating mode without swirl, but with a swirl-induced annular jet as well (Figure 1c). Fuel (gaseous propane for reacting cases, CO_2 for non-reacting cases) was introduced through the jet centrally located in the centerbody.

In addition to the CBC geometry, an independent "Dilute Swirl Combustor" (DSC) geometry (Figure 1d) was designed to satisfy the established criteria and address limitations observed with the no-swirl and swirl operation of the CBC. In addition to propane for the reacting cases and CO_2 for the non-reacting cases, the DSC was also operated with liquid isooctane injected through either a twin-fluid or pressure atomizer.

Both the CBC and DSC modules were operated at atmospheric pressure, with ambient inlet temperature. Axial mean and rms velocity measurements were made using the two component laser anemometry system (Figure 3b).

High-speed photography was used to qualitatively document the flame structure and investigate dynamic aspects of the flame. The camera (Fastax Model WF3) was run at a frame speed of approximately 1000 frames/second. Black and white film (Kodak 7277, 16 mm, 400 ASA) was used and pushed 2 stops during processing.

4.1.1 No-Swirl CBC

Swirl is one of the primary features required by a test bed geometry to be useful as a supporting data case for the identified modeling efforts. The no-swirl CBC was investigated as a point of reference and because it is the configuration used at the Air Force Wright Aeronautical Laboratory (AFWAL).

Laser anemometry measurements were made to:

(1) Identify the basic flow patterns including the extent and structure of the recirculation zone.

22

(2) Characterize the recirculation zone in terms of turbulence intensity levels and velocity gradients.

(3) Investigate the fuel jet/recirculation zone interaction.

Figure 5a illustrates the Laser Anemometry (LA) results for 7.5 m/s, ϕ = 0.05, isothermal (COLD) flow and reacting (HOT) flow. The formation of a recirculation zone downstream of the centerbody face is clearly evident. The fuel jet is contained within the recirculation zone in the case of isothermal flow. Reaction changes the flow structure. For the reacting case, the fuel jet penetrates the recirculation zone. This is attributed to the higher temperature and thus lower density of medium into which the fuel jet is issuing. A similar result was established for the isothermal case by doubling the jet velocity.

Visually the flame is comprised of two regions, an upstream region with the shape of a semi-ellipsoid attached to the centerbody face and a downstream region with the appearance of a diffusion flame. To the eye, the flame appears steady and symmetric with the exception of a rugged trailing edge on the diffusion flame and occasional oscillations about centerline. Both regions are luminous yellow and substantial soot build-up occurs on the centerbody face, indicative of a close proximity of the reacting gases to the solid boundary.

The high-speed photography revealed a visually undetected cyclic change in the flame structure occurring at a frequency approximately 110 Hz. The no-swirl flame oscillates both axially and, at a random interval, radially about the centerline. During each axial oscillation of the flame, a mass of reacting fluid separates from the trailing edge of the flame, traveling independently downstream in the form of a flame turbule (Figure 5b). This phenomenon is consistent with that observed in the larger scale (AFWAL)

23

a) **Axial and Radial Mean Velocity Probes (ϕ = 0.05, COLD/HOT)**
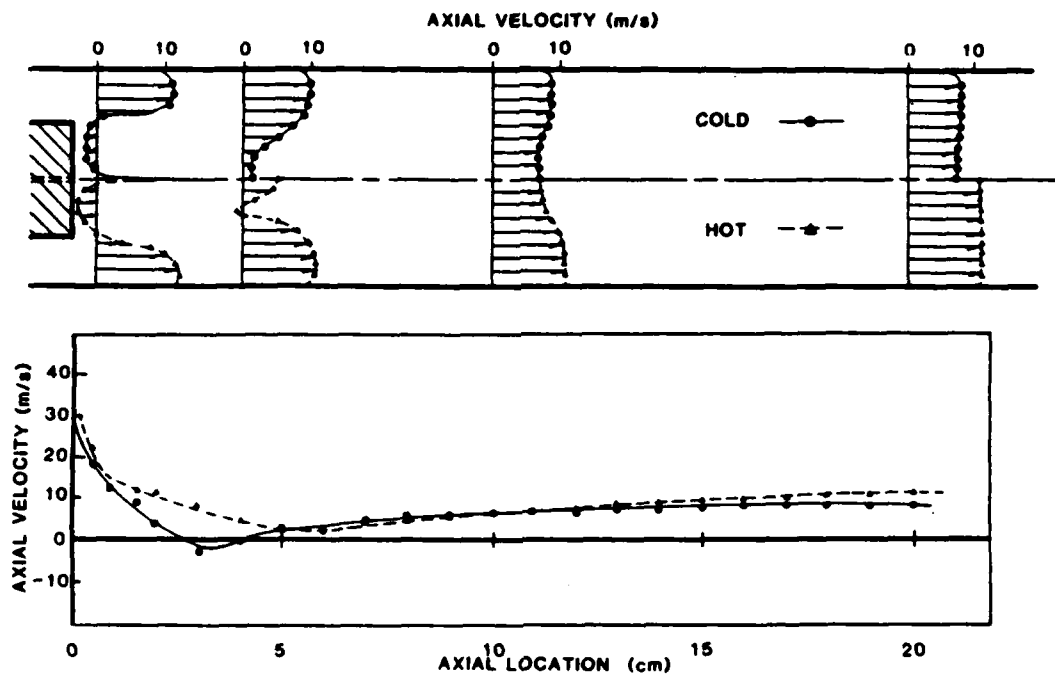
b) **High-Speed Photography (ϕ = 0.10, HOT)**
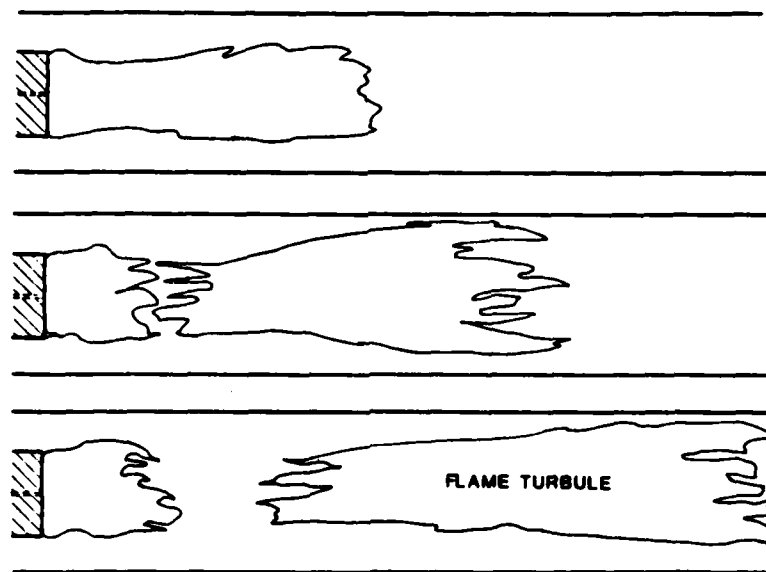
Figure 5. Centerbody Combustor Evaluation (7.5 m/s)

system, combustor (Roquemore, et al., 1982) and is attributed to vortex shedding off the centerbody face.

These observations established that, although the no-swirl CBC geometry has value for diagnostic tool development (e.g., as employed at AFWAL), not all the criteria delineated above are satisfied. In particular, (1) the geometry does not have swirl, (2) the no-swirl flames exhibit random asymmetry and flame turbule shedding, and (3) the flame is attached to the centerbody face, producing carbon deposits and establishing an intimate association between the solid boundary condition and flame performance, a difficult if not impractical condition to model. This established a point of reference to identify the effect of swirl which was next added to the geometry.

4.1.2 Swirl CBC

Swirl was added to the CBC geometry by placement of 45° straight blade swirl vanes upstream of the centerbody face (Figure 1c). Qualitatively, swirling flows in the CBC configuration produce a much more intense and, to the eye, stable flame. Swirl tends to shorten the flame and produce a smaller, but more intense reaction zone with little flame oscillation apparent to the eye.

High-speed photography of the swirl flame revealed that the flame undergoes a lengthening and shortening cycle (on the order of 2:1 in magnitude) at a frequency of about 100 Hz. Several hundred cycles were observed (on the film) and, although the period would sometimes vary ± 50% in duration, it was surprisingly regular. The pictures also revealed that (1) the swirl flame is axisymmetric even though it oscillates in length, and (2) reacting gases do not separate from the trailing edge of the flame during these oscillations, as was the case for the no-swirl flame.

Figure 6a shows the effect of adding swirl to a 7.5 m/s (bulk velocity)

25

a) Axial and Radial Mean Velocity Profiles (7.5 m/s, COLD, No Fuel Jet)
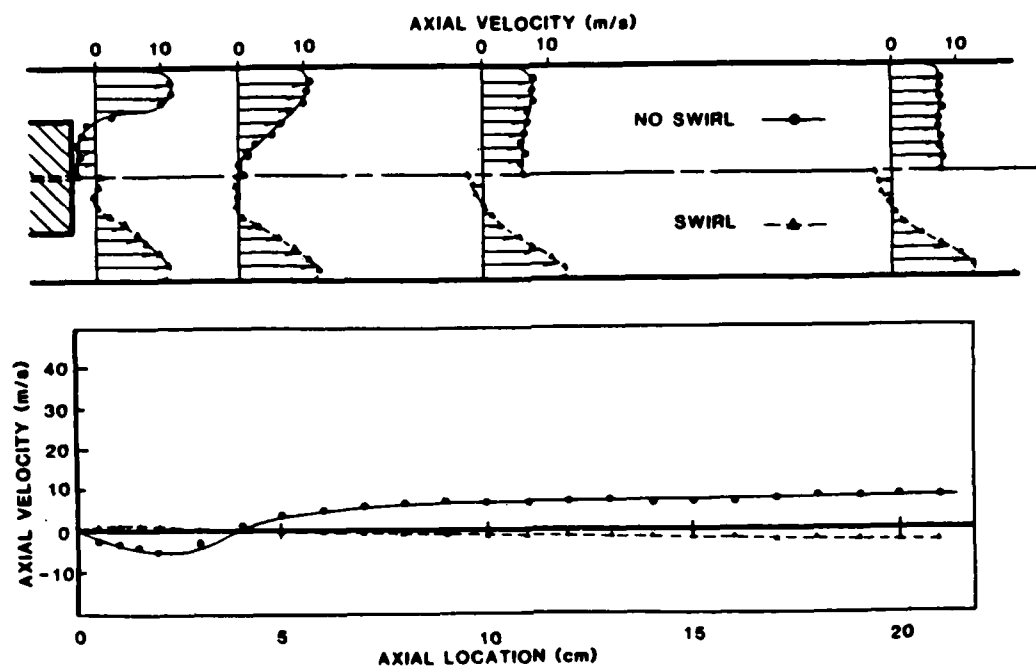
b) Axial and Radial Mean Velocity Profiles (Swirl, HOT, ϕ = 0.05)
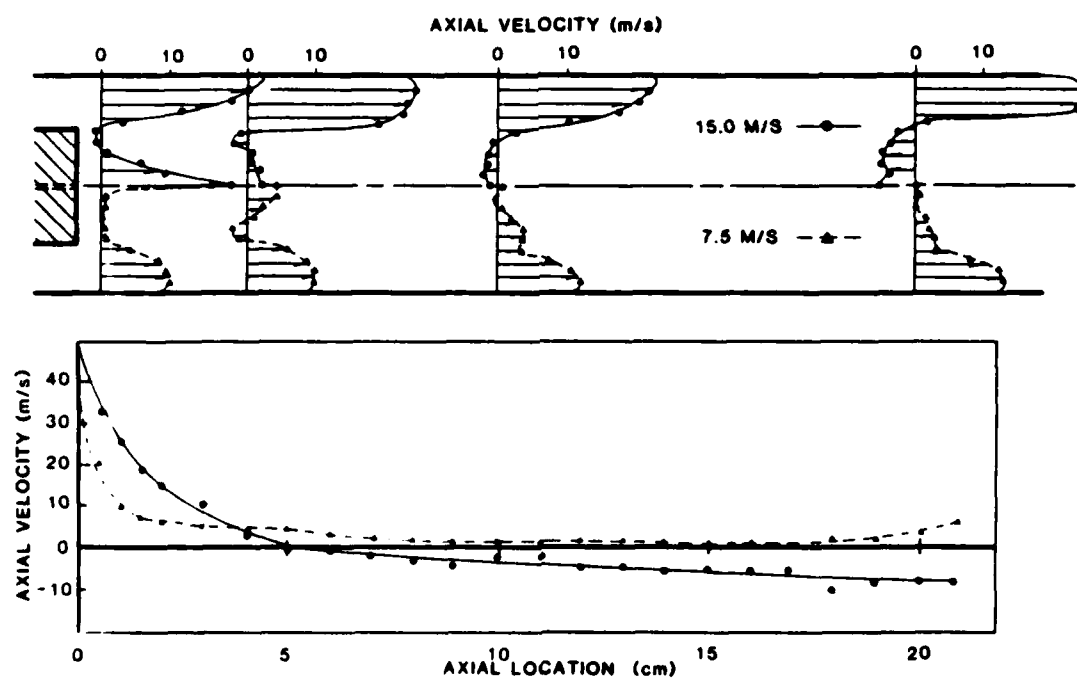
Figure 6. Centerbody with Swirl Evaluation

cold flow with no central fuel jet. Both the recirculation zone length and structure experience significant change. With swirl, the recirculation zone extends beyond the 20 cm test section with negative centerline velocities increasing monotonically with axial distance from the centerbody face. The extent of recirculation was first shown by laser anemometry and later verified via smoke traces to reach beyond the end of the 70 cm long duct and produce a suction of gaseous material (combustion products and room air) from the exit plane to the centerbody face. In contrast, the no-swirl case has a recirculation zone contained within the test section with high negative velocities starting near the centerbody and reaching a stagnation point about two centerbody diameters downstream.

Heat release tends to suppress exit plane suction as illustrated by Figure 6b which shows the same swirl case with reaction (7.5 m/s, ϕ = 0.05). However, an increase in reference velocity increases swirl strength and can again induce suction for the reacting, as well as the non-reacting flows.

Previous experimental analyses of complex flow combustors in which all the inlet air is swirled reveal the presence of indefinitely long recirculation zones as evidenced by suction at the exit plane of the combustor (e.g., Khalil, et al., 1976, — low-intensity swirl tube combustor). Other examples of 100% inlet swirl configurations susceptible to suction, include hi-intensity swirl tube combustors (e.g., Appleton and Heywood, 1973), swirl dump combustors (e.g., Buckley, et al., 1980) and swirl expansion combustors (e.g., Lilley and Rhode, 1982). Published modeling results do not, as a general rule, indicate suction at the exit plane. However, this may be an artifact of the modeling process. Exit plane suction can be, and is, predicted by elliptic flow codes, but the possibility is generally ruled

27

unrealistic by the modeler and excluded by setting the exit plane boundary condition to preclude a reverse flow.

A similar approach might be employed experimentally, that is by controlling the exit plane boundary conditions to suppress suction. Flow straighteners, for example, could be positioned in the combustor to retain the zone of recirculation upstream of the exit plane. In practical gas turbine combustors, however, this is not realistic and aerodynamic methods (i.e., radial jet injection and dilution air) are employed to confine the zone of recirculation to the primary zone and thereby prevent reverse flow from extending to the exit plane.

Several development tests were conducted in an attempt to eliminate the swirl induced suction while maintaining the CBC geometry as close as possible to the original one described in Figure 1c. Downstream swirl suppression devices such as orifice plates with varying size holes were installed. They were found to suppress suction but in doing so modify the structure of the recirculation zone and thereby compromise flame stabilization. Flames were stable only at very low equivalence ratios and were invariably attached to the centerbody face. Honeycomb and other anti-swirl devices installed downstream did not prevent suction but only moved the point of flow reversal upstream to the location selected for the device.

4.1.3 Dilute Swirl Combustor (DSC)

A swirl-stabilized geometry was developed to address the deficiencies observed with the swirl CBC geometry and satisfy the identified criteria. The geometries of practical (gas turbine) combustors were used as a guide in these development tests. The strong swirl required to produce a stable flame must be dissipated downstream prior to reaching the exit plane by the addition of non-swirling dilution air. Adding this air downstream of the recirculation

zone through radial wall jets would properly represent gas turbine combustors but compromise the criteria to retain (1) clean and well prescribed boundary conditions, and (2) clear optical access. Therefore, an alternative approach, amenable to subsequent transformation to radial jet addition, was adopted and evaluated (Figure 1d).

Swirl Strength. The DSC was initially evaluated to determine the ratio of swirl to dilution air (S/D) required to suppress exit plane suction. It was found that if the swirl flow was less than seventy (70) percent of the total flow, no suction occurred. Whereas the upper limit of percent inlet swirl air is dictated by the onset of suction, the lower limit is bounded by the minimum necessary to produce swirl-induced centerline recirculation. A typical scenario is depicted in Figure 7. At zero (0) percent inlet swirl air (Figure 7a, S/D = 0), the flame is similar to that of a no-swirl CBC, (i.e., the flame is long, luminous yellow, and attached to the fuel tube face). At the onset of swirl-induced recirculation, the flame shortens, becomes more intense, separates from the fuel tube face, and the regions of luminous yellow soot are suppressed (Figure 7b, S/D = 1/4). At fifty (50) percent swirl air (Figure 7c, S/D = 1/1), the flame is 100% blue, intense and compact. A 50% inlet swirl (i.e., a swirl/dilution air ratio (S/D) of unity) was selected as a baseline operating point. For a swirl-to-dilution ratio of unity, the value used in the present study, the swirl number (SN) obtained by integrating across the swirl vanes is 0.8; that obtained by integrating the total inlet mass flux is 0.3.

Performance. Radial and centerline profiles of axial mean and rms velocities are shown in Figure 8a for the DSC operating under reacting (HOT) flow at a swirl/dilution ratio (S/D) of 1/1. Gaseous propane is introduced through a cone annular nozzle with an overall equivalence ratio of 0.1. A

a) S/D = 0
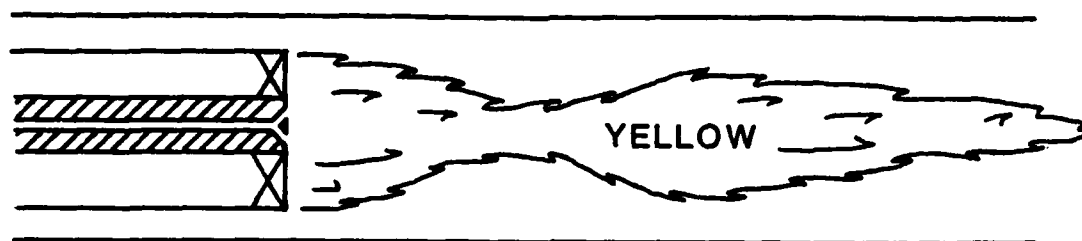
b) S/D = 1/4
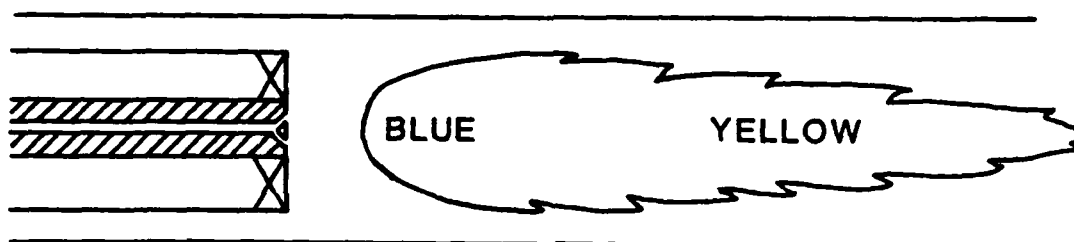
c) S/D = 1/1
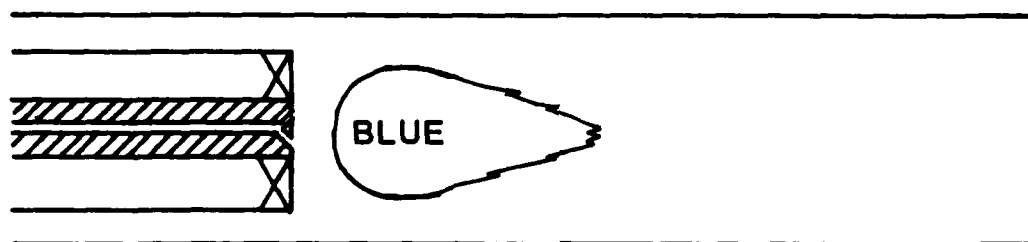
Figure 7. Visual Effect of Swirl/Dilution Air Ratio (S/D)
(7.5 m/s, HOT, ϕ = 0.1)

a) Centerline and Radial Mean and RMS Velocity Profiles
(15 m/s, HOT, $\phi = 0.1$)
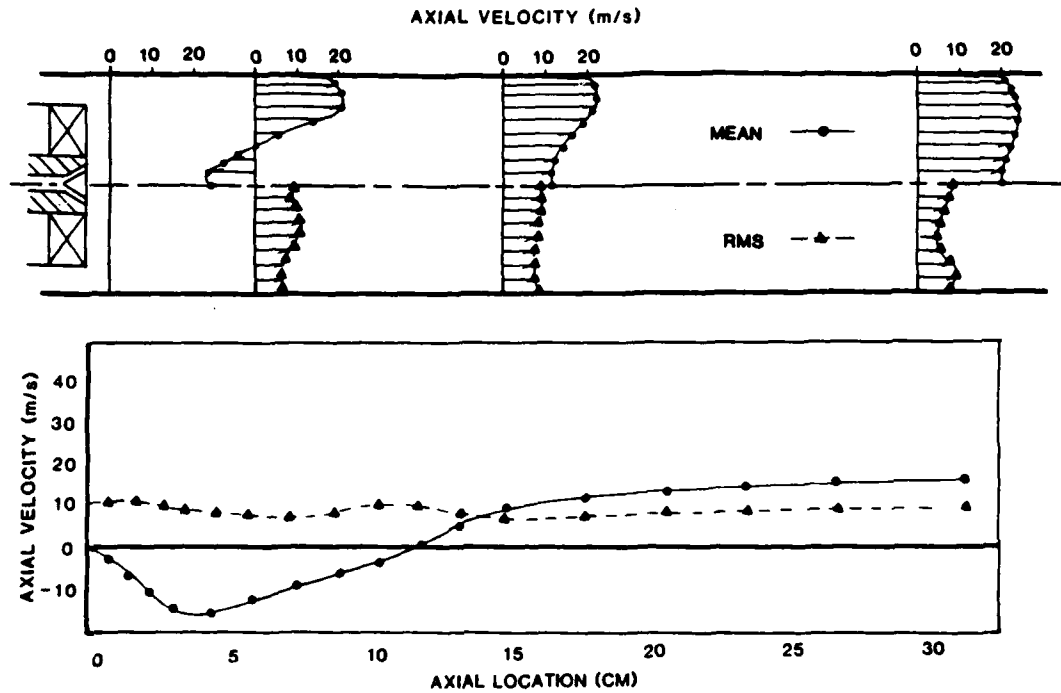
b) Fuel Injection Nozzles

Round Jet

Delavan W/A

Cone-Annular
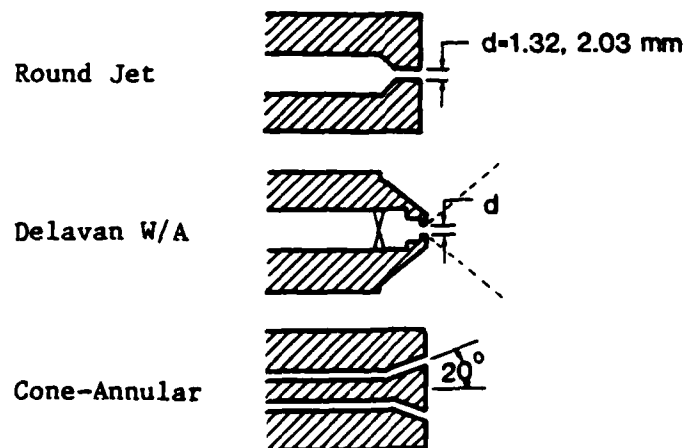
Figure 8. Dilute Swirl Combustor Evaluation
(S/D = 1/1)
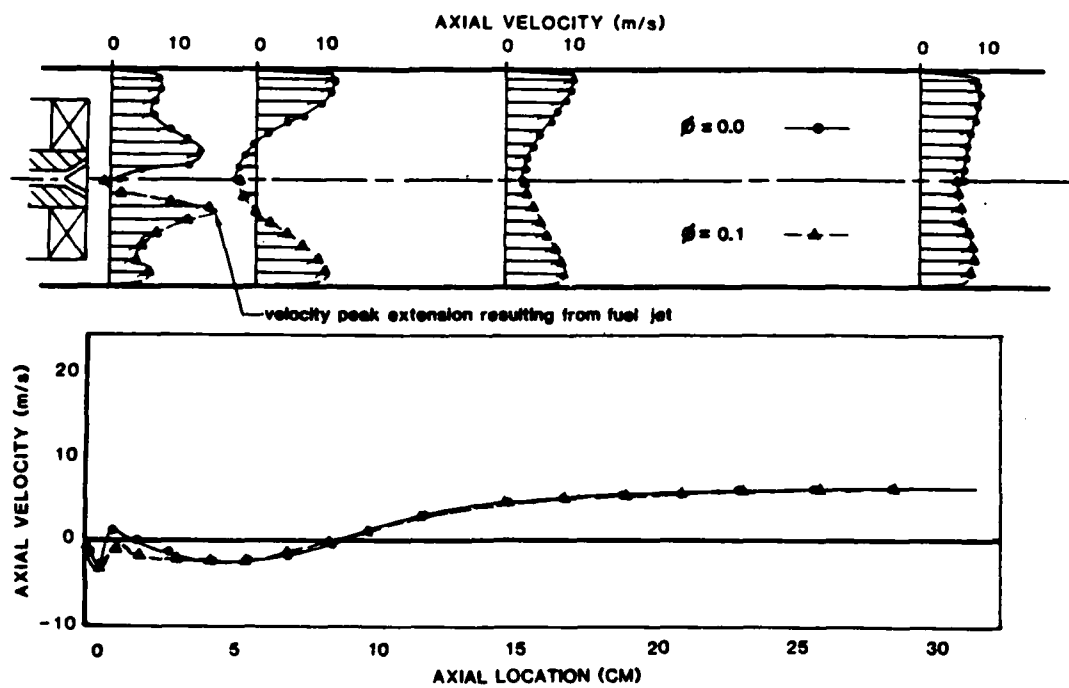
Figure 8. (concluded)

strong, compact recirculation zone is produced and positive centerline velocities are established well before the exit plane.

High speed cinematography of the DSC reveals a steady and symmetric flame. No regular or periodic change in either flame shape or luminosity is observed. This behavior is attractive especially with respect to the application of time-averaging modeling.

Fuel Injection. Both combustor aerodynamics and fuel injection play an important role in dictating the flame intensity, blow-off limits, and final products of combustion. Mellor (1980), for example, describes the use of differential nozzle pressure to control the location into which the bulk of the fuel is injected in the wake of a stabilizer disk. At low injection pressures, the fuel is contained within the recirculation zone with a concomitant promotion of soot formation. At high injection pressures, the fuel penetrates the bulk recirculation zone and enters the shear layer resulting in lower soot production and increased flame stability.

Tests of various fuel injection nozzles (Figure 8b) were conducted in the present study to identify the influence of spray pattern in the DSC flowfield. In general, it was found that the fuel injection pattern was a principal determinate in the control of blow-off limits, flame shape, and emission of soot particulate.

Round fuel jet injection was first assessed for both gaseous (propane) and liquid (isooctane) fuels. For propane, jet diameters of 1.32 mm (0.052-inch) and 2.03 mm (0.080-inch) ID were tested and, for the liquid isooctane, a straight jet Delavan air blast atomizer (Model 30609-4) was evaluated. Results were similar for both fuels. At lower equivalence ratios (eg., $\phi = 0.05$), the fuels were contained within the recirculation zone resulting in luminous soot production. As equivalence ratio was increased,

33

the jet momentum increased and the fuel penetrated the recirculation zone resulting in, first, a diffusion type flame downstream of the recirculation zone and finally, blow-off at relatively low values of overall equivalence ratio (ϕ = 0.2).

Solid cone liquid pressure atomization nozzles (Delavan WDB 1.5 and 1.0, 45°) were tested using isooctane at a differential pressure of 125 psi. Injection of a portion of the fuel into the center of the recirculation zone once again resulted in luminous soot formation although less than was observed for straight jet injection.

Hollow cone nozzles for both liquid (Delavan WDA 1.5, 80°) and gaseous fuels (cone/annular, and Delavan WDA 16, 80°) were tested. For propane and isooctane, these nozzles resulted in virtually no visual soot production and extended the blow-off limits to equivalence ratios greater than 1.0. Laser anemometry data (Figure 8c) illustrates the zone of injection. Cold flow is selected for this example to demonstrate the effect of the jet. The effect of fuel injection is evident by comparing the radial profiles at the 1.0 cm station for ϕ = 0.0 (no jet) and ϕ = 0.1 for the cone/annular gas injection nozzle. The fuel is injected into a region of high velocity gradients which results in high turbulence levels and enhanced mixing of the fuel with thermally and chemically excited intermediates from the recirculating core flow and oxygen from the outer flow.

4.1.4 Summary

Criteria were established for a common, laboratory scale, complex flow combustor, and an evaluation was conducted of candidate geometries. A no-swirl centerbody combustor (CBC) was first evaluated. The no-swirl flames exhibit random asymmetry and vortex shedding off the trailing edge of the flame. In addition, for many of the no-swirl cases, the flame is attached to

the centerbody face, a difficult if not impractical condition to model.

All of the inlet air to the CBC was swirled and it was found that this often resulted in exit plane suction, a condition not representative of practical devices, and for which downstream boundary condition specification is difficult. A development study was conducted to establish a swirl stabilized geometry that controls both the strength and extent of swirl.

The configuration developed and evaluated, the dilute swirl combustor (DSC), is comprised of a combination swirl, no-swirl inlet and exhibits clean and well-defined boundary conditions as well as a detached symmetric recirculation zone. Laser anemometry measurements were made to identify the strength and extent of the recirculation zone and baseline methods of fuel injection, equivalence ratios and swirl strength were identified.

Papers presented on this work include Brum, Ikioka, and Samuelsen (1981), Brum, Ikioka, and Samuelsen (1982), and Brum and Samuelsen (1982a). A manuscript has been submitted for publication (Brum and Samuelsen, 1984a). More detailed information is provided in a M.S. Thesis (Ikioka, 1982) and a Ph.D. Dissertation (Brum, 1983).

4.2 Element B: Physical and Chemical Processes in Complex Flows

Attention under this element was directed in the present program to (1) the acquisition and interpretation of detailed flowfield data in the premixed Opposed Jet Combustor (OJC) and the non-premixed Dilute Swirl Combustor (DSC), and (2) the performance of elliptic flow modeling in predicting the acquired experimental data. Experiments were conducted for the following conditions: COLD (non-reacting), HEATED (non-reacting), and HOT (reacting). The justification of conducting non-reacting flow experiments (COLD and HEATED) was to develop an experimental data base for testing elliptic flow models in the absence of reaction. Such tests are both useful

35

and necessary to detect shortcomings of the models prior to tests for the cases in which the complication of reaction is added.

4.2.1 Opposed Jet Combustor (COLD Experiments)

Two COLD, non-reacting opposed jet combustor experiments were conducted under the present program. One was conducted in the Laboratory Combustor Facility (LCF) and the second in the Hydrodynamic Facility (HDF).

LCF Tests

The opposed jet module, depicted in Figure 1a, was operated in a nonreacting (isothermal) mode wherein the main stream flow was air and the jet stream flow was carbon monoxide. The baseline main stream and jet stream velocities were 15.24 m/sec (50 ft/sec) and 140 m/sec (460 ft/sec) respectively. The Reynolds and Mach numbers of the main flow were 50,000 and 0.05 respectively, and 11,000 and 0.4 respectively for the jet flow. Reynolds numbers were sufficiently high to insure turbulent flow in both the pipe and jet, and both flow sources had entrance lengths sufficient to provide fully developed pipe flow conditions. Mach numbers were sufficiently low to avoid compressibility effects. This operating condition produced a recirculation zone which extended approximately 4 cm (0.78 combustor diameters) upstream of the jet exit plane. A second operating condition was established in which the velocity of the main stream was reduced by 50 percent to 7.62 m/sec (25 ft/sec). This operating condition resulted in a substantially larger upstream extension of the recirculation zone (6.3 cm, or 1.2 combustion diameters).

The objective of the experimental measurements was to provide a basis for judgment of modeling results as well as to assist in the specification of the flow inlet boundary conditions. The key diagnostics included:

(1) a <u>laser anemometer</u> for the measurement of instantaneous velocity and the subsequent determination of time-averaged velocity and turbulence intensity,

(2) a <u>pitot probe</u> for the measurement of mean velocity to provide a check for and extend the laser anemometer measurements, and

(3) a <u>nondispersive infrared analyzer</u> and extractive probe sampling system for the measurement of the diffusion of the tracer (carbon monoxide) throughout the flowfield.

The specific data developed were axial velocity profiles at ten stations within the combustor, contours of constant turbulence intensity, and contours of constant mass concentration of the carbon monoxide tracer species.

Two sets of experimental data were obtained: (1) momentum transport measurements using laser anemometry and pitot probe techniques, and (2) mass transport measurements defining the diffusion of the CO tracer species using probe sampling and nondispersive infrared detector measurements.

Laser anemometer measurements were restricted to that region forward of the jet exit plane because of the interference of the jet body with the laser beams. The key results of the laser anemometer measurements obtained were:

(1) definition of the combustor inlet velocity and turbulence intensity profiles,

(2) definition of the flow development in the main combustor tube, and

(3) definition of the velocity and turbulence intensity in the region surrounding and in the outer portion of the recirculation zone.

Figure 9a shows the inlet velocity profile at the combustor inlet for the baseline 15.24 m/sec main flow test condition. Shown are two full diameter profiles folded about the axis of symmetry to display both profile symmetry and repeatability.

37

a) Inlet Velocity Profiles

MEASUREMENT STATION 18cm
UPSTREAM OF JET EXIT

O PROFILE 1   LASER SIDE
◊ PROFILE 1   PHOTODETECTOR SIDE
△ PROFILE 2   LASER SIDE
▽ PROFILE 2   PHOTODETECTOR SIDE
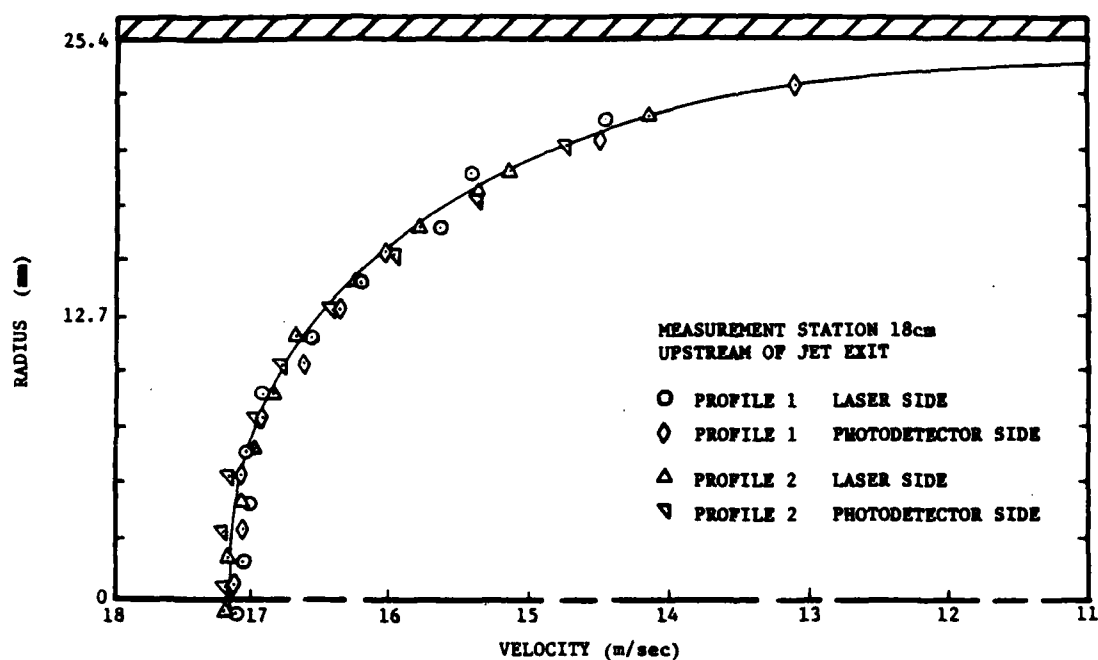
b) CO Tracer Concentration Profiles
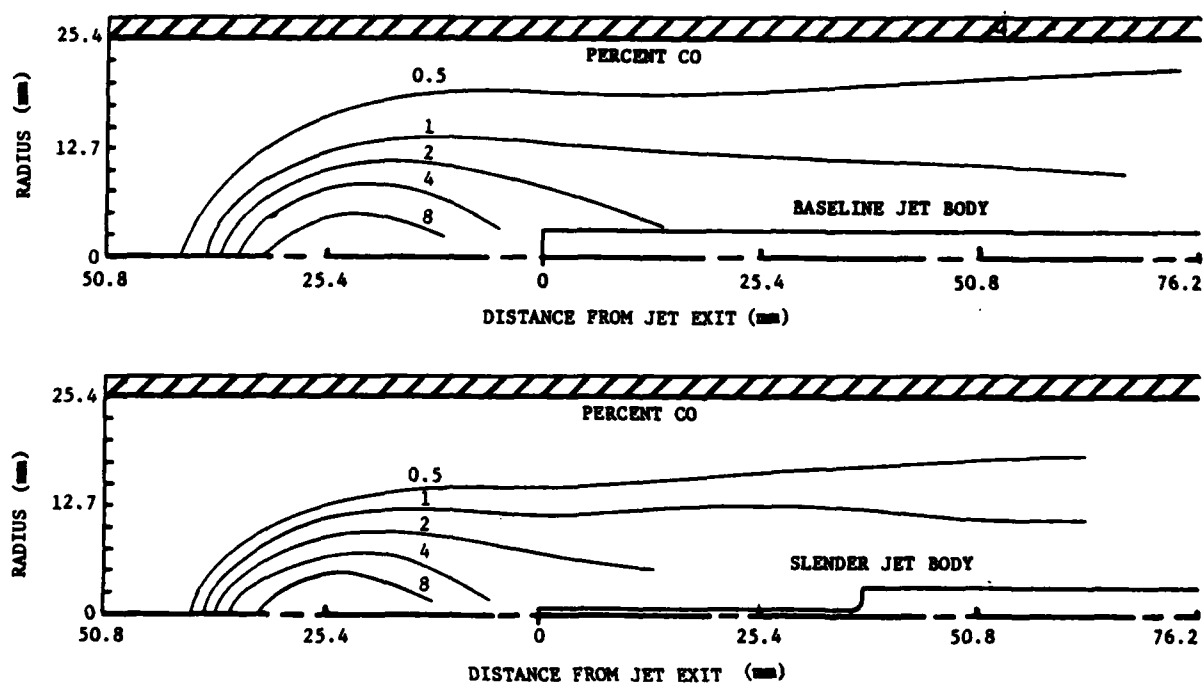
Figure 9. Opposed Jet Combustor COLD Flowfield Data
(15.24 m/s)

Mass diffusion was measured within the recirculation zone and the wake. Proper design of sample probe configurations allowed mapping those regions of the flowfield where the concentration ranged from 0.5 to 8 percent (Figure 9b). Numerical results were obtained for the (1) velocity components (u and v), (2) turbulence kinetic energy (k), (3) turbulence kinetic energy dissipation rate (ε) , (4) effective viscosity (μ_{eff}), and (5) tracer species (carbon monoxide) concentration (CO).

The sensitivity of the numerical solution to various features of the analytical models (e.g. transport models, model parameters, and boundary conditions) were investigated. Specifically, the following model requirements were addressed:

Case	Subject
(1)	turbulence model specification,
(2)	density of the numerical grid
(3)	turbulence kinetic energy dissipation rate on jet body face,
(4)	inlet turbulence kinetic energy for the main and jet flows,
(5)	inlet turbulence energy dissipation rate for the main and jet flows,
(6)	inlet velocity profiles for the main and jet flows,
(7)	variations in main and jet flow rates, and
(8)	turbulence model parameters (C_1, C_2, C_μ, C_D).

Velocity and species concentration predictions could be <u>directly</u> compared to the experimental measurements. As a result, these comparisons were used as the primary means of evaluation of the analytical results. The findings are summarized in Table I and discussed below by case.

Case 1. The algebraic viscosity model did not exhibit the capability to adequately predict the complex flowfield of the combustor (Figure 10). The resultant constant turbulent viscosity could not simultaneously produce the trends observed experimentally of jet penetration and mass diffusion in the wake. Solutions using this model, however, were valuable in pointing out the magnitude of the turbulent viscosity needed to produce the diffusion of momentum and mass observed experimentally and facilitating a first solution with a minimum of independent variables.

The two-equation k-ε model did produce a distribution of turbulence within the flowfield, and displayed the potential to more satisfactorily predict the combustor flowfield. However, certain deficiencies were apparent in the ability of the model to predict experimental trends. For example:

(1) The velocity profiles (Figure 10a) show that the predicted momentum exchange between the main stream and the recirculation zone is insufficient. (This result is evident from inspection of the velocity profile at the station $X/R_0 = 1.0$).

(2) The predicted velocity profiles adjacent to the outer wall of the jet display a momentum deficit.

(3) The predicted concentration gradients (Figure 10b) in the vicinity of the stagnation region are significantly steeper than those measured.

(4) The predicted radial diffusion of mass in both the recirculation zone and the wake was limited.

TABLE I

- Summary of Opposed Jet COLD Modeling Study -

Case	Sensitivity Investigated		Results
1.	Turbulence model	algebraic model	μ = constant, could not simultaneously match penetration and radial diffusion of jet
		k-ϵ model	limited radial diffusion of momentum and mass, high concentration gradients predicted
2.	Numerical grid	18x31 grid	4 horizontal gridlines in jet, 9 vertical gridlines in recirculation zone, provided a realistic solution
		25x49 grid	14 horizontal gridlines in jet, 22 vertical gridlines in recirculation zone, provided improved solution
3.	Recirculation zone wall boundary conditions	0.1 ϵ_w(nom)-- 1.0 ϵ_w(nom)	high sensitivity, solution develops unrealistic character for specification of off nominal condition
4.	Inlet turbulence kinetic energy	k(nom) = .0054 $\bar{U}^2$ 1.0k(nom)--6.0k(nom)	no significant sensitivity noted
5.	Inlet turbulence kinetic energy dissipation rate	$\epsilon = k^{3/2}/\ell$ ℓ(nom) = 0.10R .05ℓ(nom)--1.0ℓ(nom)	no significant sensitivity noted
6.	Inlet velocity profiles	square	realistic solution
		turbulent pipe profiles	no significant change
7.	Main and jet flow rate variations	0.9$\bar{U}_j$(nom) and 1.1$\bar{U}_m$(nom)	no significant change
		0.5$\bar{U}_m$ (nom)-- 1.0$\bar{U}_m$ (nom)	significant increase in extent of recirculation zone as main stream velocity decreased
8.	Turbulence model parameters	1.0C (nom)-- a. 0.5 C_1(nom) b. 1.5 C_2(nom) c. 0.5 C_D(nom d. 1.5 C_μ(nom)	jet penetration decreased, radial diffusion increased, and stagnation zone gradients decrease for all cases
		f. 0.875 C_1(nom)	most improved solution

a) Momentum Transport

U/Ū₀   • MEASURED VALUE   → PREDICTED VALUE

18 X 31 GRID, ALGEBRAIC TURBULENCE MODEL, SQUARE INLET VELOCITY PROFILES

18 X 31 GRID, 2-EQUATION TURBULENCE MODEL, SQUARE INLET VELOCITY PROFILES

AXIAL STATION X/R₀

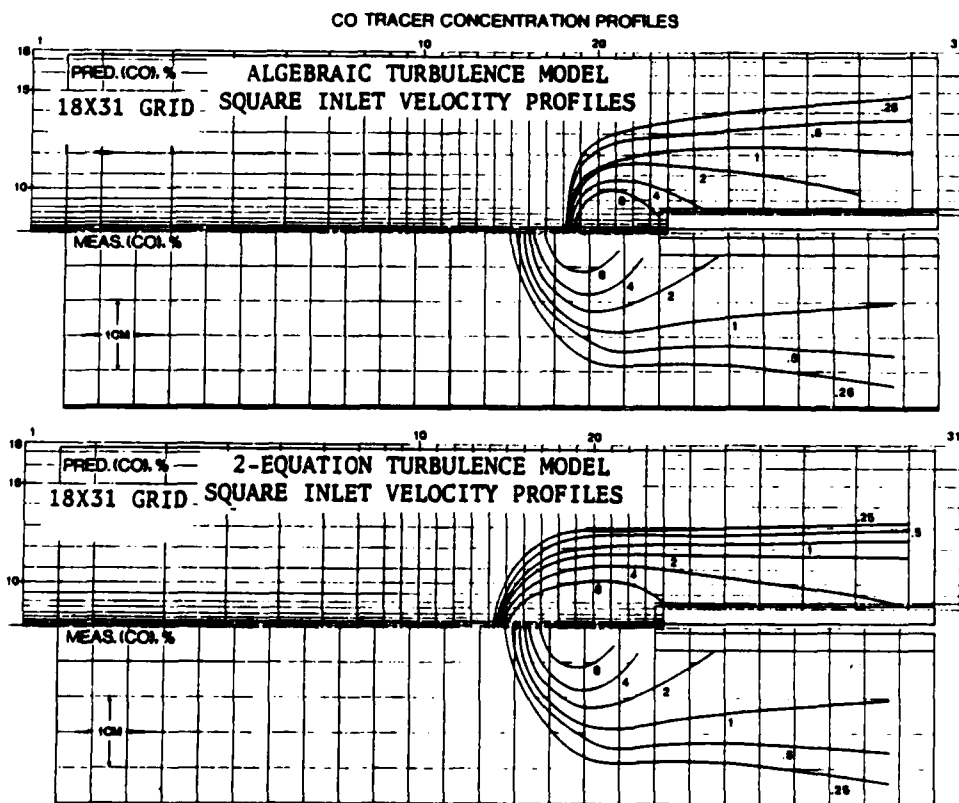## b) Mass Transport

CO TRACER CONCENTRATION PROFILES
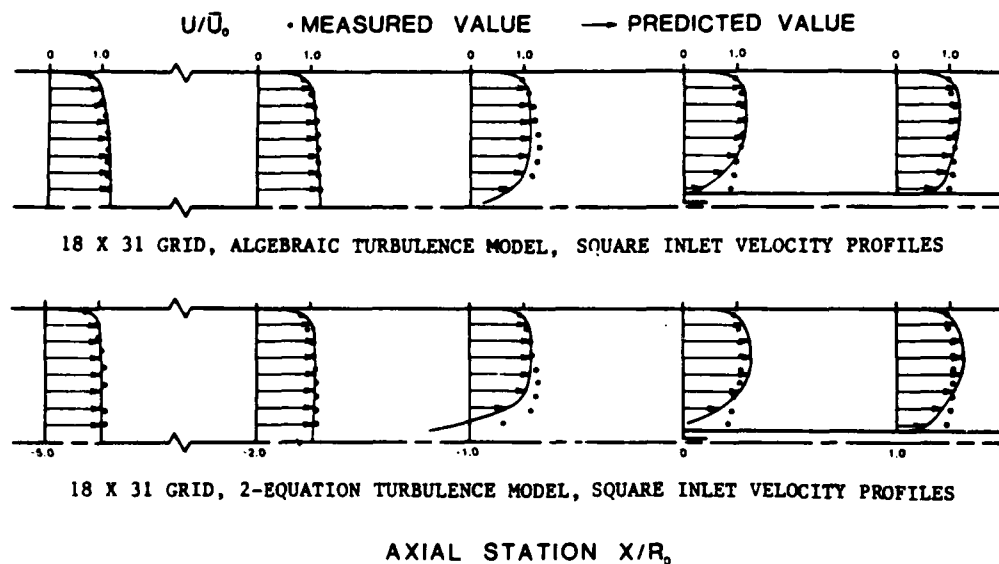
Figure 10. Opposed Jet COLD Combustor Flowfield Data:
Sensitivity to Turbulence Model
(15.24 m/s)

42

These results indicate that the magnitude of the predicted turbulent viscosities is underestricted and that the spatial distribution of viscosity is not adequately predicted.

Case 2. Refinement of the computational grid to provide greater detail within the jet, near the jet exit, and within the recirculation zone resulted in a significant change in the character of the resultant solution. The changes reflect an improved match of the predicted and experimental results (Figure 11), and result from the reduction of numerical error in the application of the finite difference procedure.

Case 3. Previous studies have noted that in confined flows, where the recirculation zone may contact solid boundaries, the specification of near-wall turbulence energy dissipation rate may significantly influence the mixing characteristics (Peck and Samuelsen, 1977). This proposal was tested in the present investigation both experimentally and numerically by reducing the outer diameter of the jet tube from 6.4 to 1.6 mm.

Experimentally measured profiles of turbulence intensity mass show less turbulence and less mass mixing for the case where the small outside diameter jet was used. The differences, however, are quite small and do not support the proposal that the presence of the jet body face in the vicinity of the recirculation zone has a large influence on the structure of the resultant flowfield.

In contrast, the predictions were found to be quite sensitive to the specification of the energy dissipation rate on the upstream facing step of the jet tube. The use of other than the nominal value of the energy dissipation rate on solid boundaries does not appear justified and may in fact mask fundamental shortcomings of the model.

Case 4 and 5. The predictions were found to be not sensitive to the

43

a) __Momentum Transport__

18 X 31 GRID, 2-EQUATION TURBULENCE MODEL, SQUARE INLET VELOCITY PROFILES

25 X 49 GRID, 2-EQUATION TURBULENCE MODEL, SQUARE INLET VELOCITY PROFILES

AXIAL STATION X/R_0
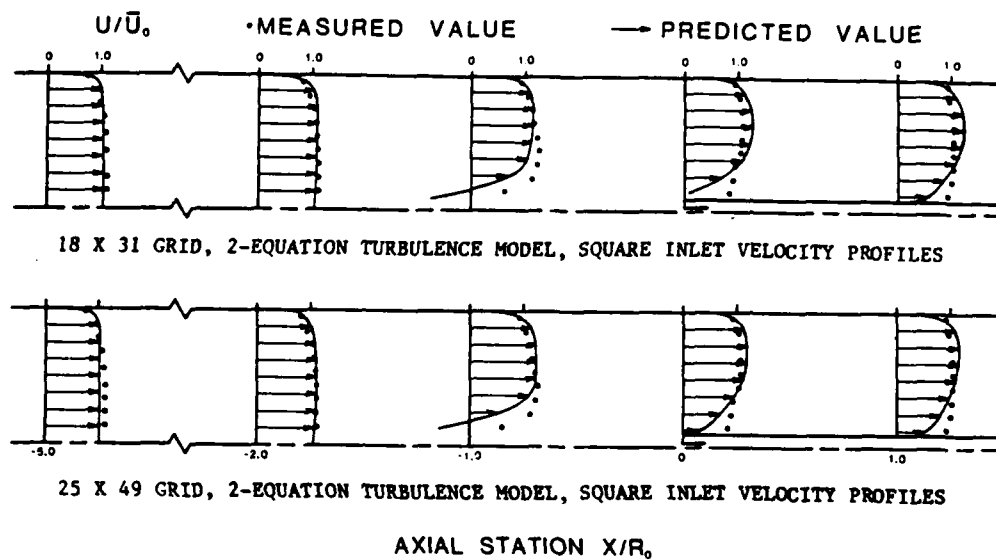
b) __Mass Transport__

Figure 11.   Opposed Jet Combustor COLD Flowfield Data:
Sensitivity to Numerical Grid
(15.24 m/s)

specification of inlet turbulence kinetic energy and inlet turbulence energy dissipation rate. Comparable magnitudes of turbulence intensity were developed in the zone of primary activity (i.e. recirculation zone) for a sizeable range o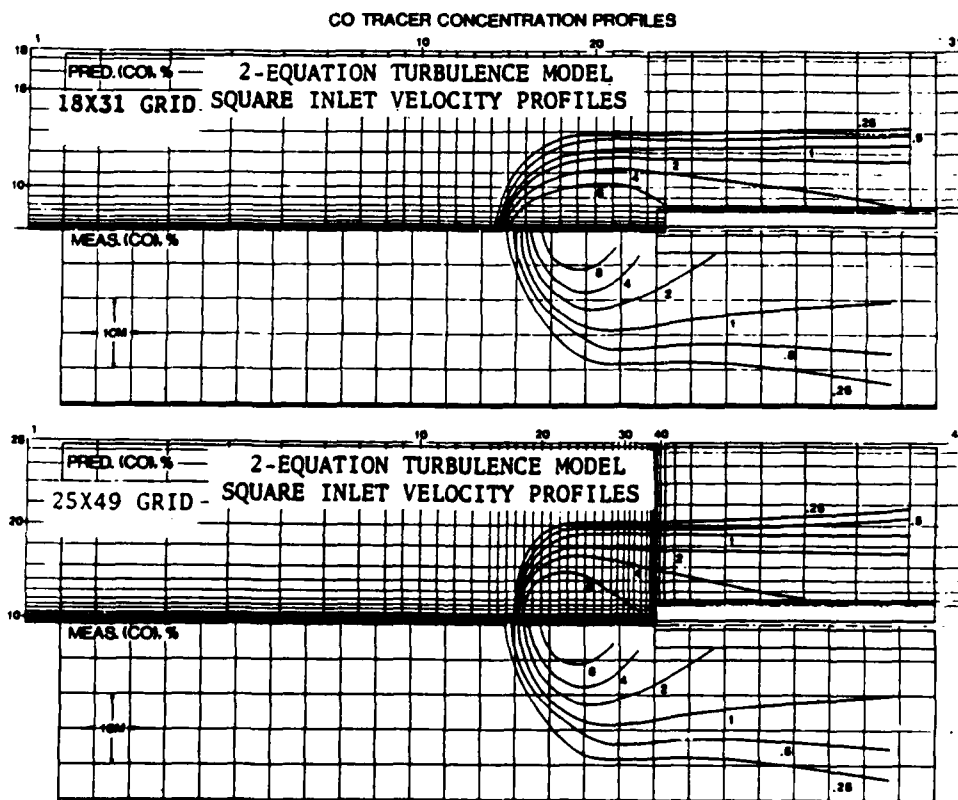f values for both parameters. The reason for the insensitivity observed is attributed to the separation of the recirculation zone from the flow entrance planes in terms of pipe diameters and/or jet diameters. As a result, the viscosity model dominates the flowfield development rather than the flow inlet boundary conditions. Were the recirculation zone located in close proximity to the flow inlets, the solution would be expected to be sensitive to the inlet flow boundary conditions.

Case 6. To add to the realism of the boundary condition specification, velocity profiles were input for both the main and jet flow inlets. The measured velocity profile (Figure 9a) was input for the main flow and a one-seventh power law turbulent pipe flow was input for the jet flow. No significant change in the resultant solution occurred as a result of this refinement. The reason for the insensitivity to this refinement is identical to that given for the insensitivity to inlet k and ε specification. That is, the primary zone of activity (i.e., the recirculation zone) is sufficiently removed from the flow entrance prolanes in terms of pipe diameters and/or jet diameters. Were this not the case, the solution would be expected to be sensitive to the specification of the inlet momentum distribution.

Case 7. The sensitivity of the flowfield to both small and large changes in input flow momentum was investigated. Small changes in input flow momentum were first investigated to examine the potential influence of experimental flow rate errors on the resultant solution. Insignificant change in the solution was observed for a simultaneous +10 percent change in the main flow rate and -10 percent change in the jet flow rate. These perturbations
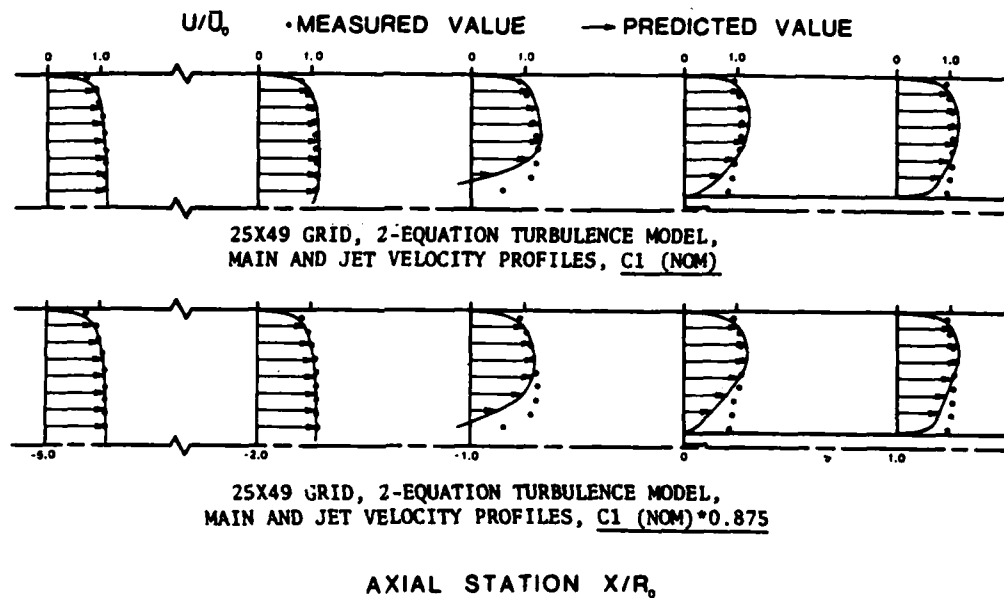
45

significantly exceed any errors present in the experimental procedure and show

an insensitivity of the experimental results to potential flow rate errors.

A significant change in the flowfield character resulted when the

main flow velocity was reduced to 50 percent from 15.24 m/sec to 7.62 m/sec.

The axial extent of the recirculation zone approximately doubled as a result

of the perturbation. The same general disagreement between prediction and

experiment was noted for the 7.62 m/sec flow as for the 15.24 m/sec flow.

Specifically, the extent of the radial diffusion of momentum and mass was less

for the prediction and concentration gradients in the vicinity of the

stagnation point were steeper. These results demonstrate that the disparities

between experiment and prediction were consistent for a wide range of flow

conditions.

Case 8. The predictions developed thus far all indicate common

points of disagreement with the experimental data. The predictions for both

the diffusion of momentum and the diffusion of mass point to an

underestimation of the turbulent viscosity within the recirculation zone.

This is indicated by the greater predicted axial momentum of the flow in that

portion of the recirculation zone where velocities are small and by the

limiting of the radial diffusion of mass within this same region.

The key to improved solutions appears to lie in an increase in

turbulence within the recirculation zone. It has been pointed out that the

turbulence model itself can be tuned to accomplish such effects (Launder and

Morse, 1977). In the present study, the sensitivity of the resultant solution

to pertubations of various coefficients of the viscosity model was examined

(Table I). It was found that significant improvements in the solution

resulted from decreasing the coefficient of the source term in the energy

dissipation equation (Figure 12). The result, less turbulence energy

a) Momentum Transport

25X49 GRID, 2-EQUATION TURBULENCE MODEL,
MAIN AND JET VELOCITY PROFILES, C1 (NOM)

25X49 GRID, 2-EQUATION TURBULENCE MODEL,
MAIN AND JET VELOCITY PROFILES, C1 (NOM)*0.875
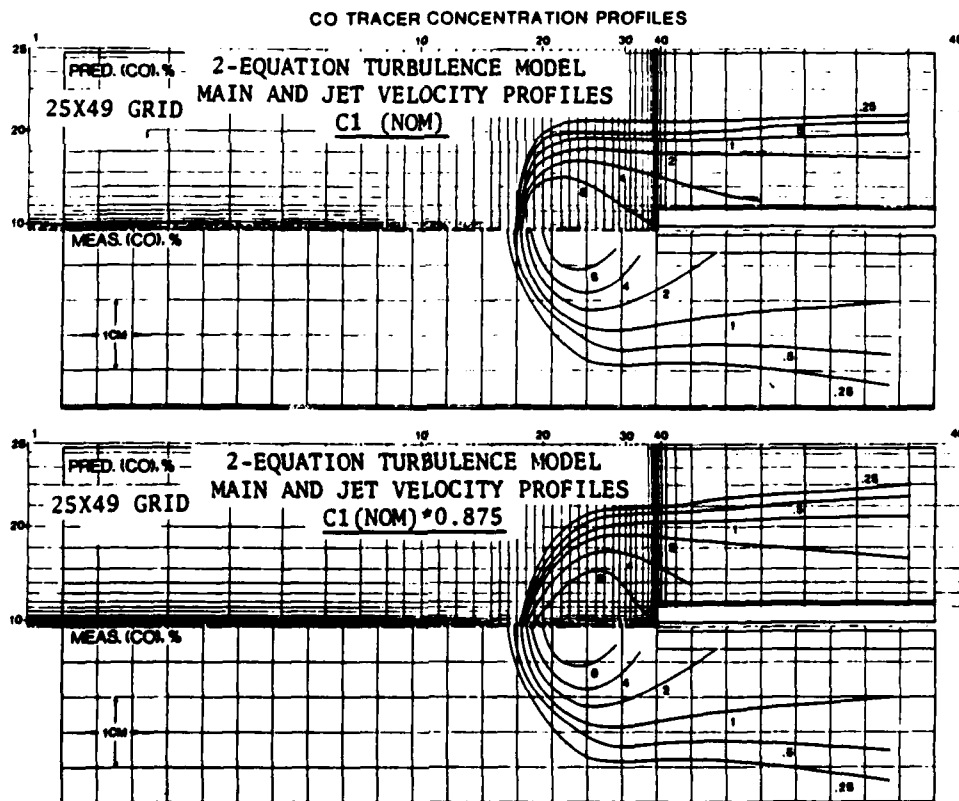
AXIAL STATION X/R_0

b) Mass Transport

Figure 12. Opposed Jet Combustor COLD Flowfield Data:
Sensitivity of Source Term Coefficient in Dissipation
Rate Equation (15.24 m/s)

dissipation, produced greater turbulence levels and the enhanced mixing of mass and momentum throughout the entire flowfield.

Summary. A turbulence model which accounts for the spatial generation of and dissipation of turbulence is essential to obtaining a realistic solution. The two-equation k-ϵ model shows limited promise in describing the complex flow adopted for the present investigation. The major shortcoming identified for the case of nonreacting (COLD) flow is in the underprediction of turbulent viscosity within the recirculation zone and the wake. Detailed information is available in a Ph.D. Dissertation (Wuerer, 1978). One paper was presented on this work (Wuerer and Samuelsen, 1979), and the information is being incorporated into a manuscript planned for submission to Experiments in Fluids (Samuelsen, et al, 1984).

HDF Tests

The results of the OJC tests in the LCF described above and those described below in Section 4.2.2 made it clear that (1) a substantial advance is necessary in turbulence modeling for accurate predictions of complex flows, and (2) a need exists for spatially-resolved measurements in complex flows for conditions ranging in complexity from non-reacting (COLD and HEATED) to reacting (HOT). Such data were required to provide the foundation upon which numerical modeling can be developed and tested, and to provide the insight into the physical and chemical processes of transport and reaction as a guide to both the evolution of modeling and the understanding of these type of flows.

A second vehicle selected, in addition to the LCF, for acquisition of these data was the Hydrodynamic Facility (HDF). Data were obatined with the opposed jet configuration in the Hydrodynamic Facility (HDF) for two reasons. First, such data provide a data base amenable to isothermal

modeling. Second, water flows are more amenable than gaseous flows to flow visualization, the latter of which can be used as a check of the experimental data as well as to provide insight into both the mixing and dynamics of the flowfield.

The opposed jet flowfield was investigated in the HDF for nominal approach velocities of 0.32 m/s and 0.64 m/s at a constant jet velocity of 5.8 m/s. As shown in Table II, these velocities were selected to yield the identical Reynolds numbers of both the mainstream and jet examined in the LCF. The variation in mainstream approach vellcity provides a means of examining recirculation zone strength and also demonstrates the influence on experimental and analytical trends of large changes in differential flowrate between the main and jet streams.

Representative experimental and predicted profiles of the axial component of mean velocity are presented in Figure 13 for both mainstream flowrates. Figure 13a presents centerline velocity profiles, while Figure 13b provides a radial profile at an axial location in the recirculation zone near the stagnation point.

The trends exhibited in the analytically determined mean velocity profiles using a 18 x 31 grid and plug velocity profile in the jet agree qualitatively with those established experimentally. The axial penetration of the opposing jet as determined numerically, however, extends farther upstream than indicated experimentally; this effect is observed for both the low Reynolds number (0.32 m/s average velocity) and the high Reynolds number (0.64 m/s average velocity) mainflow cases. The jet expansion also is overestimated by the analytical model in both cases.

TABLE II

- HDF Test Conditions -

MAINSTREAM				JETSTREAM			
HDF Velocity (m/s)	HDF Flowrate (ℓ/m)	OJC Velocity (m/s)	Re	HDF Velocity (m/s)	HDF Flowrate (gpm)	OJC Velocity (m/s)	Re
0.32	87	7.5	25,000	5.8	0.28	135	11,500
0.64	174	15	50,000	5.8	0.28	136	11,500

a) Centerline Mean Velocity Profiles
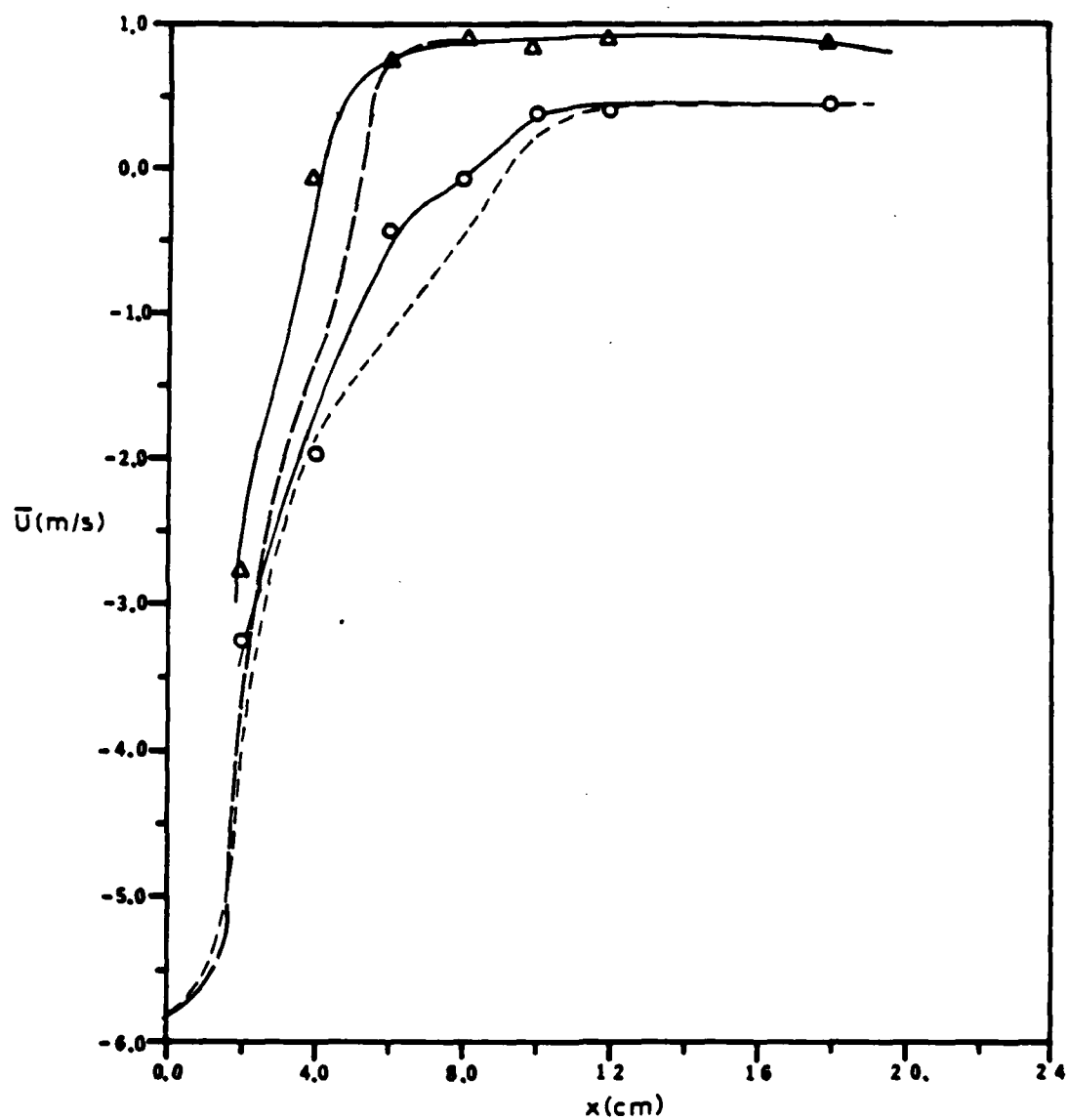
Figure 13.   Opposed Jet Combustor COLD (HDF) Flowfield Data
             (0.32 m/s   0.64 m/s)
             o——o——o Experiment ——△——△——△)
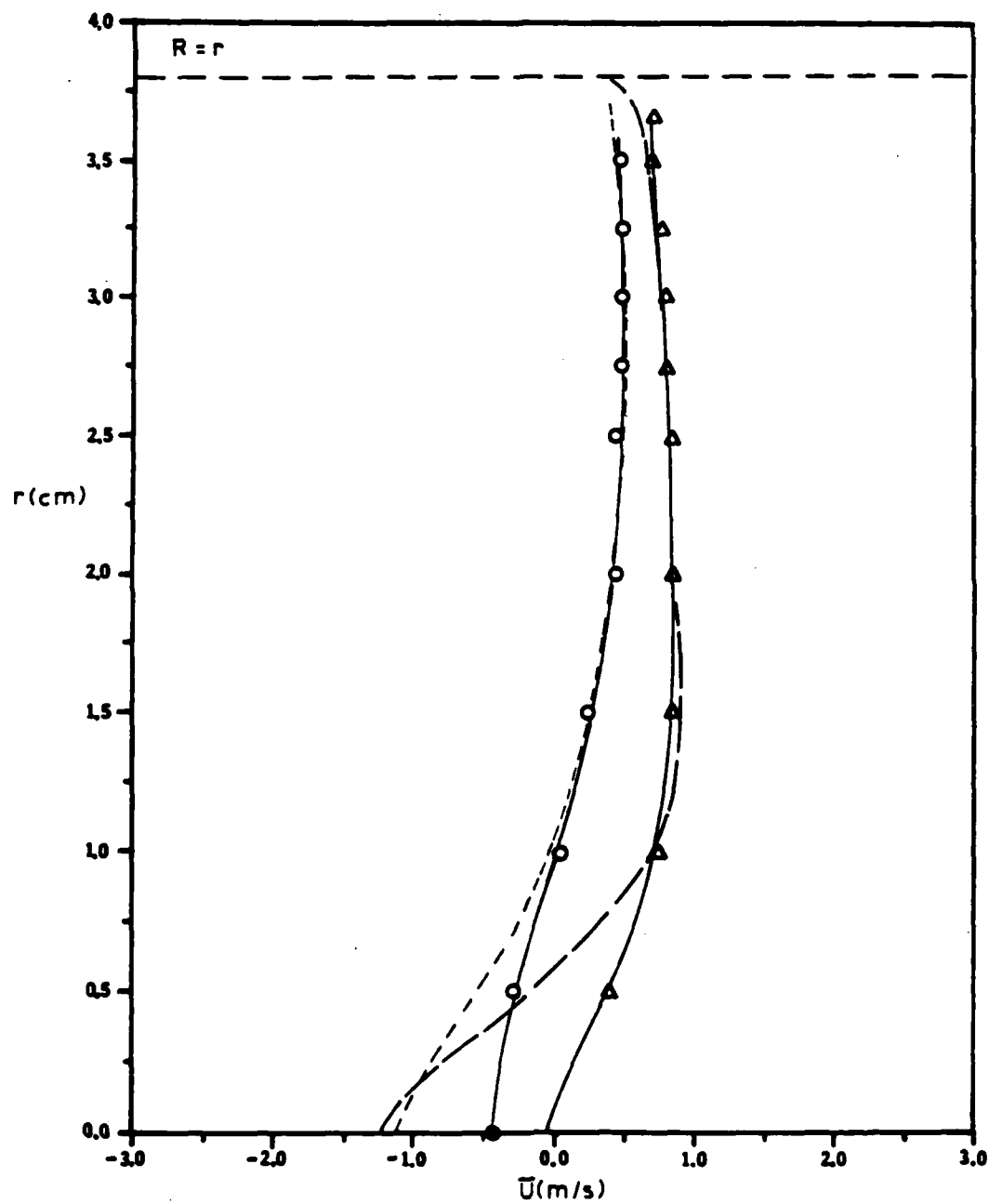   ————————————Prediction————————————

51

Figure 13. (continued)

c) Flow Visualization

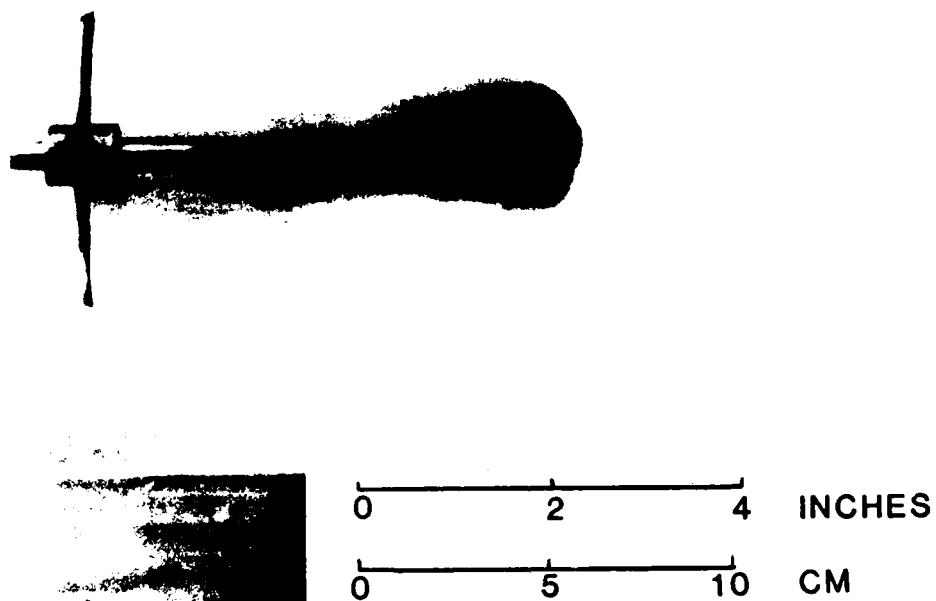| 0	2	4	INCHES
0	5	10	CM

Figure 13. (concluded)

53

The experimentally determined jet penetration distance is 8.4 cm (1.1 pipe diameters) for the 0.32 m/s mainstream approach velocity; in contrast, the numerical code predicts a stagnation point at 9.2 cm (1.2 pipe diameters). LA measurements for the high Reynolds number case indicate a jet penetration of 4.2 cm (0.55 pipe diameters) in the axial direction; this result compares with a numerically predicted value of 5.4 cm (0.71 pipe diameters). In Table III, these data are compared to those obtained in the LCF. The overestimate of jet effects in the HDF is consistent with those observed in the LCF for a course numerical grid and plug velocity profile in the jet.

Finally, flow visualization (Figure 13c) using a dye in the jet serves as a check of the LA data and graphically illustrates the jet penetration and size of the recirculation zone.

Additional details are provided in a M.S. Thesis (Acroumanis, 1980) and a M.S. Project Report (Grudovich, 1983).

4.2.2 Opposed Jet Combustor (HEATED Experiments)

In the work described above, tests for the description of mass and momentum transport were conducted in the absence of reaction and heat release. Heat transport was assessed by heating the jet in the LCF and comparing predicted values of mean and rms temperature with experimentally measured values. The opposed jet was operated for this study at rounded values of the mainstream velocity, 7.50 and 15.0 m/s, instead of the 7.62 and 15.24 m/s reference velocities used above.

The temperature signals were obtained by means of 0.125 mm diameter glass coated thermistors and a 1.25 μm diameter resistance ("cold wire") thermometer. The cold wires were platinum and 0.48 mm in length for $U_{m,i}$ = 7.5 m/s, and platinum-10 percent rhodium and 0.66 mm in length for $U_{m,i}$ =

TABLE III

- Location of OJC Stagnation Point -

FACILITY	TECHNIQUE	NUMBER of pipe diameters from jet exit	
		Re = 25,000	Re = 50,000
HDF	LA	1.1	0.55
	Prediction	1.2	0.71
	Flow Visualization	0.92	0.66
LCF	LA	1.2	0.60
	Prediction	1.3	0.70

15.0 m/s. The cold wires were operated with a root mean square current of 255 microampers.

The radial profiles of θ/θ_{max} and T'/θ_{max} at x/d = 2.56 for the 7.5 m/s flow are shown in Figure 14a where θ is the time-mean temperature difference $(T - T_1)$ between the local and inlet temperature. (Because of interference between the probe and jet body, measured values were not obtained at radial locations of r/R less than 0.15.) The predictions depict a peak at r/R of 0.1 in the T'/θ_{max} distribution; this is associated with the steep gradient in θ/θ_{max} at that radial location. In the outer region, the predictions are in fair agreement with measurements.
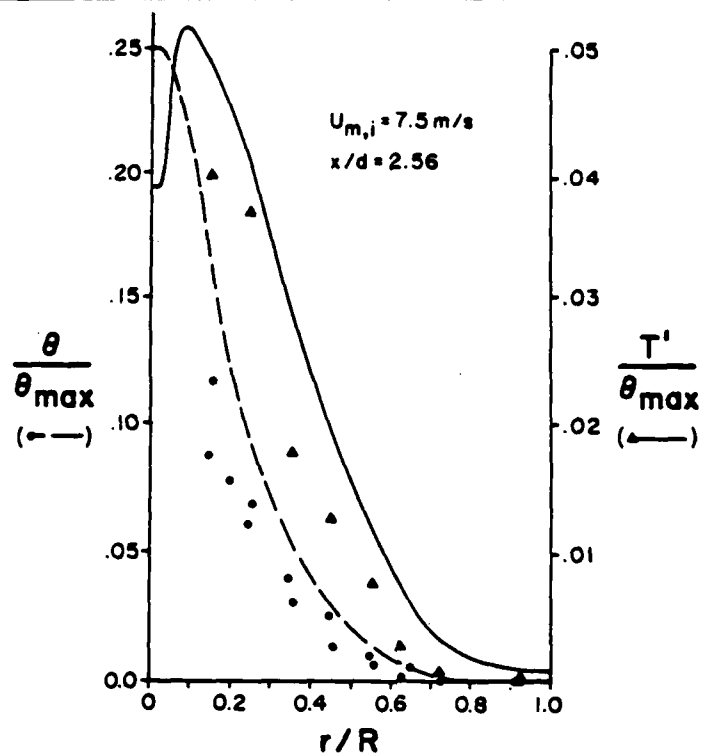
Figure 14b shows the radial profiles of θ/θ_{max} and $T'\theta_{max}$ at four axial locations for the 15 m/s flow. The axial and radial thermal extent of the heated jet is shown on both figures. It is interesting to note that, as expected, the radial extent of the temperature fluctuations is larger than that of the mean temperature at all the four stations.

The mean temperature is well predicted at stations farther from the jet exit and overpredicted near it. This may be attributed to overpredicted turbulent diffusion coefficients which could be due to underpredicted values of the rate of dissipation of kinetic energy, ε , or due to the use of constant σ_H.

At the station x/d = 2.95, the predicted θ/θ_{max} is in excellent agreement with the experimental data. However, at the same station, the temperature fluctuations are underpredicted.

It should be mentioned here that the transport equation for the mean square fluctuation of a scalar quantity (LaRue, Deaton, and Gibson, 1975) has been validated for turbulent free jets (Lockwood and Naguib, 1975) and for

56

a) Radial Profiles of Mean and RMS Temperature (7.5 m/s)

$U_{m,i} = 7.5 \, m/s$

$x/d = 2.56$

$\dfrac{\theta}{\theta_{max}}$ (-- --)

$\dfrac{T'}{\theta_{max}}$ (——)

b) Radial Profiles of Mean and RMS Temperature (15 m/s)

Experimental	Predictions	x/d
●	———	3.35
△	— —	3.15
■	—·—·	2.95
◇	—··—··	2.75

$U_{m,i} = 15 \, m/s$

$\dfrac{\theta}{\theta_{max}}$
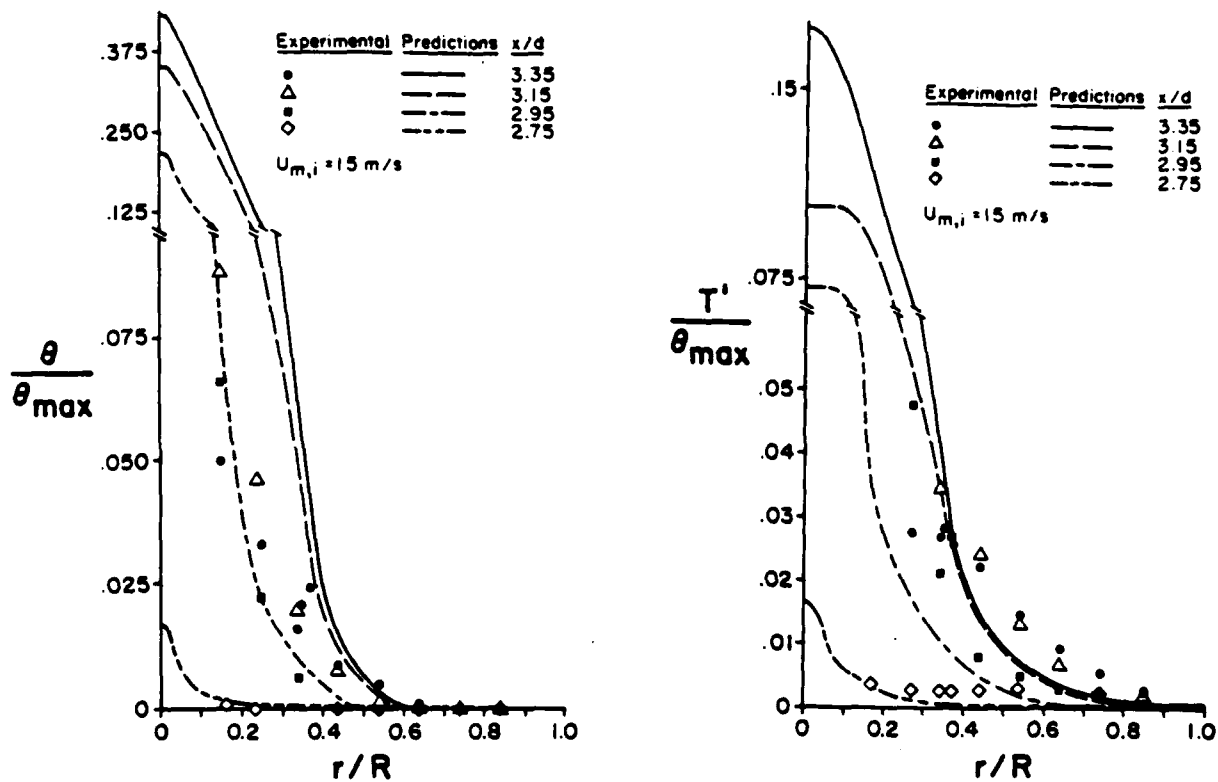
$\dfrac{T'}{\theta_{max}}$

Figure 14. Opposed Jet Combustor HEATED Flowfield Data

confined turbulent recirculating flows (Elghobashi, Pun, and Spalding, 1977). The same equation (with both the values of C_{T2} of 2.0 and 1.4) did not accurately predict the measured values of rms temperature fluctuations under the experimental conditions of this study. This stresses the need to solve a transport equation for the dissipation of the temperature fluctuation. These data also reinforce the need for a closer examination of the ε equation and the assumption of the constant turbulent Prandtl and Schmidt numbers. One such example is Hanjalic, Launder, and Schiestel, 1979.

Detailed information of this study is available is publication (Elghobashi, et al, 1981).

4.2.3 Opposed Jet Combustor (HOT Experiment)

The objective of the present study was to provide a general characterization of the chemical and flame structure of the OJC (Figure 1a) for a range of parametric variations of the four primary controlling variables: Main and jet stream equivalence ratios, main and jet stream velocities. Exit plane and detailed flowfield profiles are presented and analyzed for NO_x, carbon monoxide (CO), total hydrocarbons (HC), and temperature. The goals are to provide (1) insight into the performance of a reverse jet, aerodynamic flameholder, (2) guidance for practical applications of aerodynamic flameholding, and (3) a data base for future code testing.

For detailed flowfield maps, radial traverses were taken at twelve axial locations, with the distance between axial locations ranging from 2.54 mm (0.1-inch) in regions of steep gradients (e.g., the nose of the recirculation zone) to up to 24.13 mm (0.95-inch) in regions of near zero gradients (e.g., downstream of the jet tube exit). Radial locations were at 3.05 mm (0.12-inch) increments between the jet tube wall and the chamber wall.

The test conditions are tabulated in Table IV. The following conditions

TABLE IV
- OJC HOT Test Conditions -

U_m(m/s)	U_j(m/s)	ϕ_m	ϕ_j	Parametric variation
7.5	135	1.0	1.0	BASE CASE
7.5	135	1.2	0.8, 1.0, 1.2	
		1.0	0.8, 1.0, 1.2	ϕ_m, ϕ_j
		0.8	0.8, 1.0, 1.2	
		0.6	0.8, 1.0, 1.2, 1.4, 1.6	
7.5	70	1.0	1.0	U_j
15.0	135	1.0	1.0	U_m

represented the BASE CASE:

- Main Stream Reference Velocity $U_m = 7.5$ m/s
- Jet Stream Reference Velocity $U_j = 135$ m/s
- Main Stream Equivalence Ratio $\phi_m = 1.0$
- Jet Stream Equivalence Ratio $\phi_j = 1.0$

Results are presented for the BASE CASE. Second, parametric variations are presented in the order listed in Table IV. Each of the four controlling variables (ϕ_m, ϕ_j, U_j, U_m) were evaluated. Note (Table IV) that the mainstream equivalence ratios (ϕ_m) were biased to fuel lean mixture ratios because of the interest in lean mainstream emission performance. The jet equivalence ratios (ϕ_j) were biased to the fuel rich mixture ratios to extend the lean limit of the main stream mixture. The range of main stream (U_m) and jet velocities (U_j) allowed an examination of the effects of recirculation zone size and stoichiometry on flame structure and pollutant emission.

Finally, emission indexes are presented to summarize the emission behavior of the combustor at the conditions considered, and to provide a practical perspective to the utility of opposed jet flameholding.

Base Case. The detailed flowfield maps and exit plane profiles for the base case are presented in Figure 15a. Two distinct regions can be deduced from the results (Figure 15b). One is the recirculation zone, which is a zone of strong backmixing driven by the jet flow. The other is a radially propagating reaction in the wake of the recirculation zone. For example, the oxidation of hydrocarbons and formation of carbon monoxide (CO) occurs within the recirculation zone where there is intense mixing of reactants with hot products, and along the radially propagating wake reaction

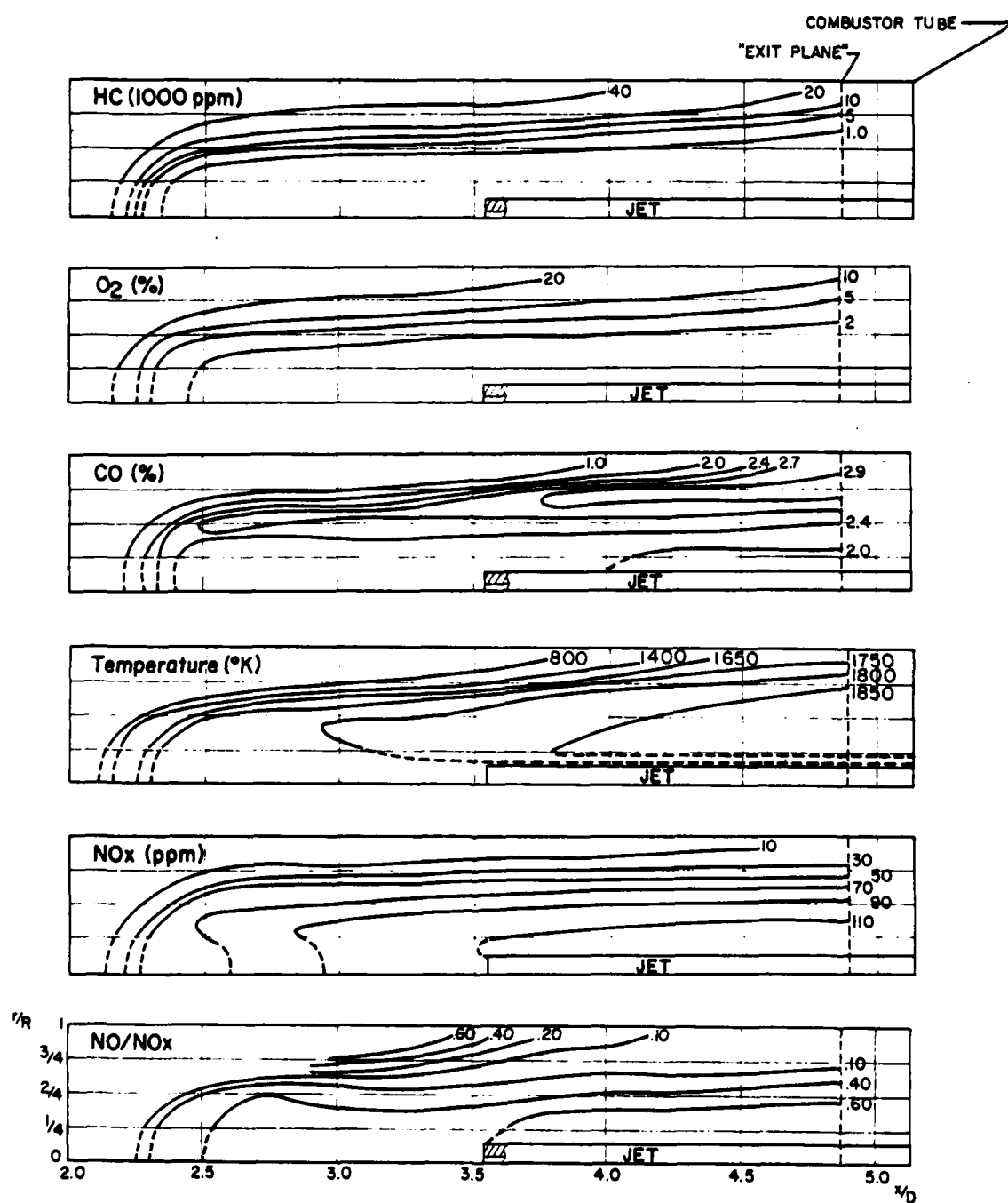a) Base Case (U_m = 7.5 m/s, U_j = 135 m/s, $\phi_m = \phi_j$ = 1.0)
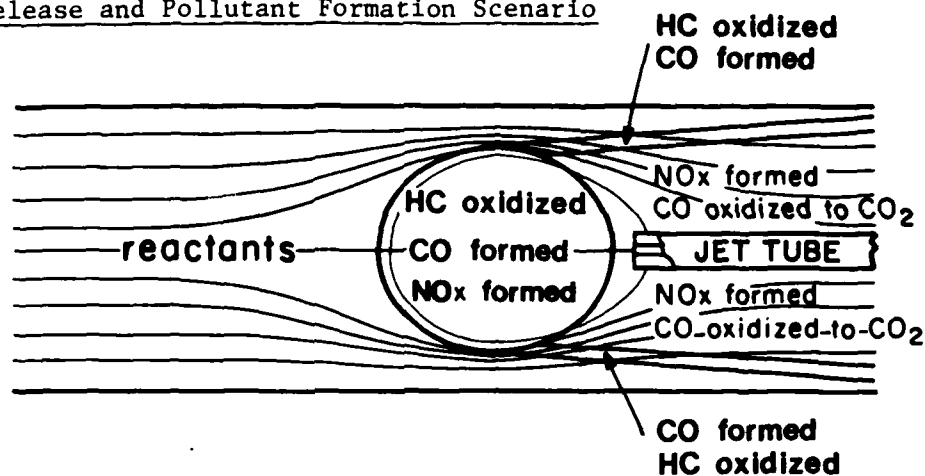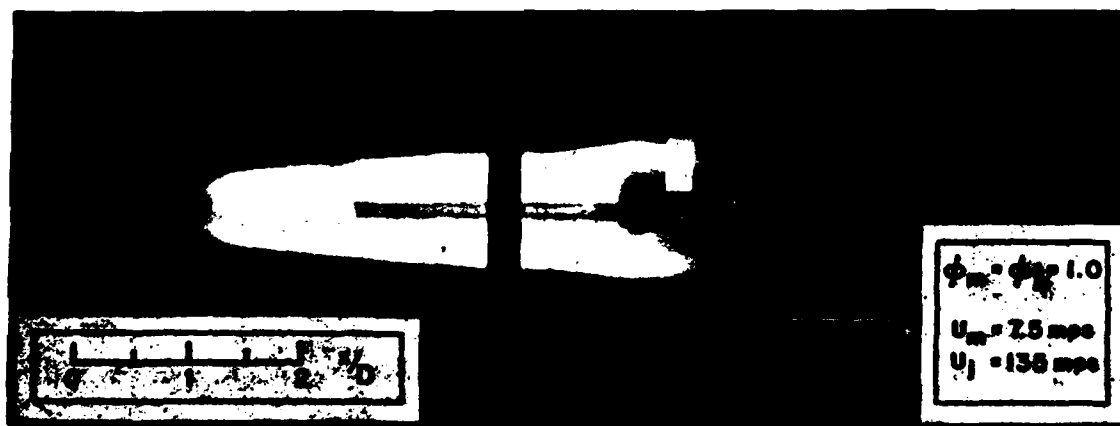

Figure 15. Opposed Jet HOT Flowfield Data

b) **Heat Release and Pollutant Formation Scenario**

c) **Parametric Study: Effect of U_m and U_j (Flame Shape)**

Base case

Elevated mainstream velocity (U_m)
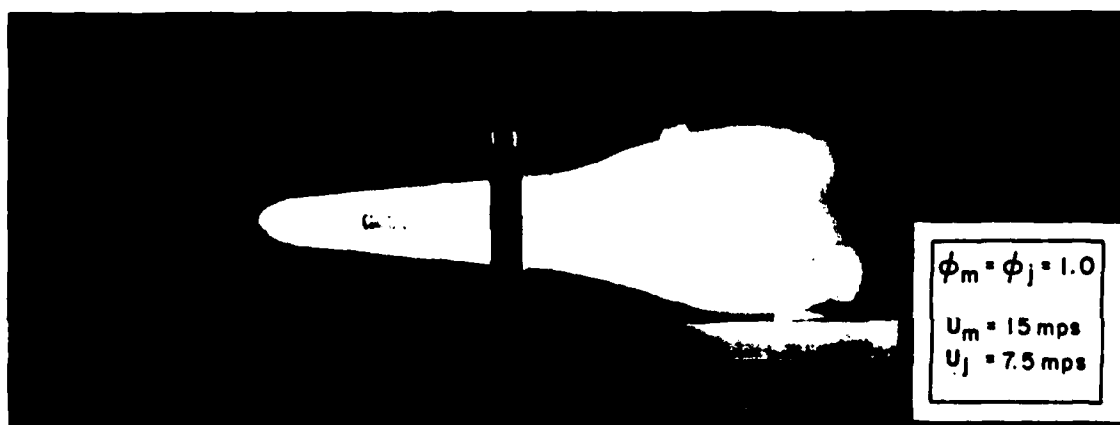
Figure 15. (continued)

d) Parametric Study: Effect of U_m and U_j (T)
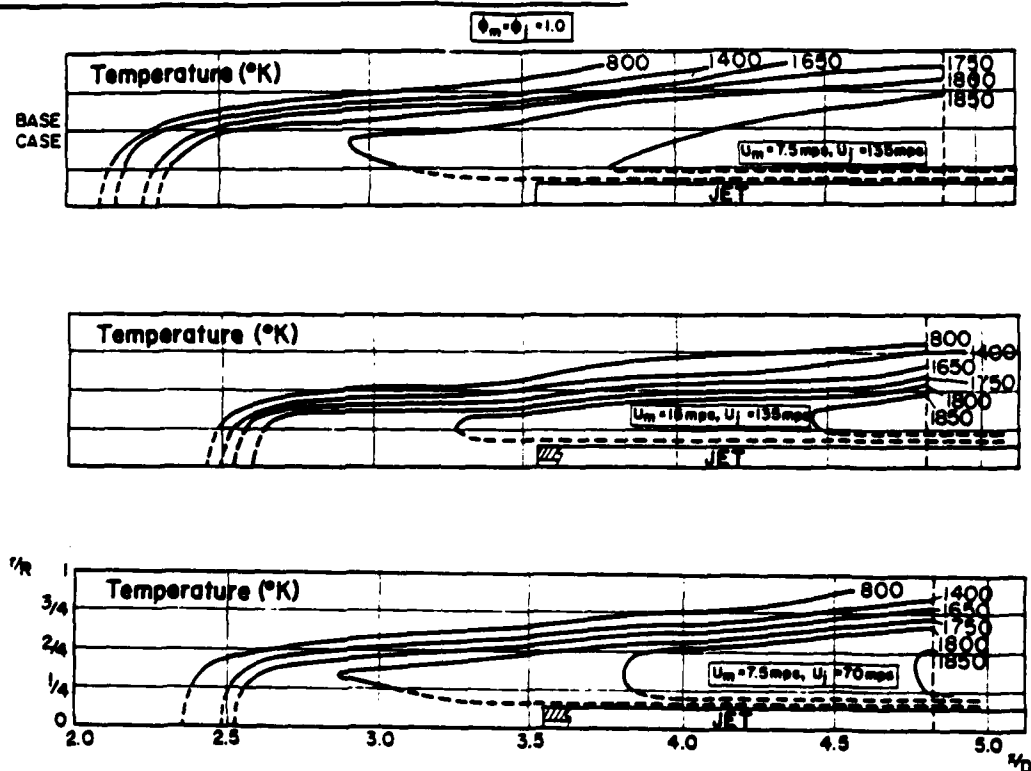
e) Parametric Study: Effect of U_m and U_j (NO_x)

Figure 15. (continued)

f) Parametric Study: Effect of ϕ_m and ϕ_j (HC, CO, T)
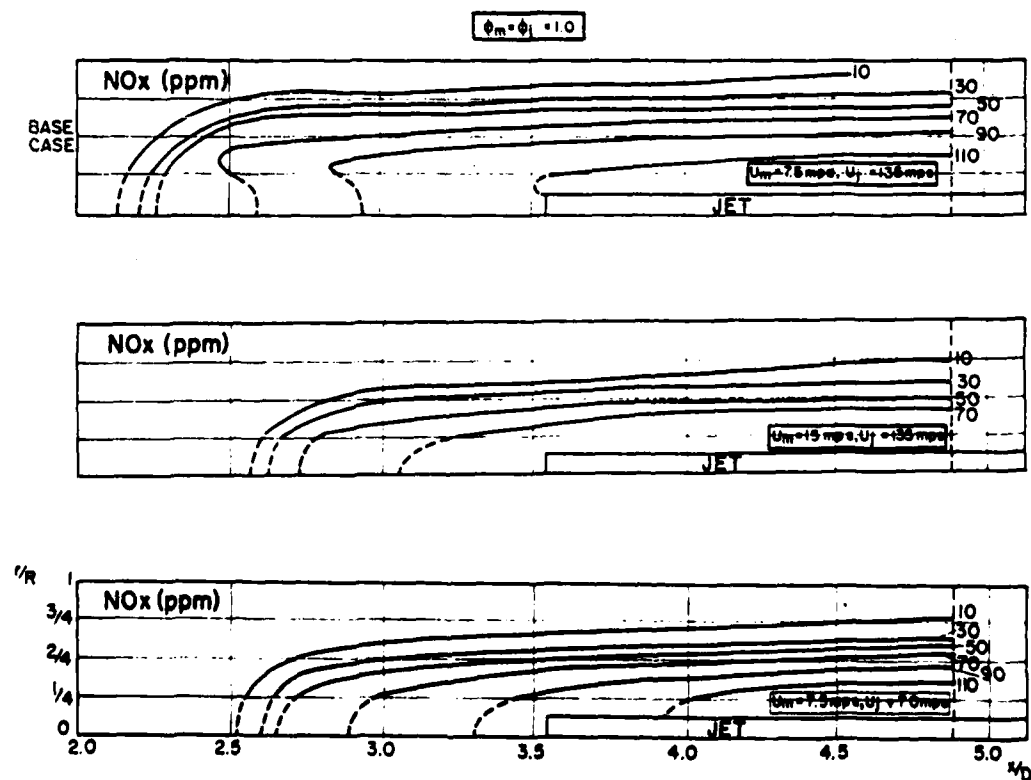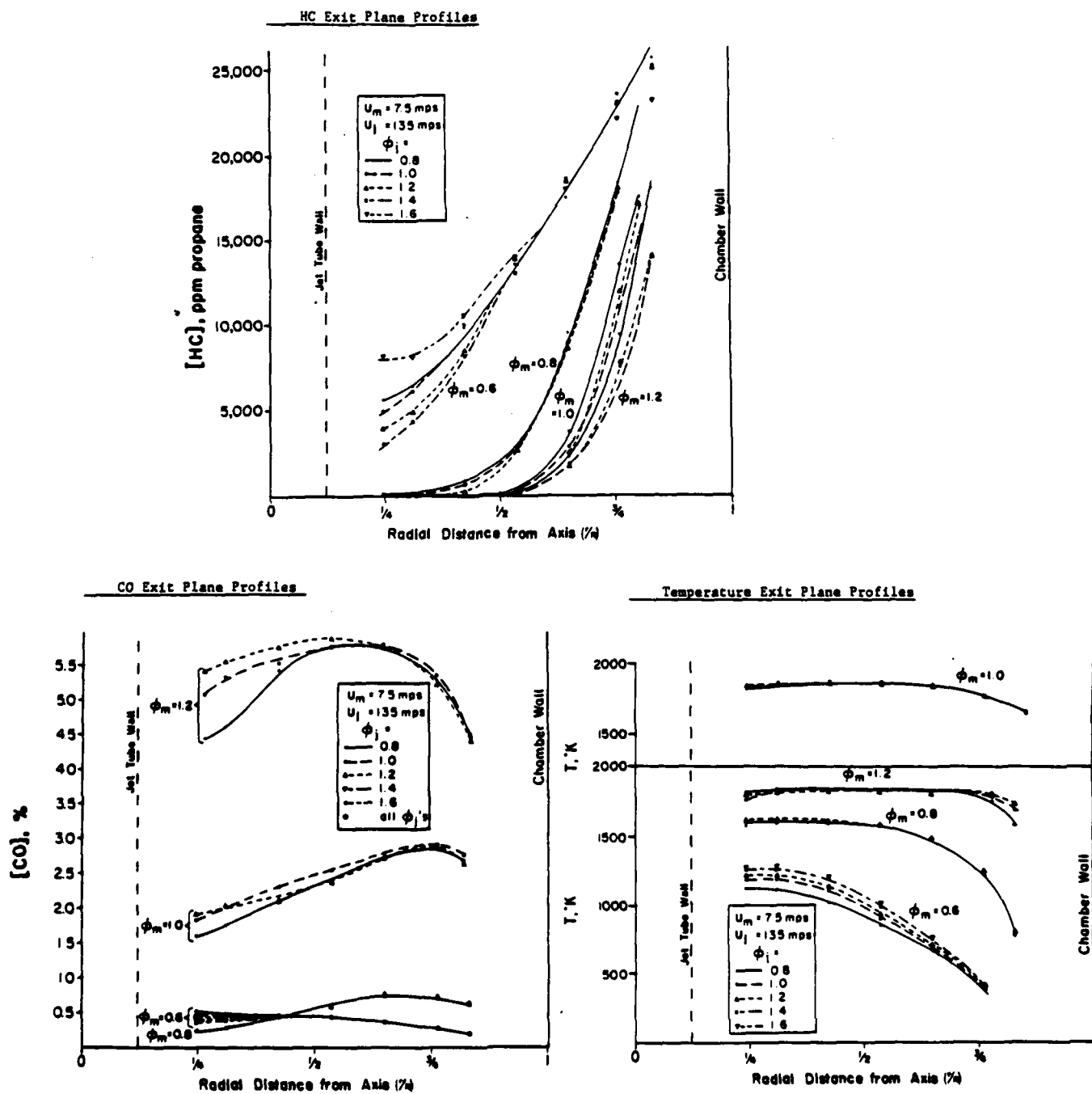

Figure 15. (continued)

g) Parametric Study: Effect of ϕ_m and ϕ_j (NO$_x$)
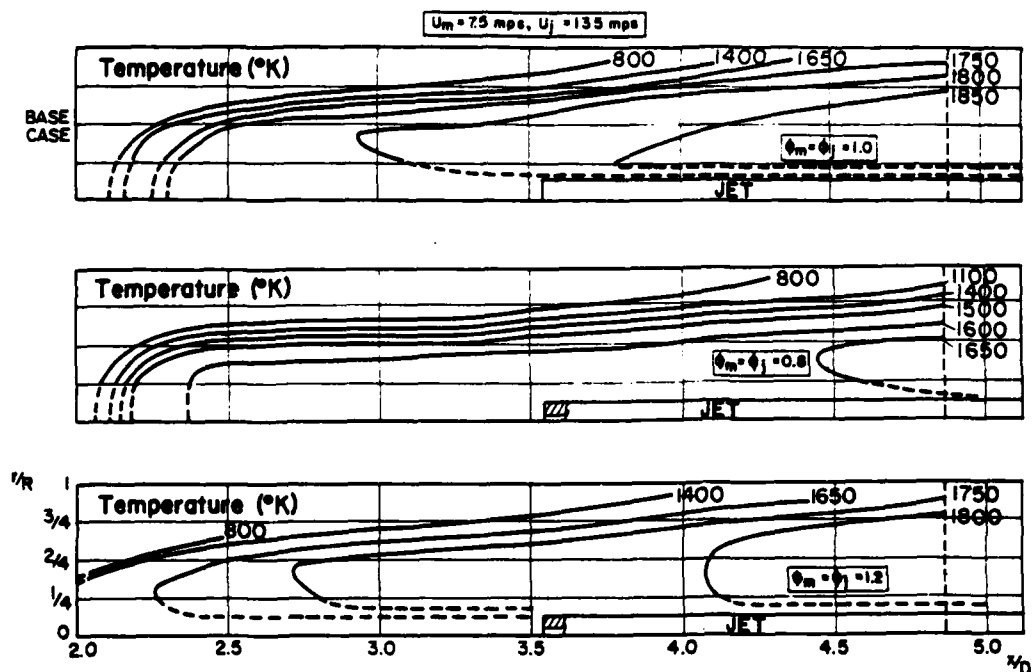
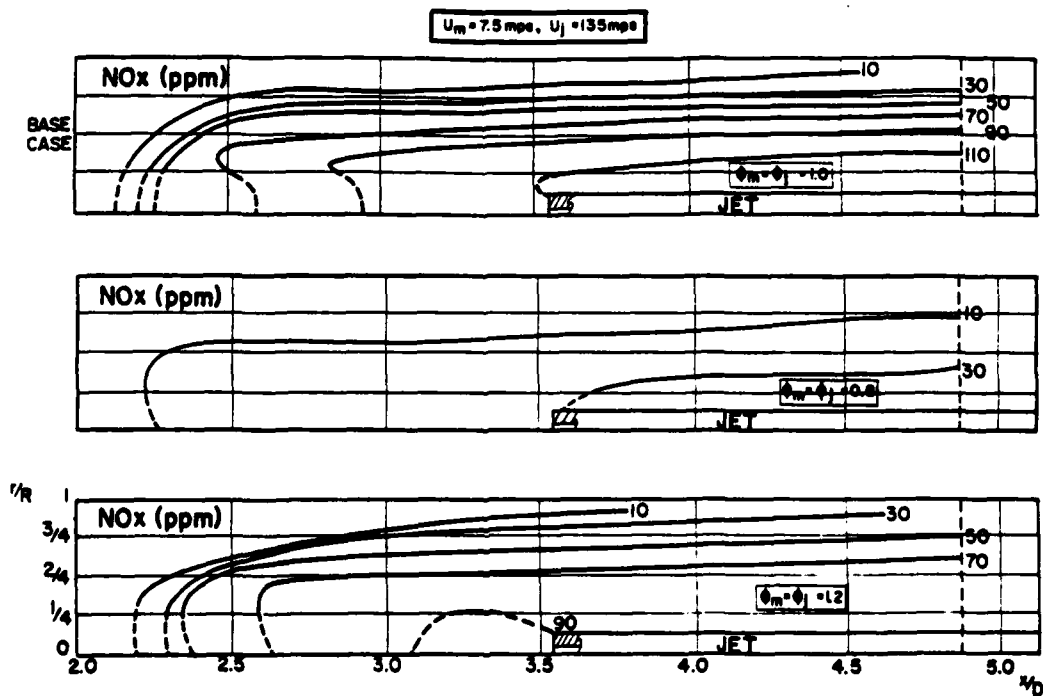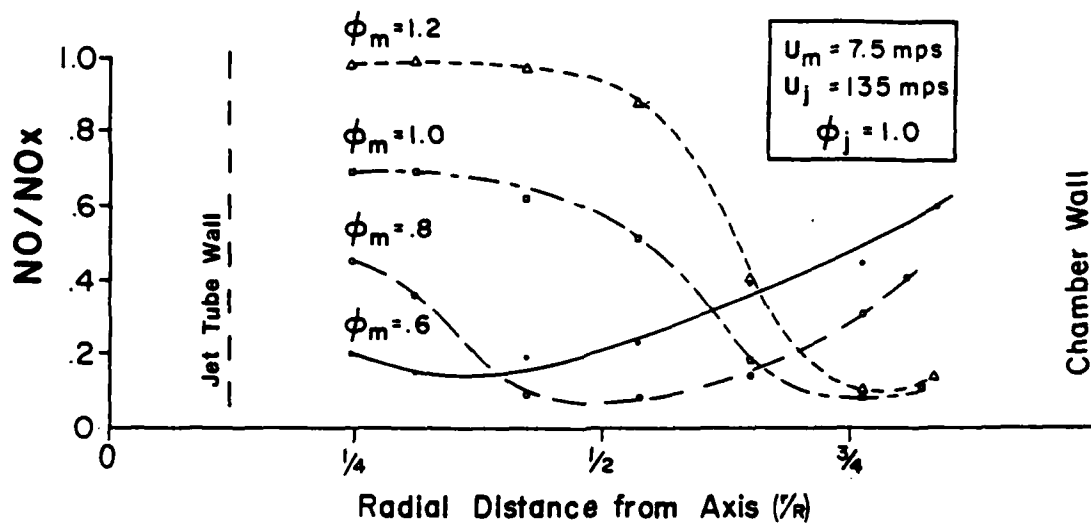h) Parametric Study: Effect of ϕ_m and ϕ_j, (NO/NO$_x$)

Figure 15. (continued)

65

h) Parametric Study: Effect of ϕ_m and ϕ_j, (NO/NO_x)
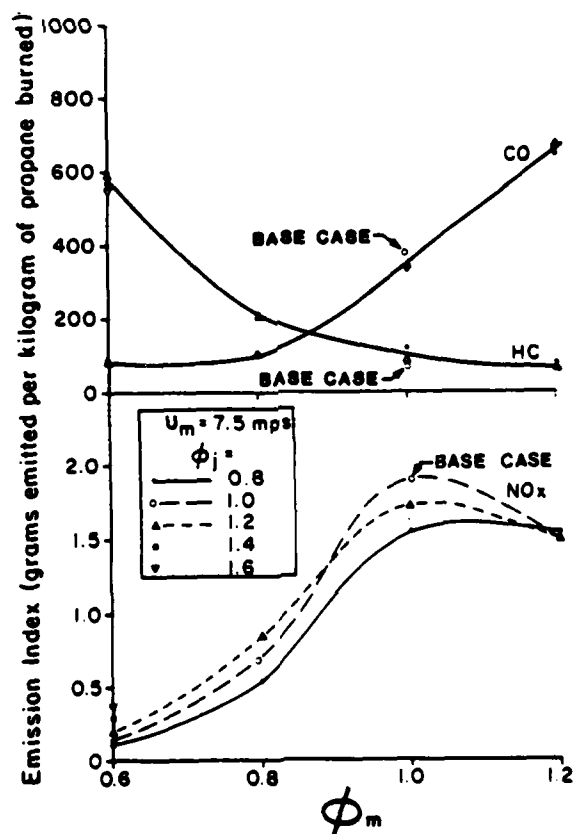

i) Emission Indexes

Figure 15. (concluded)

front. Within the wake, temperature, oxygen, and residence time are sufficient to ensure nearly complete HC consumption, and to initiate the oxidation of CO to carbon dioxide (CO_2) as demonstrated by the decrease in CO concentration adjacent to the jet tube proceeding downstream toward the exit plane. Proceeding toward the combustor wall, the concentrations of HC and O_2 approach those of the reactants. As a result, the source of the hydrocarbons emitted at the exit plane is the area outside of the wake.

Oxides of nitrogen (NO_x) are formed thermally in both the recirculation zone and wake as a result of elevated temperatures, sufficient residence time, and available oxygen. Area-averaged concentrations calculated at both the "jet exit plane" and combustor "exit plane" (Figure 1a) indicate that 75 percent of the total NO_x emitted is formed in the recirculation zone for this base condition.

The exit plane profiles show the general structure of the wake. Within the wake and proceeding from the jet tube to the combustor wall, HC and oxygen concentrations and temperature remain relatively constant, while CO concentrations increase slowly and NO_x concentrations decrease. At approximately r/R = 0.55, the concentrations of HC, CO_2, and O_2 change sharply. Oxygen and HC rise, CO_2 drops and CO peaks. Eventually, the HC and O_2 rise to the reactant concentrations.

Finally, it is noteworthy that the NO/NO_x ratio drops abruptly at the flame front. This is attributed to the rapid mixing of hot products and cold reactants at the flame front which produce radical relaxation reactions and associated populations of hydroperoxy radicals (HO_2) sufficient to oxidize NO to NO_2. Unfortunately, these events can be influenced by the probe, and the extent to which the measured levels of NO_2 are real or artifacts of the probe remains unanswered. However, an evaluation (Chen, et al., 1979) of

67

similar observations in a premixed combustor (Oven, Gouldin, and McLean, 1979) concluded that, although measurements within high temperature reaction zones (e.g., within the recirculation zone and wake) are likely biased by probe-induced oxidation of NO, elevated levels of NO_2 in areas of rapid flame quench (e.g., the flame front) are likely real and not artifacts of the probe.

Mainstream and Jet Velocities. The major effect of changing mainstream and jet velocity is to change the size of the recirculation and wake region. This is demonstrated in the present study by independently increasing the mainstream velocity (U_m) and decreasing the jet velocity (U_j). The effect of either is to decrease the size of the recirculation and wake regions.

The visual appearance of the flame for the base case and two variations on the base case is shown in Figure 15c. Both the penetration of the jet and the radial propagation in the wake are restricted by increasing the mainstream velocity or by decreasing the jet velocity. This is confirmed by the detailed temperature maps presented in Figure 15d.

A decrease in the size of the recirculation and wake reaction zones produce a net reduction in the residence time and, hence, a net reduction in the NO_x production (Figure 15e).

Mainstream and Jet Equivalence Ratios. The mainstream equivalence ratio (ϕ_m) is the dominant variable controlling the heat release and, ultimately, the pollutant emission. The effect on heat release is shown in Figure 15f.

HC, CO, T. As indicated by HC exit plane profiles (Figure 15f), the wake reaction propagates further radially as the mainstream mixture is enriched. This is a consequence of the decrease in air dilution as ϕ_m is increased from 0.6 to 1.0. The increase in wake reaction as ϕ_m is enriched

68

from 1.0 to 1.2 is attributed to an increased availability of hydrocarbon radicals. Peak flame velocities for propane-air flames generally occur at equivalence ratios rich of stoichiometric (Fristrom and Westenberg, 1965).

The highest temperatures occur for the base case (ϕ_m = 1.0). Peak temperatures are about 300°K lower for ϕ_m = 1.2 and 500°K lower for 0.8.

Carbon monoxide concentrations increase with mainstream equivalence ratio as the amount of available oxygen to oxidize CO to CO_2 decreases. For all conditions, the temperature is sufficient for the oxidation to occur. For equivalence ratios of 0.8 to 1.0, peak concentrations correspond to the location of the wake reaction front. Inside the front, CO is oxidized to CO_2. This accounts for the increase in temperature in the wake. Ahead of the front, CO diffuses into the cold reactant gases.

At ϕ_m = 1.2 , the absence of oxygen in the wake results in relatively constant CO concentrations and an absence of a distinct CO peak at the flame front.

For all cases except ϕ_m = 0.6, temperatures are fairly constant within the wake reaction zone and drop at the radially propagating wake reaction front. For ϕ_m = 0.6, the temperatures drop immediately adjacent to the axis, and HC concentrations remain elevated while CO concentrations fall, instead of rise, when proceeding from the axis to the chamber wall. This suggests that reaction in the wake is suppressed and CO formation, for example, is restricted to the recirculation region upstream with radial diffusion in the wake. Note that CO concentrations for ϕ_m = 0.6 are not appreciably lower than for ϕ_m = 0.8. In fact, near the jet tube, concentrations are lower for ϕ_m = 0.8. The additional oxygen available at ϕ_m = 0.6 is offset by lower temperatures.

Varying the jet stream equivalence ratio (ϕ_j) allows determination

of the effect of recirculation zone mixture ratio. The effect on exit plane profiles of HC and temperature is pronounced only at $\phi_m = 0.6$. Higher jet equivalence ratios result in lower HC concentrations near the jet tube wall and higher temperatures, and this effect diminishes as distance from the jet tube wall increases. This is attributed to higher temperatures in the recirculation zone that result from recirculation zone mixture ratios closer to stoichiometric. This effect is not as pronounced for the other equivalence ratios because each effectively sustains a fully developed reaction in the wake.

The effect of jet equivalence ratio on carbon monoxide is noticeable only near the jet tube. For $\phi_m = 0.6$, richer jet mixtures result in lower CO emissions because of higher temperatures in combination with the elevated concentration of oxygen. This same trend occurs, but to a much lesser extent, for $\phi_m = 0.8$. At $\phi_m = 1.2$ and 1.2 this trend is reversed. For these cases oxygen, and not temperature, limits the CO oxidation.

$\underline{NO_x}$. The NO_x profiles are presented in Figure 15g. Peak concentrations are highest for the base case ($\phi_m = 1.0$). The concentrations are slightly lower at $\phi_m = 1.2$. For the leaner cases, there is a significant drop in concentrations.

For all cases the shape of the NO_x exit plane profile is similar, decreasing almost linearly from the jet to the combustor wall. The shape indicates that most of the NO_x is formed in the recirculation zone, and diffuses by turbulent transport downstream. This is confirmed in the detailed flow maps presented in Figure 15g. These trends correspond well with the trends observed for temperature (Figure 15f) reflecting the temperature dependence of NO_x formation reactions.

Note that the $\phi_m = 1.2$ exit plane profiles (Figure 15g) intersect

70

the $\phi_m = 1.0$ profiles with higher concentrations near the chamber wall. This is attributed to the additional production of NO_x in the larger wake reaction zone associated with the rich mainstream. Although the recirculation zone is larger as well, the data indicated that NO_x production in the recirculation zone is not increased, a consequence of suppressed oxygen availability and temperature.

Jet equivalence ratio (ϕ_j) directly impacts both the mixture ratio and temperature of the recirculation zone. As a result, the effect of jet equivalence ratio on NO_x production is predictable. Production of NO_x is increased with jet enrichment for lean mainstream ($\phi_m = 0.6, 0.8$), decreased with jet enrichment or jet leaning for stoichiometric mainstream ($\phi_m = 1.0$), and increased with a lean jet or decreased with a rich jet for a rich ($\phi_m = 1.2$) mainstream.

The effect of mainstream equivalence ratio on the NO/NO_x ratio is shown in Figure 15h for a stoichiometric jet. (Other jet equivalence ratios are omitted for clarity.) The rapid drop in the NO/NO_x ratio occurs at the flame front for each of the cases ($\phi_m = 1.2, 1.0, 0.8$) wherein a wake reaction was supported. The low NO/NO_x ratio for $\phi_m = 0.6$ is attributed to the quench zone surrounding the hot recirculation zone in the absence of a wake reaction.

Emission Indexes. The emission indexes for NO_x, CO, and HC are presented in Figure 15i as a function of mainstream equivalence ratio (ϕ_m). The parameters are jet equivalence ratio (ϕ_j) and mainstream velocity (U_m). The procedure used to compute the emission index involved correcting the data for water vapor in the exhaust, calculating the area-averaged exit plane concentrations and the area-averaged mass emission, and taking the ratio of the mass emission to the fuel mass input.

The emission index data reflect the observations derived from the

detailed results above, and place the performance of the combustor into a practical perspective. For example, NO_x emissions are highest at $\phi_m = 1.0$, and are only slightly lower at 1.2. Values are 50 percent lower at $\mu_m = 0.8$ than at stoichiometric, and those at 0.6 are from 5 to 15 times lower than those for the base case (depending on jet equivalence ratio). The high temperatures that favor NO_x formation also favor hydrocarbon oxidation. In the absence of a developed wake reaction at $\phi_m = 0.6$, 60 percent of the fuel is emitted unburned. As suggested by the analysis of the detailed flow maps, jet equivalence ratio has a minimum impact on HC and CO emission, but does affect NO_x emission.

Summary. Aerodynamic flameholding is shown to provide control over pollutant formation and flame stability by direct, reactant injection into the recirculation zone. The data presented provide insight into the performance of the reverse jet flameholder, give guidance for practical application, and establish a data base for future testing of elliptic codes.

The reverse jet combustor, chemically and aerodynamically, consists of two distinct regions: the recirculation zone and the wake. The mainstream and jet velocity influence the size of these two regions, while the mainstream and jet mixture ratios affect the overall chemistry and heat release.

The influence of the jet on the emission of NO_x is one of the more interesting characteristics of the flameholder. Jet changes which reduce the size, lower the temperature, and decrease the residence time are favorable to the reduction of NO_x emission. For example, an enrichment of jet equivalence ratio affects recirculation zone temperature and mixture ratio, and will produce either an increase or decrease in the net emission of NO_x depending on the mainstream equivalence ratio. Such changes do not significantly affect HC and CO emissions. A primary benefit from an enriched jet is to extend the

lean blow-off limit and thereby maintain combustor stability simultaneous with

a reduction in the emission of NO_x. However, a practical limit exists beyond

which the emission of unburnt fuel is excessive. In the present experiment,

this limit occurred at a mainstream equivalence ratio of approximately 0.8.

Detailed information is available in a M.S. Thesis (McDannel, 1979),

and a Ph.D. Dissertation (Wuerer, 1978). One paper has been published

(McDannel, Peterson, and Samuelsen, 1982).

4.2.4 Dilute Swirl Combustor (COLD Experiments)

Velocity Data. Axial and tangential, mean and rms velocity

measurements were made using the two-color laser anemometry (LA) system shown

in Figure 3b. Inlet velocity profiles were measured as closely as possible to

the upstream entry plane. Tangential velocity (w, w_{rms}) was measured 1 mm and

axial velocity (u, u_{rms}) was measured 5 mm downstream of the entry plane.

Radial velocities were not measured but were estimated based on the

extrapolation of streamlines (calculated from measured data) to the entry

plane. These inlet velocity profiles are presented in Figure 16a for the

baseline case (15 m/s, swirl/dilution = 1.0, COLD, ϕ = 0.2). The spike in

the inlet tangential velocity profile is a result of the 12 discrete swirl

channels. Radial velocity measurements across the full combustor diameter

indicated that this spike was a symmetric occurrence.

Radial and centerline profile plots of mean and rms, axial (u, u_{rms})

and tangential (w, w_{rms}) velocities are presented in Figure 16b for the

baseline case, a flow condition corresponding to a 15 m/s reference velocity

and equivalence ratio of 0.2. Axial values appear on the top half of each

radial profile plot and tangential values on the bottom. Radial profiles were

measured at seven axial stations for each run condition; for clarity only four

73

a) Inlet Profiles
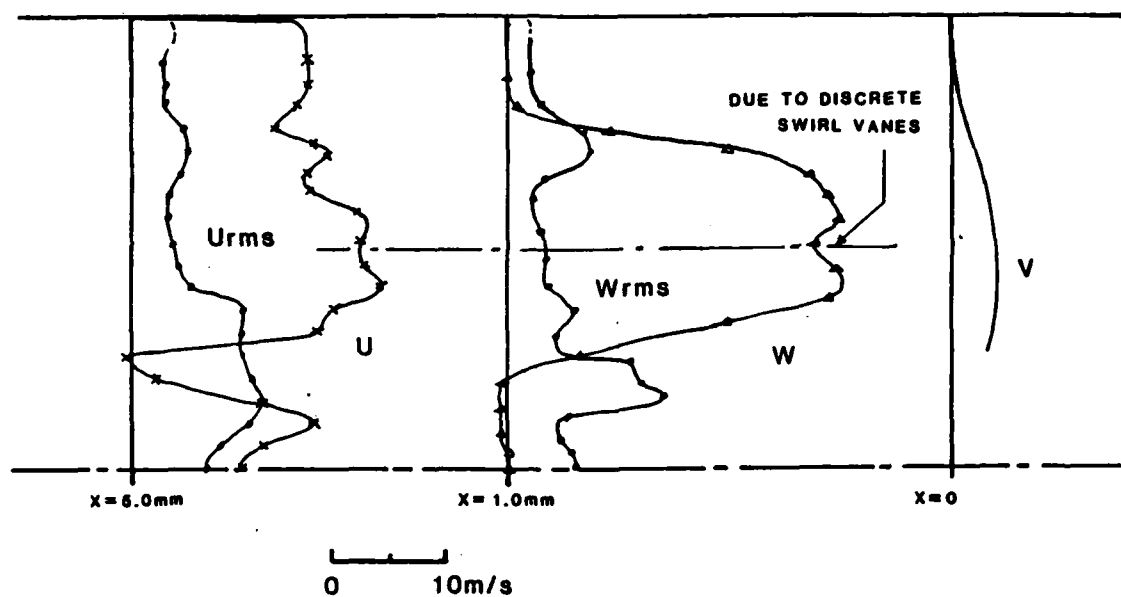
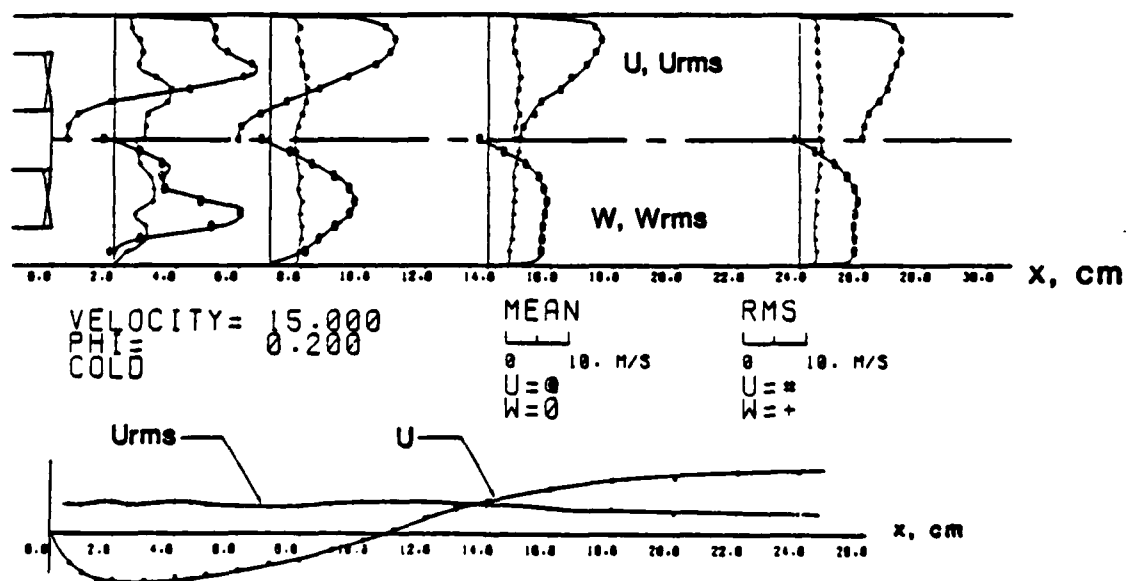b) Centerline and Radial Mean and RMS Velocities
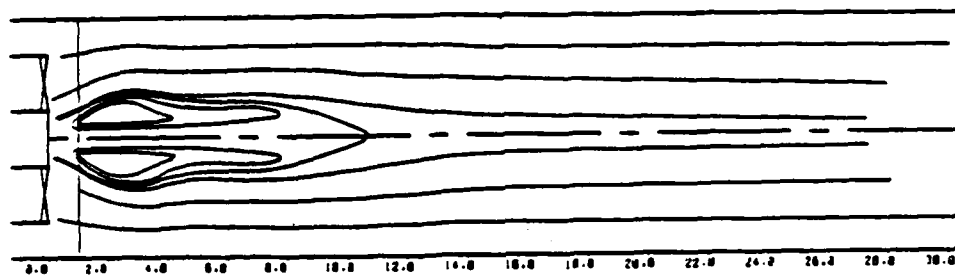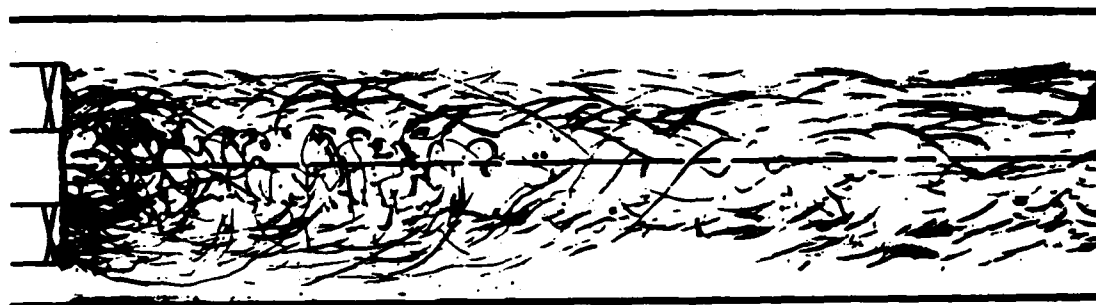

Figure 16. Dilute Swirl Combustor COLD Flowfield Data
(15 m/s, COLD, ϕ = 0.2)

c) Streamlines

d) Streak Photograph

e) Modeling

VELOCITY= 15.000
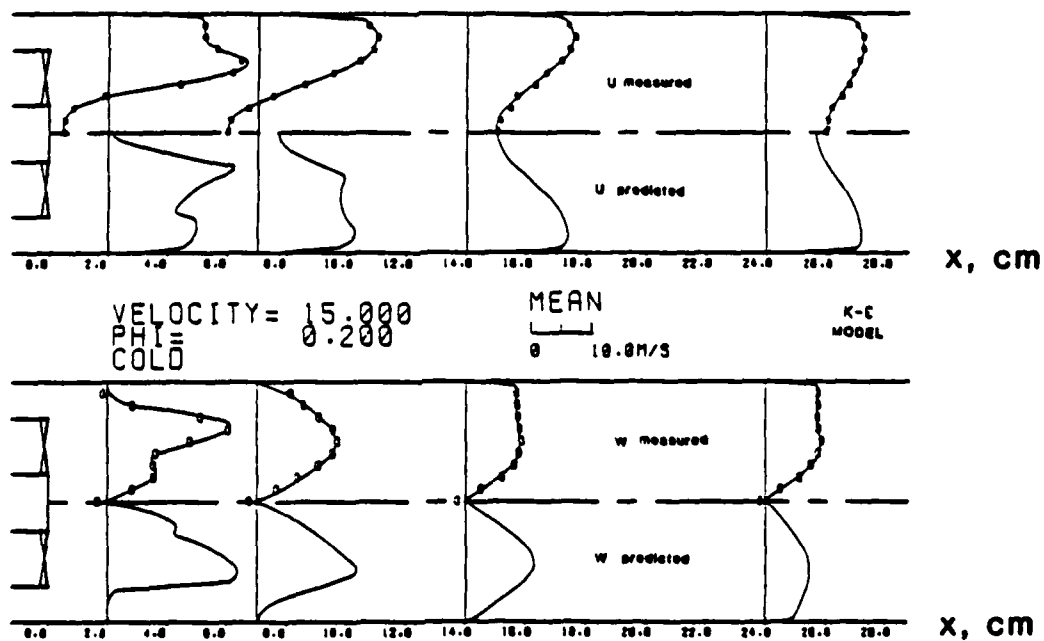PHI= 0.200
COLD

MEAN

0   10.0M/S

K-E
MODEL

Figure 16. (concluded)

are shown in the figures.

Along the centerline, tangential velocities go to zero so the rms fluctuations can be thought of as u_{rms} rather than w_{rms}. The expansion of the swirling air is shown to form a strong zone of backmixing or recirculation extending about 10 cm or 1.3 combustor diameters downstream. The peak reverse flow velocities are a significant fraction (about 50%) of the bulk velocity (15 m/s). Proceeding downstream, the radial profiles of mean axial velocity show the extent of the recirculation zone and the trend towards a pipe-flow profile.

The radial profiles of mean tangential velocity show that the initially strong concentrated swirling air mixes with the dilution air and forms a more uniform distribution of swirl downstream with a much lower maximum velocity. It can be seen that the dilution of the swirl strength corresponds with closure of the recirculation zone. At the upstream end of the recirculation zone the step in the radial profile of tangential velocity is evidence that the swirl near the centerline at this axial station is convected upstream from a downstream location. At the most downstream radial profile, the axial velocities are seen to rapidly approach a "well developed" turbulent pipe flow profile while the tangential velocities are somewhat slower in approaching a "solid body rotation" form.

Radial profiles of turbulence intensity show peaks of the regions of maximum shear. At the upstream regions of the flowfield, the axial rms velocity (u_{rms}) is generally larger than the tangential rms velocity (w_{rms}). However, isotropy seems to be a reasonable engineering assumption for the case since w_{rms} is generally within 20% of u_{rms} except in the regions where (1) the non-swirling fuel jet issues (illustrated by the peak in the u velocity curve), and (2) the non-swirling dilution air enters.

76

Using the continuity equation, stream functions ψ can be obtained by radially integrating the profiles of mean axial velocity:

$$\psi = \frac{\int_o^r rudr}{\int_o^R rudr} \qquad \text{where } r = \text{radial location of interest}$$
$$R = \text{outer radius of test section}$$

Integration at each profile allows streamlines to be drawn through points of constant ψ. These streamlines, shown in Figure 16c illustrate the form of the "time-averaged" flowfield.

Figure 16d is a photograph of streak lines created by laser illuminated, neutrally buoyant, helium-filled bubbles that were injected into the DSC to provide flow visualization. Comparison of these streak lines to the time-averaged streamlines shows agreement in the length and extent of the recirculation zone. The streak lines depict a high degree of mixing and disorder in the vicinity of the recirculation zone.

Modeling. The TEACH finite difference code with the k-ε turbulence model (Gosman and Pun, 1974) was modified to incorporate swirl following Lilly and Rhode (1982) and used to predict the DSC flowfield characteristics. The object was to demonstrate the isothermal (COLD) performance and ease of applicability of this commonly used turbulence model on a swirling complex flow.

The code was applied to the boundary conditions of the DSC flowfield for the baseline case (15 m/s, $\phi = 0.2$, COLD) without difficulty. Calculated variables were the three components of velocity (u,v,w), pressure (p), turbulent kinetic energy (k), and dissipation rate (ε). The code was run with the standard k-ε turbulence model and radial profiles of the predicted mean axial and tangential velocities are compared with measured results in Figure 16e. The code predicts a much slower radial diffusion of both u and w

77

velocity gradients than is apparent from the experimental results. It fails

to predict the strength and size of the recirculation zone. Similar results

have been reported by others when modeling swirling flows and the differences

are often attributed to streamline curvature (e.g., Srinivasan and Mongia,

1980). The DSC, as a result, is an attractive configuration in which to test

refinements to elliptic codes designed to improve performance in swirl

dominated flows as well as reacting flows.

Summary. A summary of this work is included as part of the summary

presented at the end of the next section.

4.2.5 Dilute Swirl Combustor (HOT Experiment)

Velocity Data. Detailed laser anemometry measurements were made in

reacting flow at two overall equivalence ratios (0.2 and 0.1). Centerline

profiles of mean and rms axial (u, u_{rms}) velocities appear in Figure 17a. The

recirculation zone for the $\phi = 0.1$ case appears very similar to that for the

cold flow case (Figure 16b) with three notable exceptions. The recirculation

zone in the case of reaction is (1) more intense (higher negative velocities),

(2) more compact (shorter), and (3) radially wider. Root-mean-square velocity

levels are approximately 50% higher for the reacting case except in the center

of the recirculation zone where the rms levels are about equal. From a visual

perspective, the flame was detached from the face of the fuel delivery tube

and was uniformly blue with no indication of soot formation.

As the equivalence ratio was increased to $\phi = 0.2$, a transition

occurred in the form of the recirculation zone. Visually, the flame became

attached to the upstream fuel tube face and yellow streaks of soot were

observed eminating from that point downstream along the centerline of the

combustor. The transition is clearly evidenced by the centerline profile of

u-velocity which indicates the presence of positive velocities just downstream

a) Centerline and Radial Profiles of Axial and Azimuthal
Mean and RMS Velocity
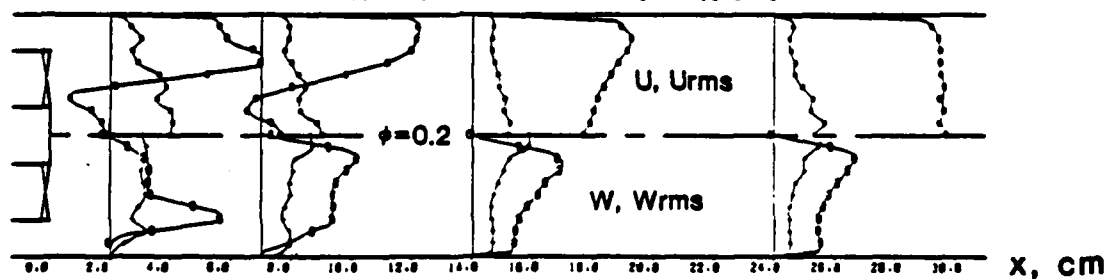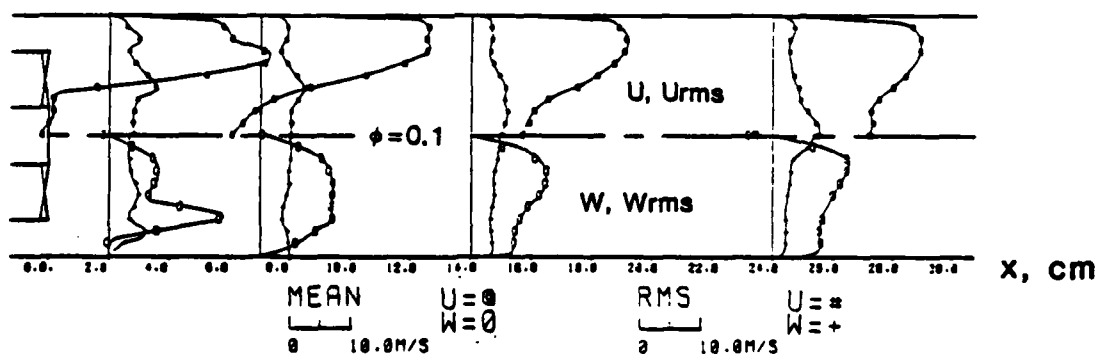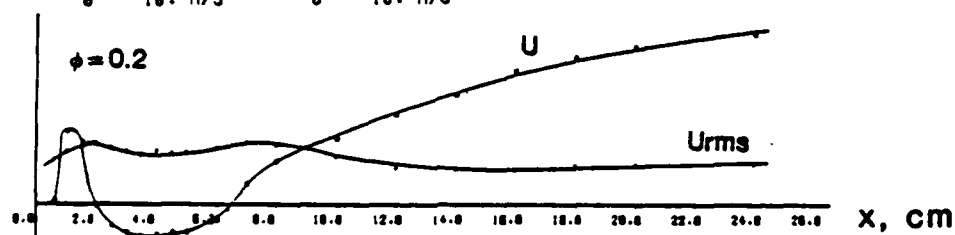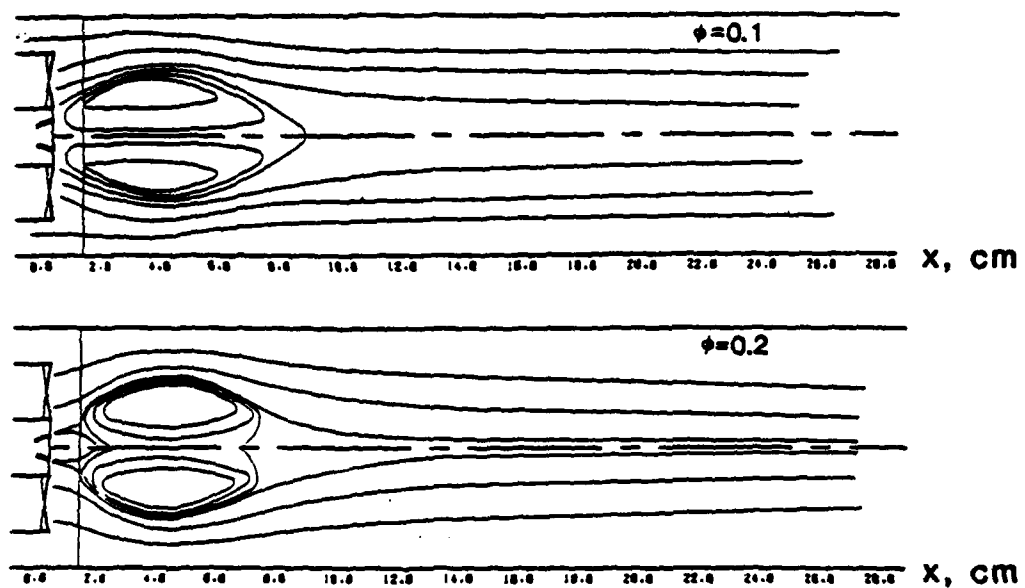(15 m/s, φ = 0.1 and 0.2)
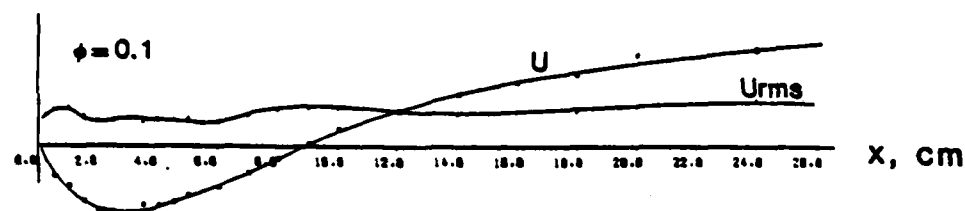
Figure 17. Dilute Swirl Combustor HOT Flowfield Data (Velocity)
(S/D = 1/1)

79

b) Streamlines (5 m/s, ϕ = 0.1 and 0.2)

c) Centerline Profiles of Mean and RMS Axial and Azimuthal Velocities
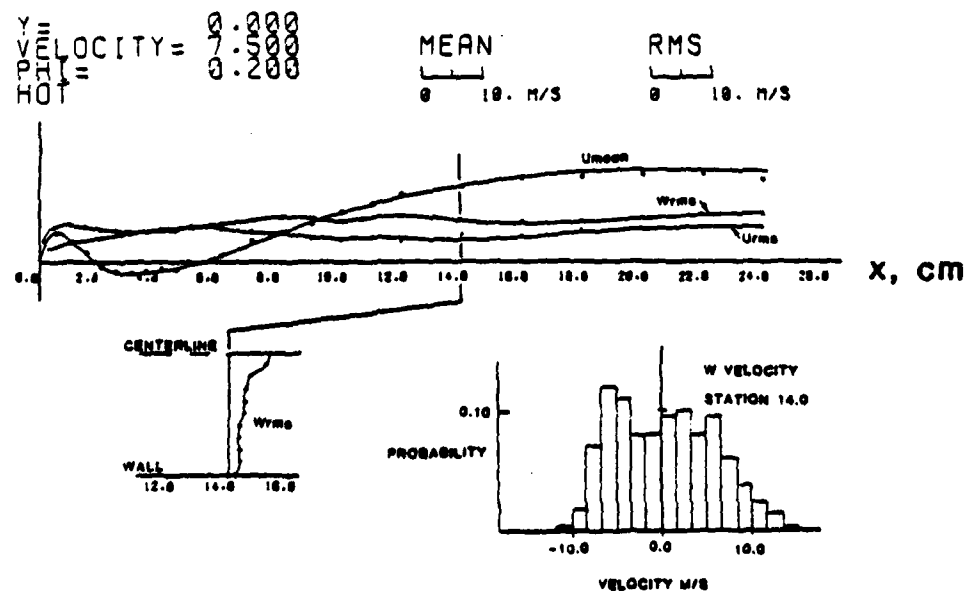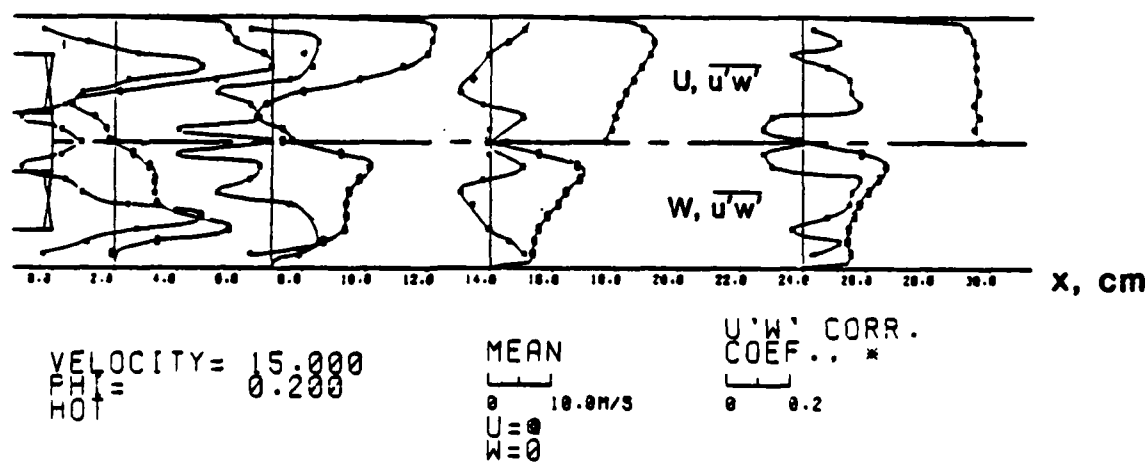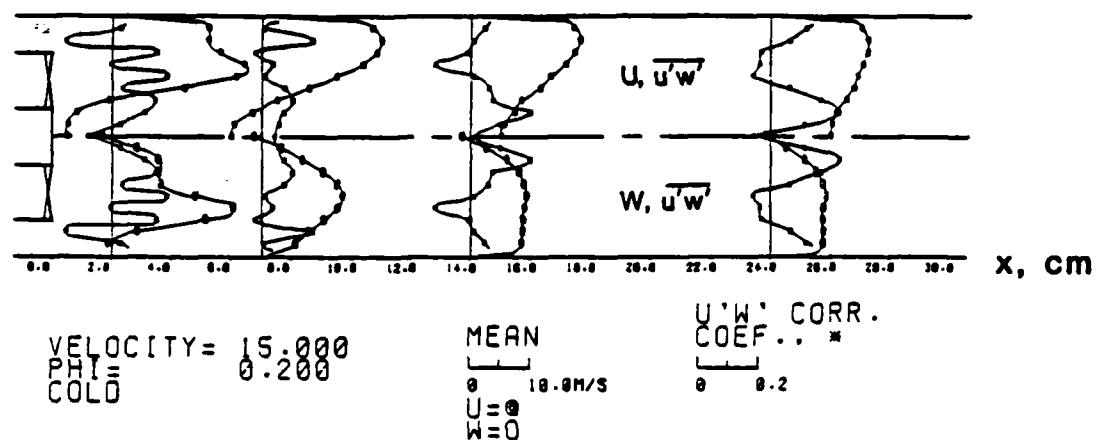(7.5 m/s, ϕ = 0.2)

Figure 17. (continued)

Figure 17. (concluded)

of the fuel delivery tube.

The effect of equivalence ratio is evident as well in the radial plots of axial and tangential velocities but is best illustrated by the streamlines which are plotted in Figure 17b. As the equivalence ratio is increased, the recirculation zone becomes shorter and wider. Eventually, the recirculation zone becomes so wide that not all the conical fuel jet is retained in the outer stream layer. Instead, some of the fuel is directed inward towards the centerline where it (1) opposes the upstream momentum of the recirculating flow and (2) ignites in the relatively oxygen deficient core of the recirculation zone resulting in visible soot production.

The change in width and length of the recirculation zone associated with reaction is a result of gases expanding in the shear layer at the boundary of the recirculation zone to create a source of pressure which tends to force (1) early closure of the recirculation zone, and (2) swirling air towards the centerline. As the swirling air is forced towards the centerline, the tangential velocity increases (conservation of angular momentum). This increase is evident by comparing the tangential velocity (w) profiles of Figures 16b and 17a. When this increased tangential velocity is convected upstream through the recirculation zone, it results in a higher radial pressure gradient that tends to widen the zone.

Turbulence intensity levels in the vicinity of the recirculation zone are noticeably higher for the $\phi = 0.2$ case (in comparison to the $\phi = 0.1$ case), whereas they are about equal downstream. Part of this increased level is attributed to intermittency in the division of the fuel jet between the inside and outside of the recirculating flowfield.

A lower reference velocity is shown in Figure 17c where centerline profiles of u_{rms} and w_{rms} velocities for the 7.5 m/s, $\phi = 0.2$ reacting case

are presented. A peak in both the u_{rms} and w_{rms} velocities occurs at the stagnation point of the recirculation zone. This characteristic has been observed by others (e.g., Owen 1976) and is attributed to "form intermittency" of the recirculation zone. Such large scale intermittency or periodic behavior of complex flows has been documented utilizing flow visualization techniques such as high speed cinematography (Brum, Ikioka, and Samuelsen 1982) and time resolved emissions techniques (Roquemore, Britton, and Sandhu, 1982).

It is also observed that, at downstream locations along the centerline, w_{rms} is greater than u_{rms}. Examination of radial profiles of w_{rms} reveals that these unusually high values occur only near the centerline. These excessive levels are most likely produced by a spiralling action of the vortex center about the stationary LA probe. This spiralling action (a type of "form intermittency" or "periodicity") is further evidence by a flattened probability distribution function (pdf) which one would expect with a spiralling center versus a Gaussian distribution more typical of "pure" turbulence. Similar high turbulence production rates have been observed by Cheng and Ng (1981) when performing LA measurement on a premixed turbulent flame. They attributed this to periodic movement of the flame sheet through the measurement volume. Hence, the "turbulence intensity" as measured by a stationary LA probe is comprised of two components: (1) rms fluctuations intrinsic to fluid mechanic turbulence production and (2) form intermittency of the complex flowfield that does not give rise to significant turbulent stress production.

Radial plots of the $\overline{u'w'}$ correlation coefficient (C) appear in Figure 17d (top and bottom) for the baseline (COLD) case along with the axial (u, top) and tangential (w, bottom) velocity profiles. These data represent

some of the first complex swirling flow velocity correlations that have been obtained by direct, simultaneous measurement. For well developed boundary layer flows, the coefficient (C) has been classically measured to be on the order of 0.4 (Liepmann, 1979). In complex flows, of course, the direction of the coefficient changes as does the direction of local gradients. For example, where both the u and w gradients with respect to y are positive:

$$\frac{\partial u}{\partial y} > 0 \qquad \frac{\partial w}{\partial y} > 0$$

then the correlation (C) is positive; when both are negative, the correlation (C) is positive. However, when the u gradient is positive and the w gradient is negative, or vice versa, the correlation is negative. In areas where there is little or no gradient in either u or w, the correlation goes to zero.

The peak value of the correlation coefficient measured was approximately 0.25, which is less than that measured in boundary layers (0.4). However, there is no reason to believe that they should be the same since, in boundary layers, there is a gradient in only one velocity component ($\frac{\partial u}{\partial y} \neq 0$) and not both as in the present case, (i.e., $\frac{\partial u}{\partial y}$, $\frac{\partial w}{\partial y} \neq 0$). Smith and Giel (1979) obtained peak values of the $\overline{u'w'}$ correlation coefficient of 0.23 via a similar direct method of measurement in a complex, but non-swirling, flow (dump combustor).

Indirect measurements of $\overline{u'w'}$ have been made in swirling complex flow geometries under isothermal conditions. For example, Janjua, et al. (1982) used a six orientation hot wire probe in an expanding swirl combustor and derived the various flow quantities algebraically based on time-averaged quantities obtained at each orientation. The peak $\overline{u'w'}$ correlation coefficient calculated from their results was on the order of 0.38. Fujii,

84

Eguchi, and Gomi (1981) used measurement of a single component LA system made in a swirling jet at various angles to algebraically determine $\overline{u'w'}$. The peak coefficient calculated from their results was about 0.40. Part of the difference between the direct and indirect measurement of the correlation coefficients may be attributed to the difference in flow geometries. For example, the level of "form intermittency" in the present complex flow geometry may be different than that in the geometries used by Fujii and Janjua. Since the stationary LA probe is not capable of distinguishing between fluctuations arising from (1) true turbulence and (2) form intermittency, and since these two fluctuating components have different time scales and are thus not well correlated to one another, the presence of the latter (form intermittency) effectively dilutes the correlation produced by the first (true turbulence).

Reynolds stress plots for the 15 m/s, $\phi = 0.2$ reacting flow case appear in Figure 17d; once again the peak correlation coefficient is on the order of 0.25.

Velocity/Temperature Data. As a next step, a fine-wire thermocouple probe was employed to obtain temperature measurements simultaneously with velocity.

First, the results of a probe perturbation study are presented where the peturbation caused by the use of probes of various shapes and orientations is assessed. Second, the effect of time constant variation is considered followed by a presentation of the temperature time series and the probability density function (PDF) of the temperature. The section concludes with the statistical properties of the combined velocity and temperature field. A tabulated data base, including measured inlet conditions, is available (Seiler, 1983b).

The probe perturbation effects are both small scale (local) and large scale (global). The former is associated with the geometrical characteristics of the probe, especially near the probe tip, while the latter is related to the overall shape, size, and orientation of the probe. The local effects can be minimized by making the probe tip as small as possible while the global effects can be minimized by probe geometry (including overall size) and probe orientation.

Probe perturbation was assessed by separately placing each of the probe configurations (Figure 4a) in the flow and determining statistical properties of the velocity field in the presence and absence of the probe. In the case of the curved probe, different orientations of the probe were also assessed. Representative results based on 500 data samples are presented in Figure 18a. The probe with minimum overall perturbation effects is identified by the solid symbol. In the central region of the flow, the curved probe has a lower perturbation effect than that of the straight probe. This may be due to the occasional occurrence of periods of reverse flow and/or suppression of the form intermittency observed by Brum and Samuelsen (1982b).

Based on this perturbation study, probe configurations and orientations were selected that minimize the perturbation. The resultant uncertainty due to probe perturbation were less than 25% throughout much of the flow field.

The effect of time constant variation on statistical features of the flow involving the temperature signal is shown in Figure 18b. The mean temperature is not significantly affected by deliberately over- or under-compensating the sensor relative to the value obtained with the sensor compensated for the mean flow conditions. For example, the measured value of the mean temperature varies by less than 10% for a ± 50% variation in the time

END

FILMED

DTIC
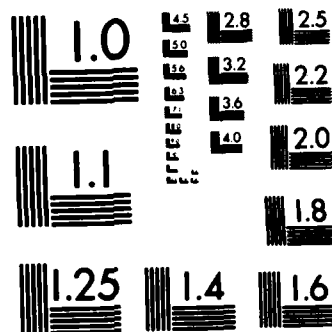
MICROCOPY RESOLUTION TEST CHART

NATIONAL BUREAU OF STANDARDS-1963-A

Figure 18.   Dilute Swirl Combustor HOT Flowfield Data (Velocity/Temperature)
(15 m/s, ϕ = 0.1, S/D = 1/1)

c) Temperature Time Series

$r/R = 0.0$ ($\overline{T} = 1560^{\circ}C$, $T_{rms} = 152^{\circ}C$)
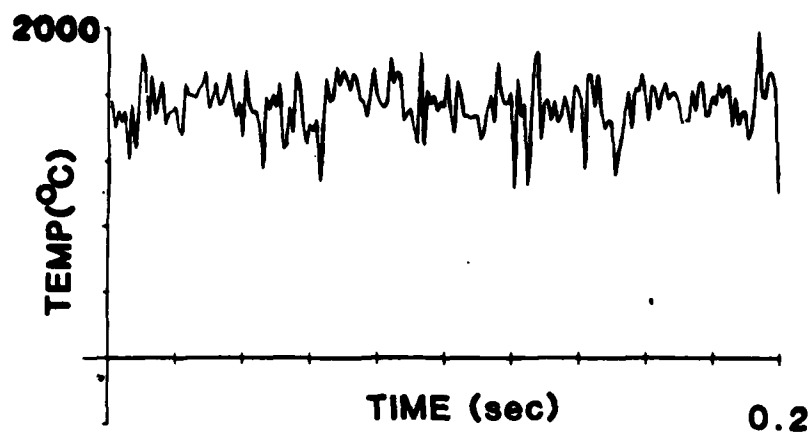
$r/R = 0.5$ ($\overline{T} = 580^{\circ}C$, $T_{rms} = 242^{\circ}C$)
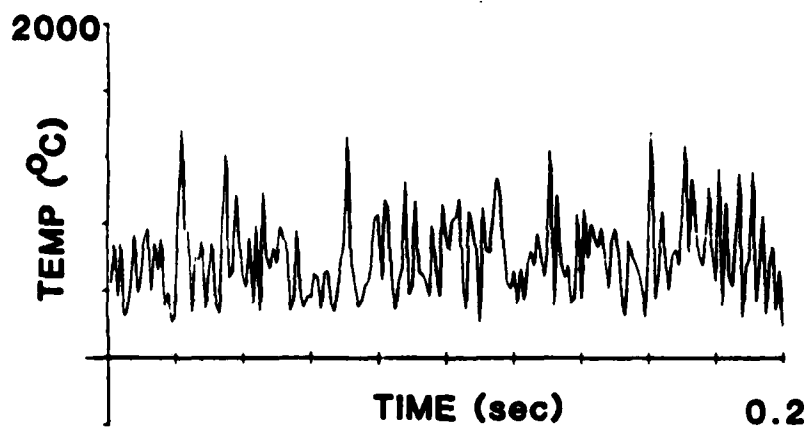
$r/R = 0.7$ ($\overline{T} = 135^{\circ}C$, $T_{rms} = 95^{\circ}C$)
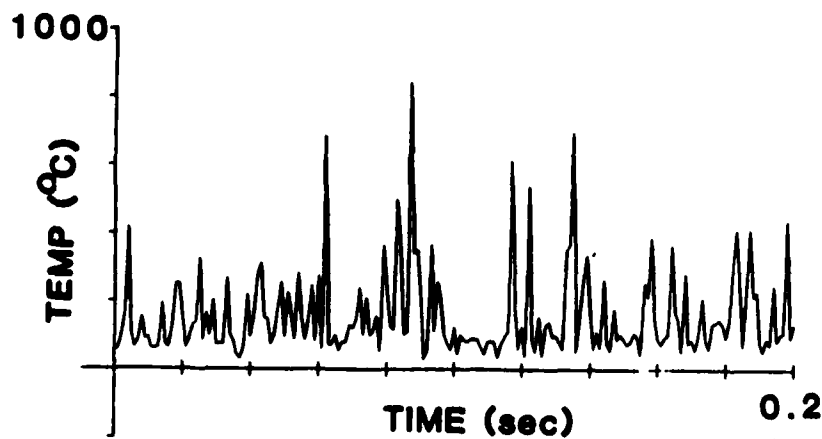
Figure 18.   (continued)

d) Probability Distribution Function of Temperature

x = 14 cm
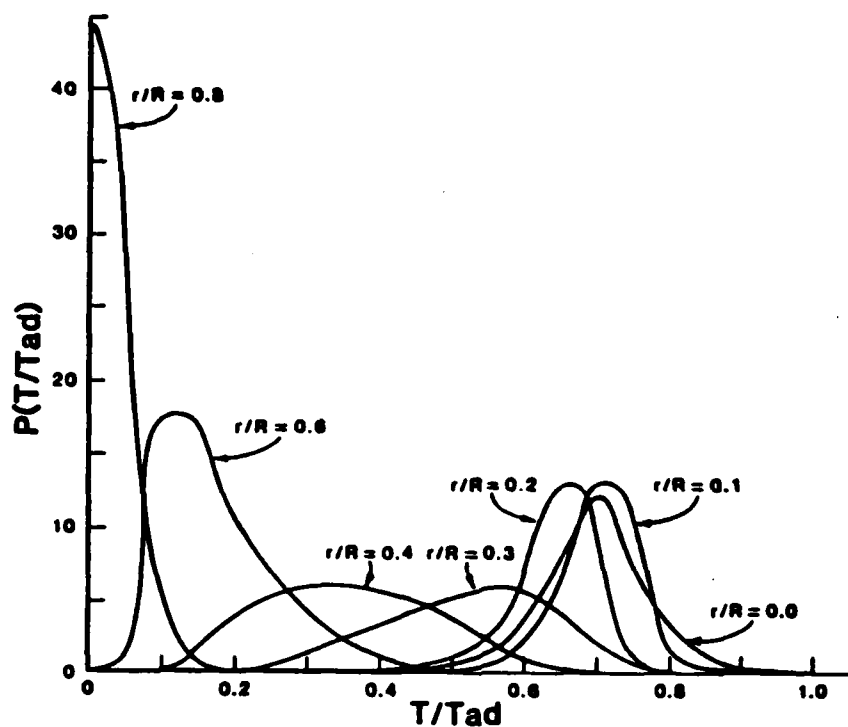
x = 24 cm
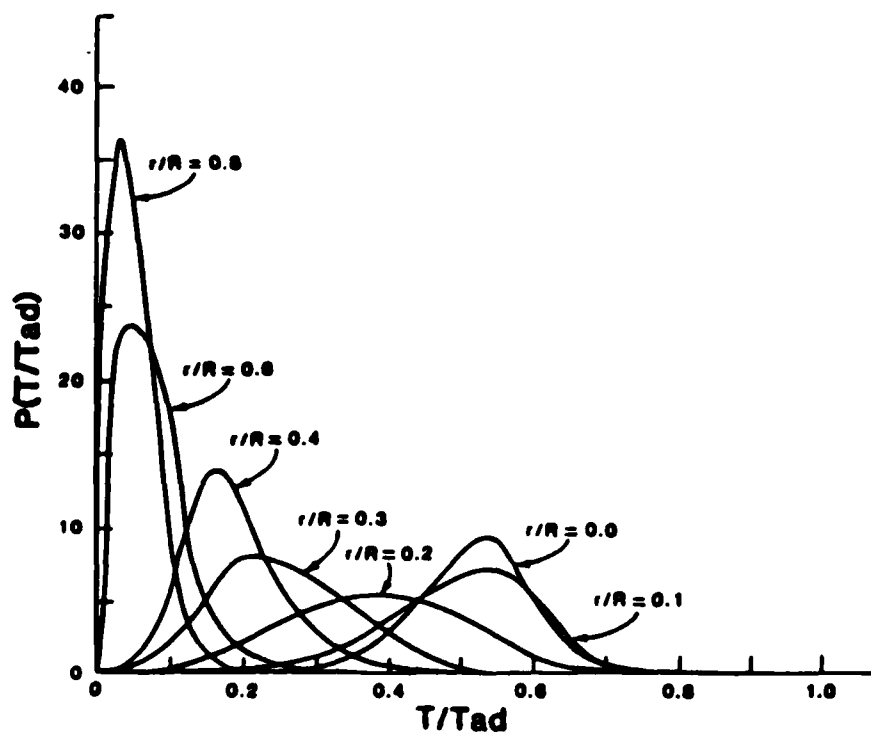
Figure 18. (continued)

e) Velocity Field with Thermocouple Probe

f) Axial Heat Flux
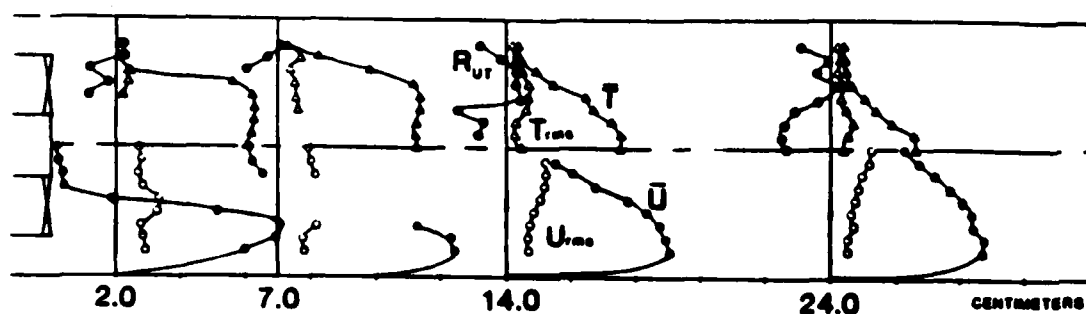
g) Azimuthal Heat Flux
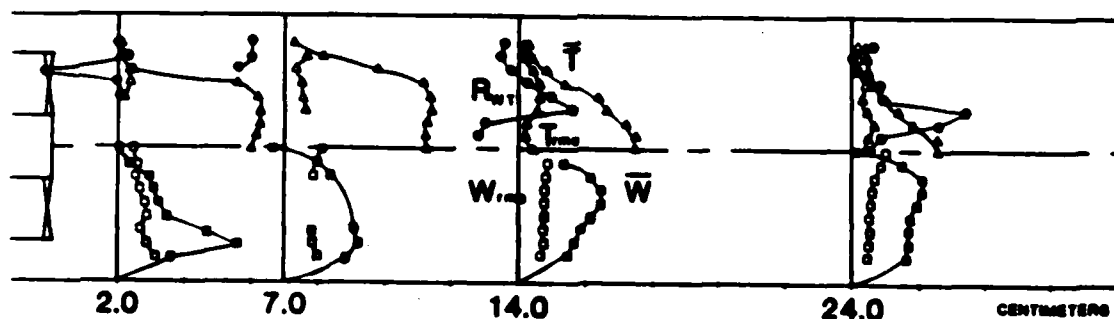
MEAN/RMS	CORR COEFF
0 10 m/s	0 0.2
0 800 °C	

Figure 18. (concluded)

90

constant. The root-mean-square temperature is also relatively insensitive to variation in the time constant. A 10% variation, has less than a 5% effect on the measured root-mean-square temperature which suggests that over- and under-compensation affects that portion of the temperature power spectrum that contributes a relatively small amount to the root-mean-square temperature. In contrast, a 20% variation in the measured axial heat flux and a 50% variation in the tangential heat flux occurs for the same 10% under-compensation in the time constant. Over-compensation has relatively little effect on the value of the heat fluxes. This observation is consistent with that of Yanagi and Mimura (1981). It is clear that both phase shift and variations in the amplitude response that are correlated with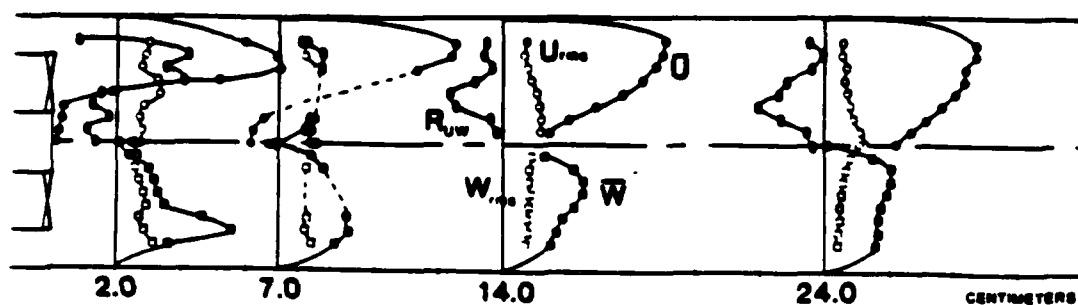 the temperature and velocity affect the value of the heat fluxes, but the difference between the effect of over- and under-compensation is difficult to explain.

Representative samples of the compensated temperature signal are presented in Figure 18c at different radial positions for the 14 cm axial station. A peak-to-peak temperature of about 500°C is found at the centerline distributed about a mean temperature of 1560°C. The fluid on the centerline is well mixed with no evidence of unheated dilution air reaching the centerline.

The temperature time series at the mid-radius position indicates that the temperature signal has positive skewness due to the presence of relative short duration, high temperature peaks. The average rate of occurrence of hot particles (defined as the average rate at which the temperature signal crosses a threshold temperature) is 42 Hz for a threshold of 1000°C. The crossings are not periodic but appear to be distributed randomly in time, and are evidence that a periodic structure is not associated with the passage of the high temperature fluid particles. Power spectral

91

measurements of the temperature signal show a relative increase in the "energy" of the temperature signal at a frequency of 90 Hz. This corresponds to the frequency of longitudinal oscillation of the recirculation zone observed in high speed photography (Brum and Samuelsen, 1982b).

Near the wall, the temperature signal is dominated by high amplitude, short duration, temperature spikes which correspond to a positive skewness. The average rate of occurrence of hot particles crossing a threshold of 400°C is 25 Hz. Again, the crossings are not periodic. The minimum temperature corresponds to about 40°C. The data obtained at the 24 cm station are similar, indicating that the sheath of dilution air near the wall of the combustor remains intact through the length of the combustor.

Representative probability density functions (PDF) are presented in Figure 18d for two axial locations, 14.0 and 24.0 cm. The data are normalized by the maximum adiabatic temperature, T_{ad} = 1996°C. The PDF's show positive skewness at locations well displaced from the centerline (r/R > 0.6). This was obtained at all four axial stations and indicates that cool, unreacted gas predominates in this region of the flow throughout the length of the combustor. In addition, the PDF's are narrow in this outer region of the flow which corresponds to low rms temperatures and indicates that only a limited amount of fluid from the hot recirculation zone mixes with the cool dilution air.

At the 14.0 cm station, the PDF's are very broad at the intermediate radial locations of r/R = 0.4 and r/R = 0.3 with peak-to-peak temperatures on the order of 1100°C, indicating the alternating presence of cool and hot fluid parcels. Maximum rms temperatures are also found at these radial locations. At r/R < 0.2, the gas is mainly high temperature (1160°C to 1750°C) combustion products with no evidence of unheated dilution air. At the 24 cm station, the

data provide evidence of additional mixing between the hot products of combustion and cool dilution and unreacted swirl air. The PDF's at $r/R < 0.2$ are broadened relative to the upstream 14 cm station, and the peak temperatures of the PDF's at the intermediate radial locations ($r/R = 0.3$, 0.4) are reduced.

Velocity data obtained with the thermocouple probe in place (Figure 18e) indicate that the statistical features of the flow field remain essentially unchanged from those found in the absence of a probe (cf., Figure 17a).

The mean and rms temperature, the axial velocity, and the normalized axial heat flux are shown in Figure 18f. The mean temperature, at all axial locations, has a maximum on the centerline. The maximum mean temperature in the recirculation region at $x = 2.0$ and 7.0 cm is nearly constant and equal to 1750°C which is approximately 200°C less than the maximum adiabatic flame temperature (1996°C). Radiation losses are estimated to account for approximately 90°C of the 200°C. The nearly constant mean temperature in the recirculation region indicates that the fluid in this region is relatively well mixed. The peak instantaneous temperature recorded was as high as 2094°C. The infrequent occurrence of measured temperature greater than the maximum adiabatic temperature occurred less than 1% of time and is due to slight over-compensation of the signal. At $x = 2.0$ and 7.0 cm for $r/R > 0.7$, the mean temperature is less than 150°C and consequently the flow corresponds to slightly heated dilution air.

Downstream of the recirculation zone (at $x = 14.0$ and 24.0 cm), the mean temperature profile exhibits a maximum of 1400°C on the centerline with a monotonic decay to a minimum near the wall of 125°C.

The axial heat fluxes at the 14.0 and 24.0 cm stations are negative

in the central region of the flow (r/R < 0.3) and are either relatively small or slightly positive in the outer region of the flow (r/R > 0.4). The negative sign of the axial heat flux in the central region of the flow indicates the presence of a relatively large number of fluid particles with high temperature (relative to the mean temperature) and low velocity (relative to the mean velocity). These fluid particles probably originate in the recirculation zone. The growth of the region of negative axial heat flux in the downstream direction is associated with the mean tangential velocity which preferentially transports low temperature, high density fluid away from the central region and high temperature, low density fluid toward the centerline.

The mean tangential velocity at the 2.0 cm station (Figure 18g) is relatively low in the recirculation region, with the peak mean tangential velocity, as expected, in line with the outer circumference of the swirl vanes. This sharp peak is quickly suppressed (x = 7.0 cm) by the interaction with the non-swirl dilution air. The tangential heat flux is very small at the x = 2.0 cm station. Downstream (x = 14.0 and 24.0 cm), the values of the tangential heat flux increase and exhibit relatively sharp peaks at radial positions (r/R = 0.2 and 0.4 respectively) corresponding to the maximum values of the mean tangential velocity.

The mean temperature in the central region at x = 2.0 and 7.0 cm is so high that the overheating of the probe required in order to determine the time constant caused the probe to fail. Therefore, rms temperature and axial and radial heat fluxes could not be determined in this region.

Conditioned sampling techniques were applied to the data in which a temperature range is specified and the statistical quantities are obtained for those data points falling within the specified range. The results verify that the central region of the combustor downstream of the recirculation zone is

dominated by parcels of high temperature, low velocity fluid. At the 14 cm station near the centerline, for example, less than one percent of the fluid parcels have simultaneously high temperature and high velocity.

Summary. Non-intrusive two-color laser anemometry has been used to perform a flowfield characterization of a model complex-flow combustor. This is an important first step toward the establishment of a "pool" of benchmark data on a common complex flow test bed geometry that can be used to (1) evaluate turbulence models, and (2) enhance the general understanding of turbulent processes in practical complex flows.

A technique was used to obtain a direct measurement of Reynolds stress ($\overline{u'w'}$); peak correlation coefficients were on the order of 0.25 which is less than that reported by others (0.40) using indirect measurement methods on somewhat different complex flow geometries.

Root-mean-square velocity results indicate that for this flow u-w isotropy is a reasonable engineering assumption. Except in a few regions (e.g., the area of the fuel jet), the values of u_{rms} and w_{rms} are generally within 20%.

The effect of reaction was to increase turbulence intensity levels and the equivalence ratio was observed to have a significant effect on the size and form of the recirculation zone. Fuel injection techniques, investigated in previous work (Brum and Samuelsen, 1982a), indicate that "tailoring" fuel distribution to the recirculation zone shape is important in controlling soot production. In the present work, quantitative flowfield measurements verify that the increased visible soot production at an equivalence ratio of $\phi = 0.2$ corresponds with a deflection of part of the fuel jet towards the relatively oxygen deficient core of the recirculation zone. Fuel injection techniques which insure the placement of fuel into the

outer shear layer of the recirculation zone reduce the dependence of sooting propensity on equivalence ratio.

There is evidence of "form intermittency" of the recirculation zone which can take one of two forms: (1) a spiralling action of the vortex center, and (2) a fluctuating interaction between the fuel jet and the recirculation zone. The magnitude of this intermittency, particularly the latter, is higher reacting flow and a function of equivalence ratio. When measured with a stationary LA probe, this form intermittency manifests itself in the form of increased turbulence intensity levels; this component tends to "dilute" the Reynolds stress correlation coefficient.

Compensated fine-wire thermocouples can be used to measure time-resolved temperature along with axial and tangential velocity in a complex flow, swirl-stabilized combustor but precautions are required, especially with respect to probe perturbation and survivability. Different probe configurations and different probe orientations must be used in the various regions of the flow to minimize probe perturbation. The sensor size required to survive in the flow depends on the mean temperature and velocity intensity and must be increased in high temperature, highly turbulent regions. In the high temperature core of the recirculation zone, the time constant cannot be accurately measured due to probe failure during the overheating process.

The mean temperature is nearly constant in the recirculation zone with peaks approximating the maximum adiabatic flame temperature. Further downstream, mixing of hot products with unreacted swirl and dilution air takes place and a gradient in the mean temperature develops in the central region. Axial heat fluxes in the central region are negative, reflecting a large population of high temperature, low velocity fluid from the recirculation region. The swirl velocity is shown to increase this population by inducing a

transport of low density, high temperatures fluid to the axis.

Detailed information is available on the two-component Laser
Anemometry data in a Ph.D. Dissertation (Brum, 1983). One paper has been
presented (Samuelsen and Brum, 1982b) and a second has been invited for
presentation at the Symposium on Experimental Measurements and Techniques in
Turbulent Reactive and Non-Reactive Flows, ASME 105th Winter Meeting (Brum and
Samuelsen, 1984b). A tabulated data set is available (Brum, 1983).

Four papers have been presented on the combined velocity-temperature
measurements (Brum, et al., 1983; Seiler, et al., 1983; Samuelsen, LaRue, and
Seiler, 1984; LaRue, Samuelsen, and Seiler, 1984) and one paper has been
accepted for publication (LaRue, Samuelsen, and Seiler, 1984). Detailed
information is available in a M.S. Thesis (Seiler, 1983a). A tabulated data
base is provided in Seiler (1983b).

4.3 Element C: Supplemental Studies

4.3.1 LA Seeder Development

Introduction. In non-premixed combustion systems, fuel and oxidant
a injected into the reaction chamber via two or more separate stream.
Velocity measurements by laser anemometry within the chamber may be biased by
individual streams unless the seeding concentrations of both streams are
uniform and constant. The present study addressed the development of a seed
generation technique for combusting flows and the evaluation of its
performance in providing both a steady rate of injection and a uniform
volumetric seed concentration for a combustion chamber featuring multiple
stream injection.

Particle Generator. The particle generation seeding system is
schematically depicted in Figure 19a. Air is delivered at line pressure
(~60 psig) to a dryer (Wilkerson Model X03-02-000) for the removal of residual

97

a) Seeding System
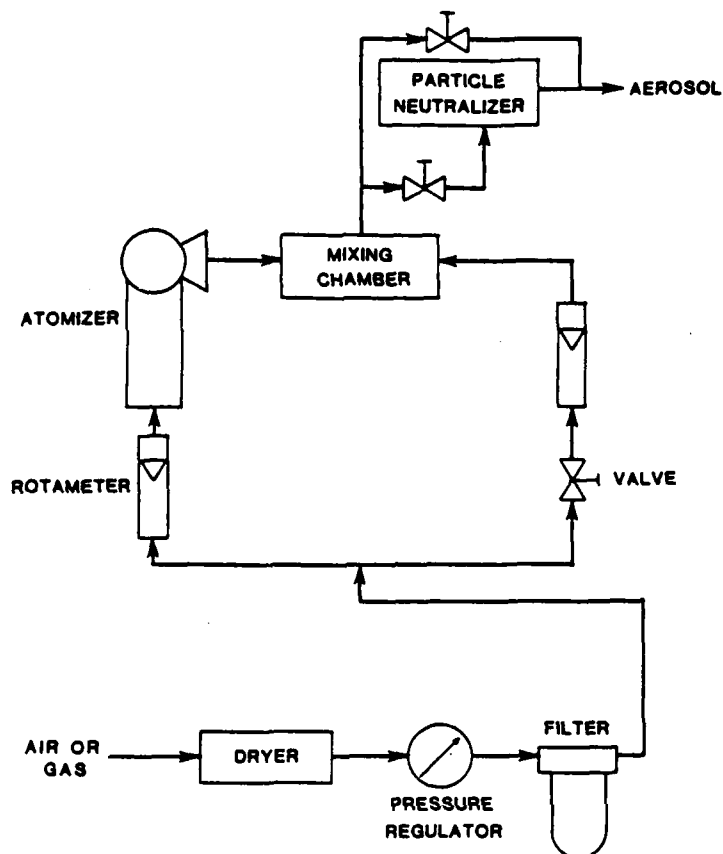
b) Particle Rate Measurement System
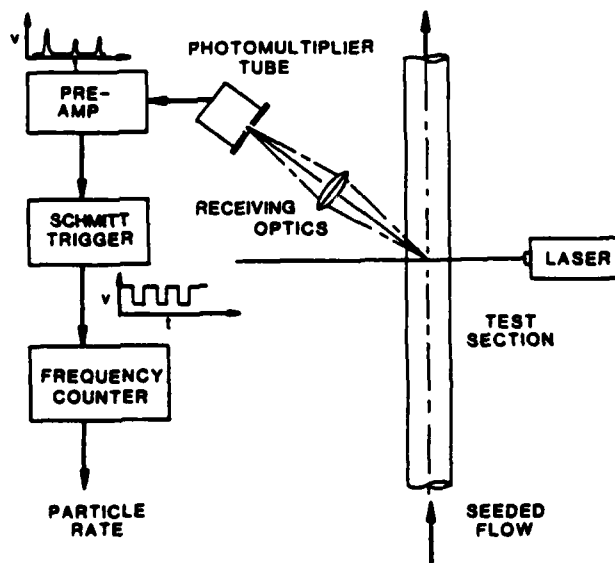
Figure 19. LA Seeder Results

c) Particle Generator Rate

DEPENDENCE ON TIME
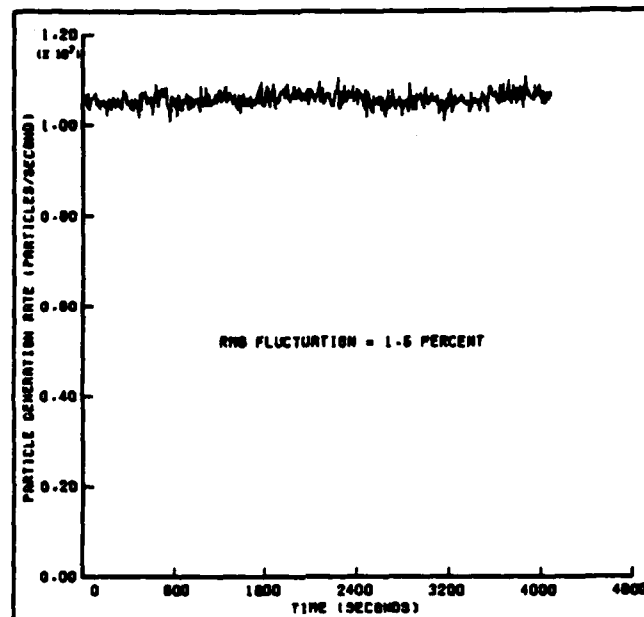
DEPENDENCE ON ATOMIZER DIFFERENTIAL PRESSURE
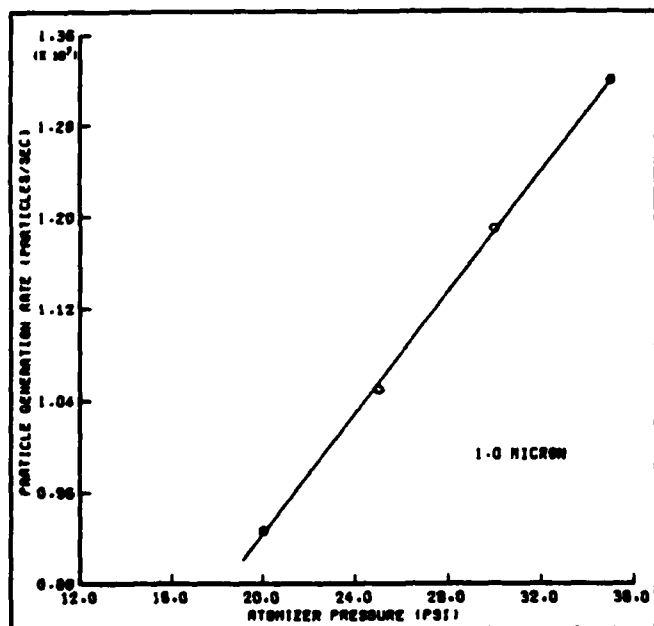
DEPENDENCE ON SUSPENSION CONCENTRATION
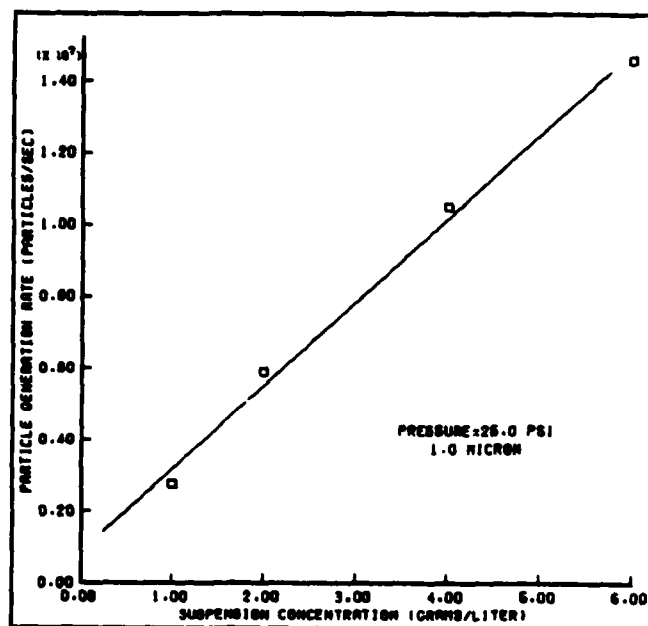
Figure 19. (concluded)

99

moisture. The air is then channeled through a high-quality filter (Balston DQ Grade), capable of 90% retention of 0.6 μm, to remove undesirable residue. The air pressure is regulated (Norgren Type R-11), usually 20-30 psig, to provide atomization conditions specified by the atomizer (RETEC X70). The atomization air and the secondary air are metered by rotameters (DWYER Models RMB-51 and RMB-54), ordinarily in 10:1 secondary to atomization air proportions. A suspension of metal oxide (aluminum oxide, Al_2O_3, in the present case) and deionized water is agitated by a magnetic stirrer to provide a uniformly mixed suspension. The suspension is mixed in proportions, usually 4 g/l, that minimize the probability of having multiple particles per drop. The atomizer produces an aerosol with a mass median diameter (MMD) of 5.1 μm with a geometric standard deviation of 2 μm. After atomization, the aerosol is carried to a mixing chamber. The secondary air is injected tangentially into the mixing chamber to induce mixing and decrease the humidity of the seeded flow. The capability of charge neutralizing the aerosol is also provided by passing the aerosol through a radiation flux produced by a 10-mC vial of Krytpon-85 gas (3M Model 3B4G).

System Evaluation. Light scattering refractory particles of sufficient size to provide adequate light but small enough to follow the flow are required for laser measurements. Thus, 1.0 μm-diam Al_2O_3 particles were selected for the present case to provide adequate scattering and representation of fluid velocity.

Al_2O_3 particles nominally sized at 1.0 μm and 1.5 μm were used. The actual size of generated particles was determined by a scanning electron microscope (SEM). Micrographs established that the nominal 1.0 μm amorphous Al_2O_3 particles were substantially smaller, approximately 0.1 μm. The significant variation from the quoted size in the 1.0-μm Al_2O_3 case was due

to the morphology of the Al_2O_3. Amorphous Al_2O_3 is composed of agglomerations of ~0.1-μm particles having an average agglomerated diameter of 1 μm. When Al_2O_3-H_2O suspensions are atomized and the moisture evaporated, the resultant particles are considerably smaller than the quoted size. In hot flow cases, the sudden heating breaks apart the remaining agglomerations that are of sufficient size to be useful, causing poor signal quality and data rate. Conversely, because of the crystalline structure of the 1.5-μm Al_2O_3 particles, there was little degradation in size due to either atomization or thermal effects.

Once it was determined that the 1.5-μm particles were to be used, a particle neutralizer was employed to assess the effect of neutralizing the charge of the aerosol. The particle neutralizer in the present tests had no significant effect on the size of the generated particle.

Particle Generator Performance. The particle generation rate was examined by utilizing the laser system shown in Figure 19b. A single beam (green, 514.5 μm) of an argon ion laser was collimated, focused, and directed through the combustor test section. Light scattered by particles passing through the laser beam at the center of the duct was focused onto a 0.25 mm-diameter aperture of a photomultiplier tube located at a 25° angle to the laser beam. The output of the photomultiplier was amplified and fed into a Schmitt Trigger which provided TTL level pulses to a frequency counter. The number of particles passing though the area of sensitiviy was recorded in ten second intervals and scaled by the area ratio (18,000:1) of the test section to the sensint area to obtain a total particle generation rate.

Particle generation rate data are presented in Figure 19c for a period of time exceeding 1 h. Using a 4 g/l Al_2O_3-H_2O suspension, 25-psig atomizer pressure, and 10:1 dilution ratio, the mean generation rate is 1.1 x

10^7 particles/s with rms fluctuation of 1.5%.

In order to match the volumetric concentration of independently seeded streams, a parameteric variation on the atomization seeding system was conducted. The particle generation rate was recorded for two conditions: (1) fixed suspension concentration with varying differential pressures across the atomizer and (2) fixed atomizer differential pressure with varying suspension concentrations. The generation rate was found to vary linearly with both atomizer differential pressure and suspension concentration (Figure 19c) for the operating conditions considered.

One question with respect to this technique of seed generation is the amount of moisture introduced by the atomization process. At a 10:1 dilution ratio, the relative humidity at the output of mixing chamber is about 50% at 72°F (0.8 weight percent of water). Since the aerosol is further diluted by an additional 10:1 when introduced into each stream entering the reactor, the presence of the moisture is considered negligible.

Summary. A particle generation system has been designed and successfully employed to introduce seed in uniform concentration to flows typical of nonpremixed combustors that feature multiple stream injection. An assessment of the system performance resulted in the following observations:

(1) Particle generation rates on the order of 10^7 particles/second can be produced at a steady rate over prolonged periods of time.

(2) rms fluctuatons of 1.5% in particle generation rate are typical for operating periods in excess of one hour.

(3) Particle generation rate is linearly dependent on (a) atomization differential pressure for fixed suspension concentration, and (b) suspension concentration for a fixed atomizer differential pressure.

(4) Crystalline rather than amophorus aluminum oxide is preferable to

ensure control over the final size of the seed particulate.

Details are provided in Ikioka (1982) and Ikioka, Brum, and Samuelsen (1983).

4.3.2 Dump Combustor

Introduction. The application of dump combustor configurations in ramjets has prompted interest in the fluid dynamics involved. As part of this effort, the UCI combustion laboratory has performed an exploratory analysis of an axisymmetric sudden expansion dump combustor utilizing a one-component laser velocimeter. The objectives were to (1) develop insight into the aerodynamics of the flowfield for both non-reacting and reacting flows, and (2) develop a database for the purpose of model evaluation and development. This task was performed under a special funding work order added to the present AFOSR grant by the Ramjet Division at the Air Force Wright Aeronautical Laboratories (AFWAL/PORT) with Dr. F.D. Stull as the technical monitor.

Experiment. The experimental dump combustor is comprised of a two-inch stainless steel inlet section which dumps into a larger quartz test section (see Figure 20a). The quartz section is removable and is capable of accommodating an 80 mm (3-inch) and 102 mm (4-inch) diameter tube. The section is 91 cm (3-feet) long, a length selected to contain the flame. These systems are typically operated at high pressures through the use of a choked exit nozzle. Because of the air flowrate limitation of the UCI facility and the safety problems inherent to the quartz test section, the experiment was performed at atmospheric pressure, thus, negating the need for an exit nozzle.

The laser velocimetry measurements were performed utilizing the UCI Combustion Laboratory laser anemometer system (Figure 3b) operating in the single component (axial) mode.

The experimental test configuration and test conditions are tabulated in Table V. The velocity measurements were performed at 17 axial stations spaced at 2 cm intervals beginning 1 cm downstream of the dump plane. At each axial station, radial traverses were made at 5 mm intervals. The reacting flow, however, was limited to 9 axial stations due to a low data rate.

In addition to the low data rate exhibited by the hot flow run, radiative heat transfer presented experimental challenges, the worst being heat transfer to the photomultiplier assembly. This was alleviated by increasing the focal length of the receiving lows to 250 mm from 120 mm, constructing a radiative heat shield with asbestos backing and by cooling the optics with an air convection system.

Results. Computer generated plots of axial and radial velocity profiles are presented in Figure 20b for the COLD cases. From the radial plots, one can see evidence of the outer recirculation zones associated with the sudden expansion. In the baseline 15 m/s case, a second recirculation zone is apparent. Also, the shear layer between the recirculation zone and the main flow is indicated by high rms velocity levels. Downstream of the recirculation, the velocity profiles approach that of turbulent pipeflow with decreasing values of RMS velocity.

The recirculation zone in the core of HOT flow remains unchanged (Figure 20c). The point of reattachment occurs at approximately 7 step heights downstream of the dump plane. Note the acceleration of the outer gases. This is attributed to the reactants of combustion passing normally through the conical flame front, reacting, and expanding.

Results are detailed in Roman and Samuelsen (1982) and Roman (1984).

TABLE V

– Dump Combustor Test Configurations and Test Conditions –

CONFIGURATION	d_1 mm(inch)	d_2 mm(inch)	d_1/d_2	$A_1/A2$	L mm(inch)	L/d
Baseline	51(2)	80(3)	0.667	0.44	91(36)	12
Off-Baseline	51(2)	102(4)	0.500	0.25	91(36)	9

MODE	RUN	VELOCITY m/s	ϕ	CONFIGURATION
COLD	V1	2.5	NA	Baseline
	V2	15	NA	Baseline
	V3	7.5	NA	Off-Baseline
HOT	H1	7.5	0.7	Baseline

a) Combustor Configuration
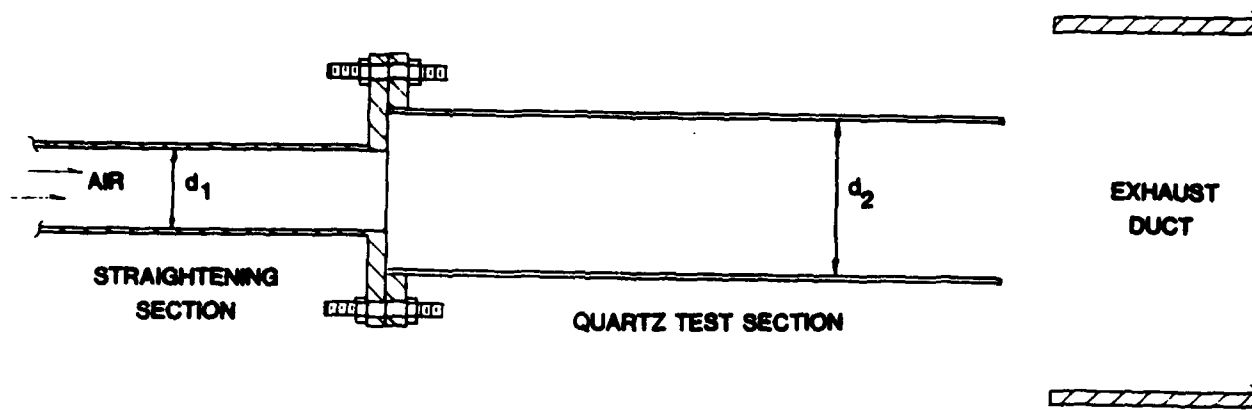
b) Axial and Radial Profiles: COLD Cases

● $A_1/A_2 = 0.44$

7.5 m/s

VELOCITY= 7.500
PHI= N/A
COLD

MEAN
●——— 10. M/S
U=■

RMS
●——— 10. M/S
U=+

LEGEND
■ = MEAN VELOCITY
+ = RMS VELOCITY
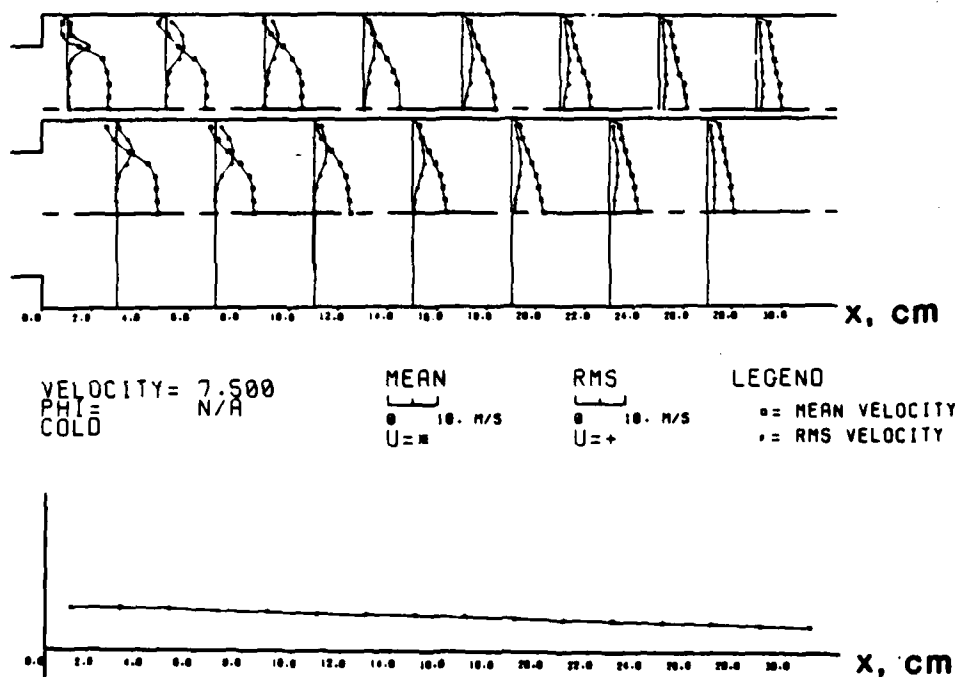
Figure 20. Dump Combustor Results
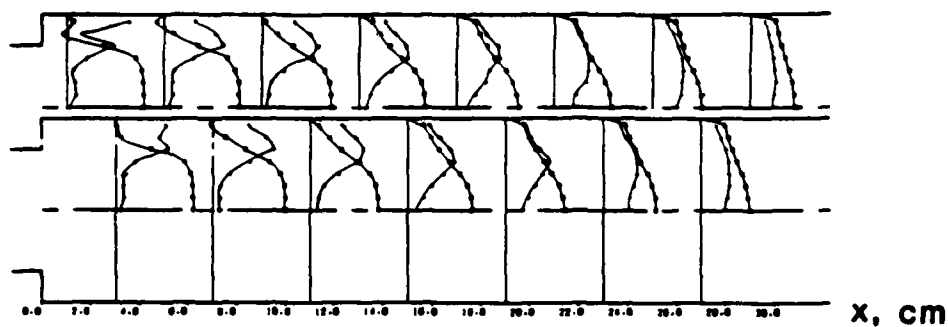
106
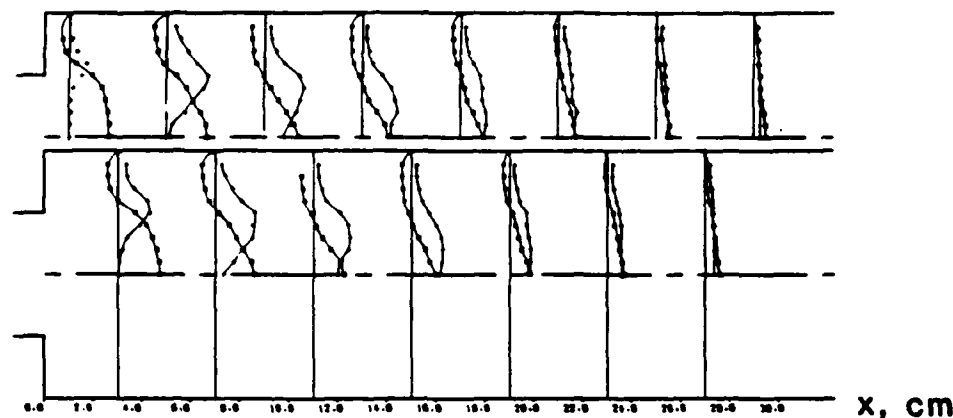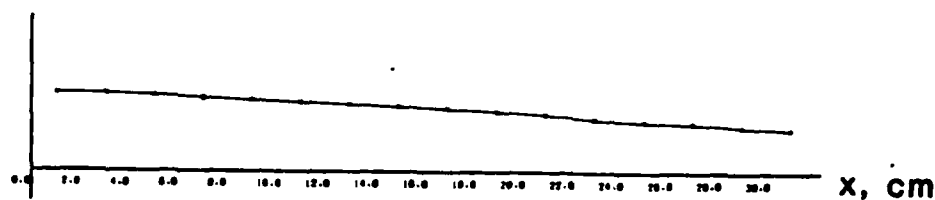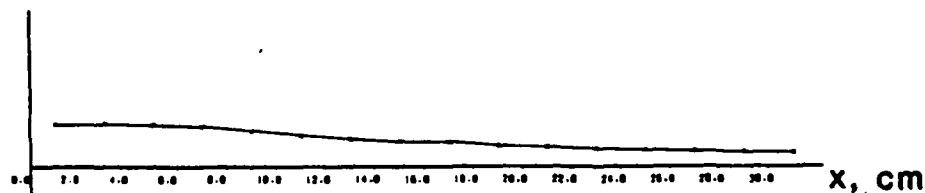
Figure 20. (continued)

c) Axial and Radial Profiles: HOT Case

● A_1/A_2=0.44

7.5 m/s

VELOCITY= 7.500
PHI= 0.700
HOT

MEAN
|—|—| 18. M/S
0
U=*

RMS
|—|—| 18. M/S
0
U=+

LEGEND
□= MEAN VELOCITY
•= RMS VELOCITY
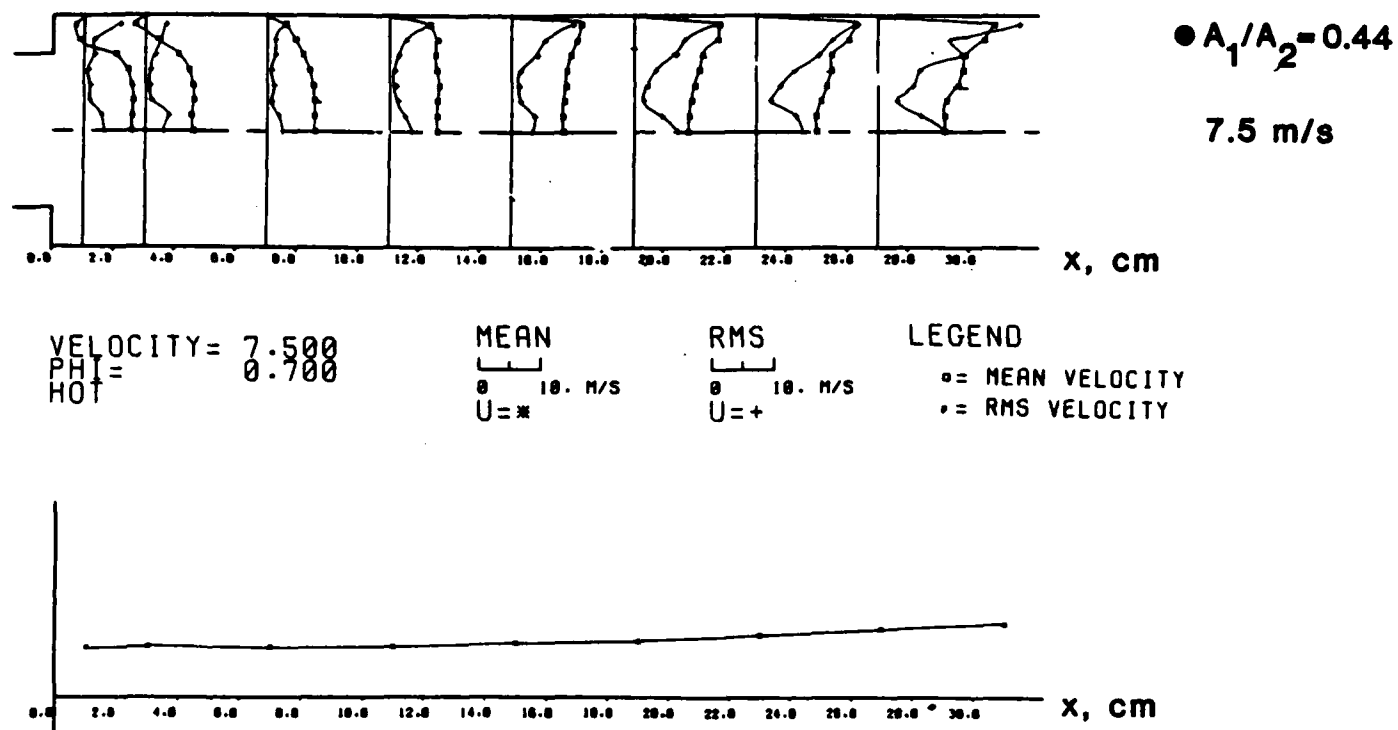
Figure 20. (concluded)

108

4.3.3 NO Sampling

Introduction. To assess the conditions under which transformations of nitrogen oxides (NO and NO_2) may occur in a gaseous sample probe, a controllable laboratory experiment was designed and used in an earlier study to systematically establish the conditions under which NO and NO_2 could be transformed and the extent of transformation (Benson, Samuelsen, and Peck, 1976; Samuelsen and Harman, 1977; Benson and Samuelsen, 1977; Samuelsen and Benson, 1979). Under the present AFOSR program at the UCI Combustion Laboratory (Grant 78-3586), the Environics Division of the Air Force Engineering and Services Center (AFESC/RDV) provided supplemental funding to modify the experiment to (1) include water vapor in the simulated combustion products, (2) provide more precise control over the temperature and history of the pollutant mixture prior to sampling, and (3) simulate gas turbine exhaust products as well as reacting zone gases, automobile exhausts, and boiler flue gases.

The experiment was successfully modified and operated. Various compositions of simulated exhaust gases, including those representative of gas turbine exhausts, were run through sample probes of varying materials and analyzed for nitrogen oxide transformations. This analysis was performed for various probe temperatures over a range (150°C to 400°C) typical of the temperatures experienced by probe materials in practical systems.

Trials were run using 2 m (79-inches) long, 6.35 mm (0.25-inch) OD tubing, and performed with and without water addition. Quartz and 316 stainless steel were the principal materials evaluated although Inconel-600 and Nickel-200 were considered as well. Type 316 stainless steel (316 SS) is the material commonly used for sampling purposes. Tubing stock and fittings are readily available, 316 SS is durable yet easy to bend during fabrication,

and the stainless quality is resistent to corrosion. However, this resistence does not preclude surface reactions that could alter the composition of a sample. Quartz tubing, in contrast, is inert to surface attack and, as a result, is attractive for sampling. However, the vulnerability of quartz to breakage renders the material impractical except for the most controlled conditions. To assess whether durable, metallic tubes are available which are less reactive than 316 SS to sample composition transformation, two nickel-containing tube materials were selected: a nickel tube (nickel-200) and an alloy of nickel (inconel-600). An investigation of stainless steel composition (Samuelsen and Harman, 1977) had indicated that the nickel content may be associated with an increase in resistivity to transformation.

Experimental. Carrier gases representative of boiler and automotive exhaust, as well as combustor reaction zones are herein referred to as STANDARD carriers; those representative of turbine jet engines are referred to as the carrier TURBINE. Compositions and concentrations of the carriers, presented in Table VI, were established based upon surveys of practical devices (Samuelsen and Harman, 1977; Samuelsen, Hamberg, and Osborn, 1978). All STANDARD carrier gases (exclusive of water and propylene) were mixed and supplied in gas cylinders by a commercial vendor. Propylene and water, if selected, were added during the experiment. The TURBINE carrier gas was also supplied by a commercial vendor except for the water, methanol, and propanol, each of which was added in the conduct of the experiment. The baseline composition was selected based on exploratory tests on the condition for which NO and NO_2 transformation was most likely.

The experimental system is shown in Figure 21a. The experiment is performed in three steps: gas preparation, probe exposure (with sampling

110

before and after the exposure), and analysis. The gas preparation begins by selecting the appropriate carrier gas by means of a toggle switch located on the control panel. Upstream carrier gas pressures are maintained constant to generate a steady flow of 7 ℓ/min. The bulk of the flow is bubbled through three 500 ml fritted glass water towers to ensure saturation if water addition ("wet trial") is to be performed. The temperature of the water in the towers is set and maintained constant per each trial to achieve the desired water concentration. For a dry trial, this carrier flow is routed around the water towers. For the TURBINE tests, a portion of the carrier is routed through Erlenmeyer flasks (1 ℓ) used to house liquid methanol and propanol.

Enroute to the furnace from the water towers, heating tape is wrapped around the Teflon tubing to prevent premature water condensation. In the furnace (Lindberg Model #51828), the carrier gas is circulated until it reaches the set furnace temperature. At this point, the carrier stream enters a mixing venturi, where the pollutant gases (NO, NO_2 and C_3H_6, if selected), are introduced in the proper amounts from high-concentration sources by means of flow restrictors. A sample (3 ℓ/min) is extracted immediately after mixing is completed. (This sample location is referred to as SP2.) A flow of 4 ℓ/ min is run though the probe to be tested. At the end of the probe, another 3 ℓ/min sample is extracted at sample point SP3, leaving 1 ℓ/min to vent.

Temperatures are monitored at SP2, SP3, in the furnace, and just downstream of the water towers; pressures are monitored at SP2, SP3, and just upstream of the water, methanol/propanol addition system. In addition, the carrier gas flow rate is monitored just upstream of the water/methanol/propanol addition system.

111

TABLE VI

- NO Sampling Carrier Gas Composition -

Carrier	Composition					
	CO_2 %	O_2 %	H_2O %	HC ppm	NO ppm	NO_2 ppm
STANDARD	12	5	0, 14	0	500	75
	12	5	0, 14	500 propylene	500	75
	12	0	0, 14	500 propylene	500	75*
	12	0	0, 14	0	500	75
TURBINE	4	14	0, 5	18 methane	500	75
				0.5 butane		
				34 ethylene		
				12 propylene		
				2.5 I-butene		
				30 methanol		
				3 propanol		

* Baseline composition (0% O_2, 500 ppm HC, 0% water)
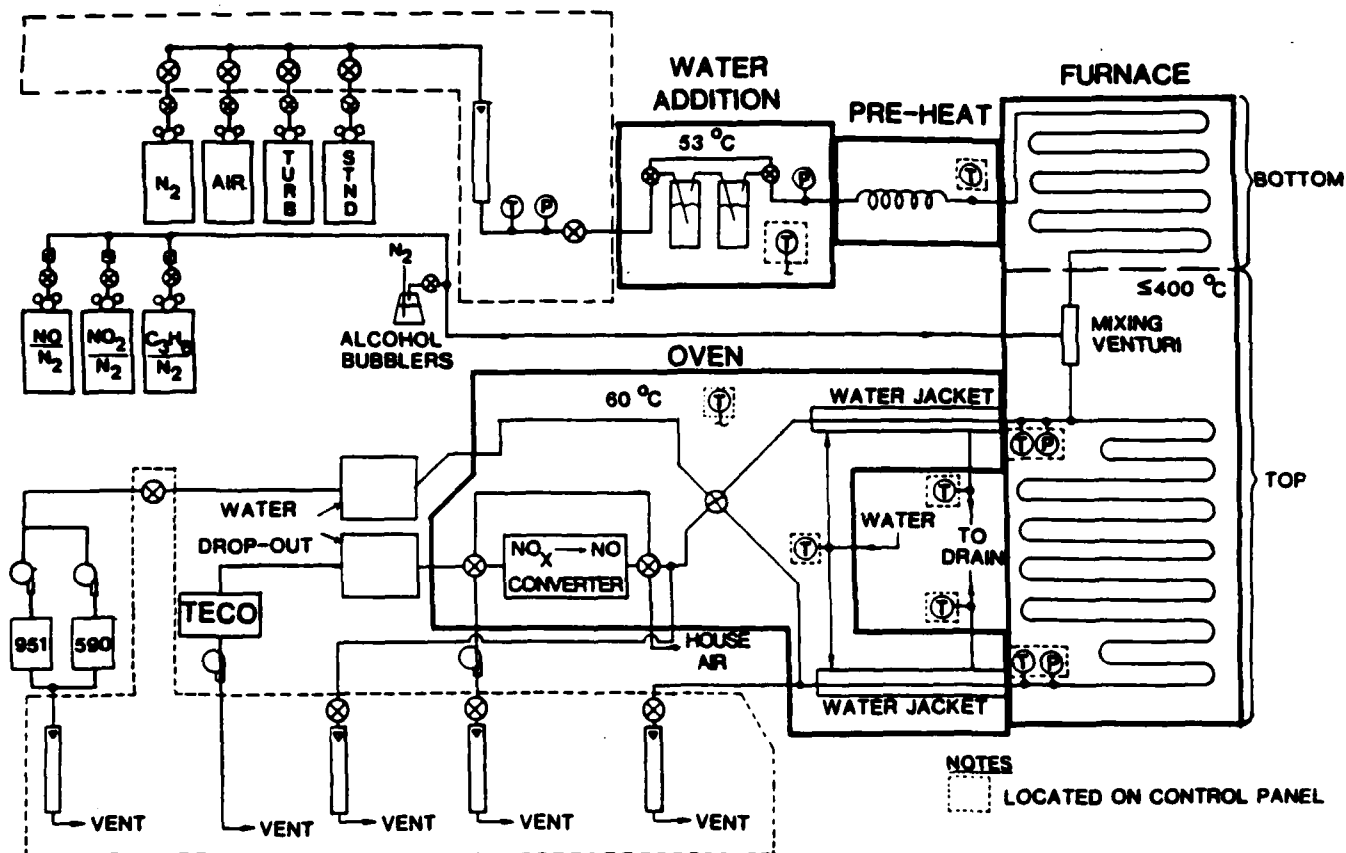
Figure 21.   NO Sampling Results

b) Sequential Exposure Cycles
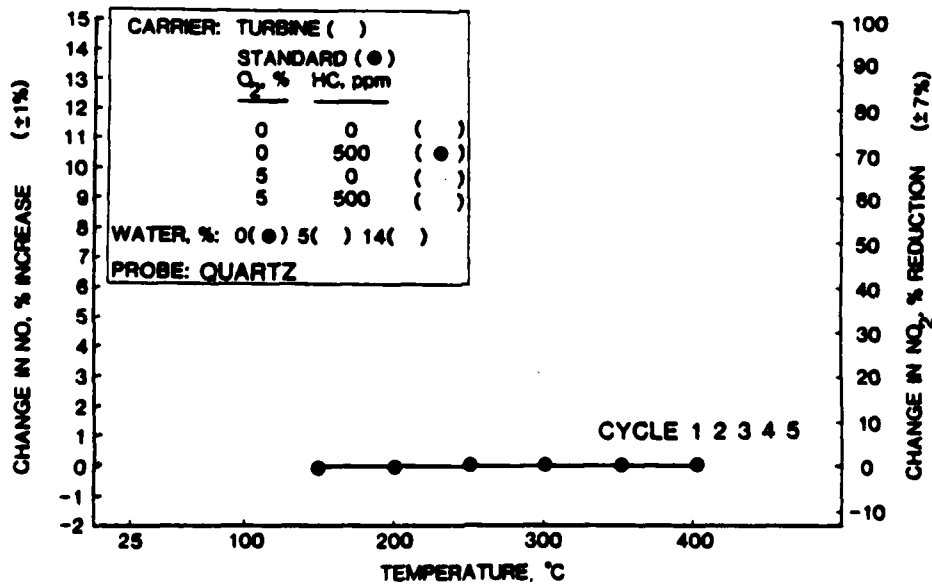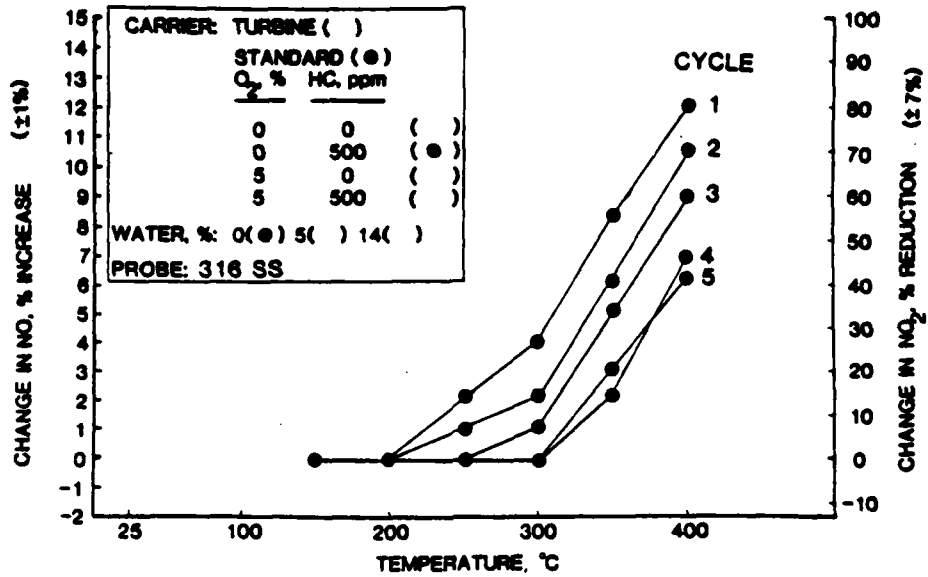
Figure 21. (continued)

c) Effect of Carrier Composition

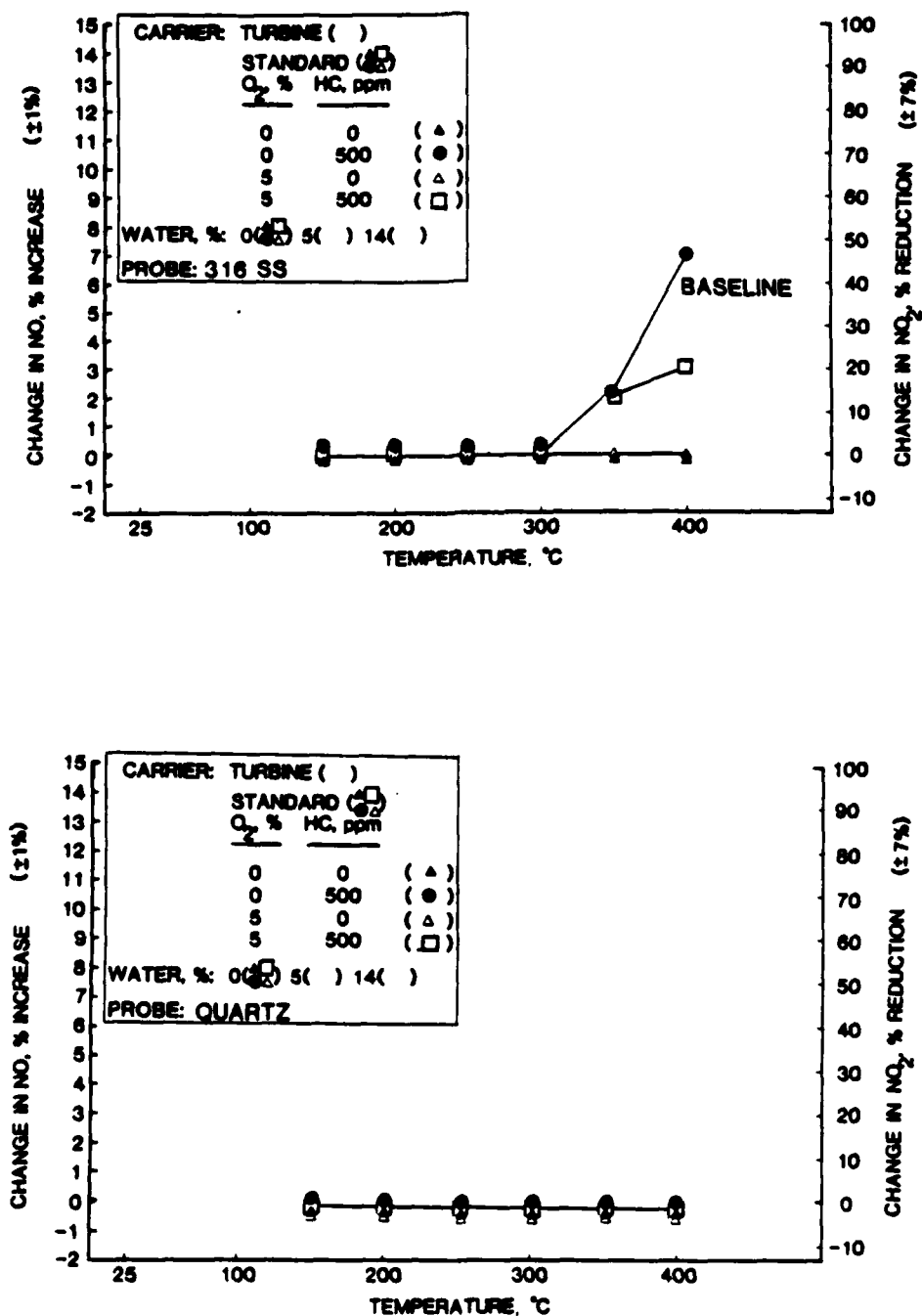Figure 21. (continued)

115

Figure 21. (continued)

116
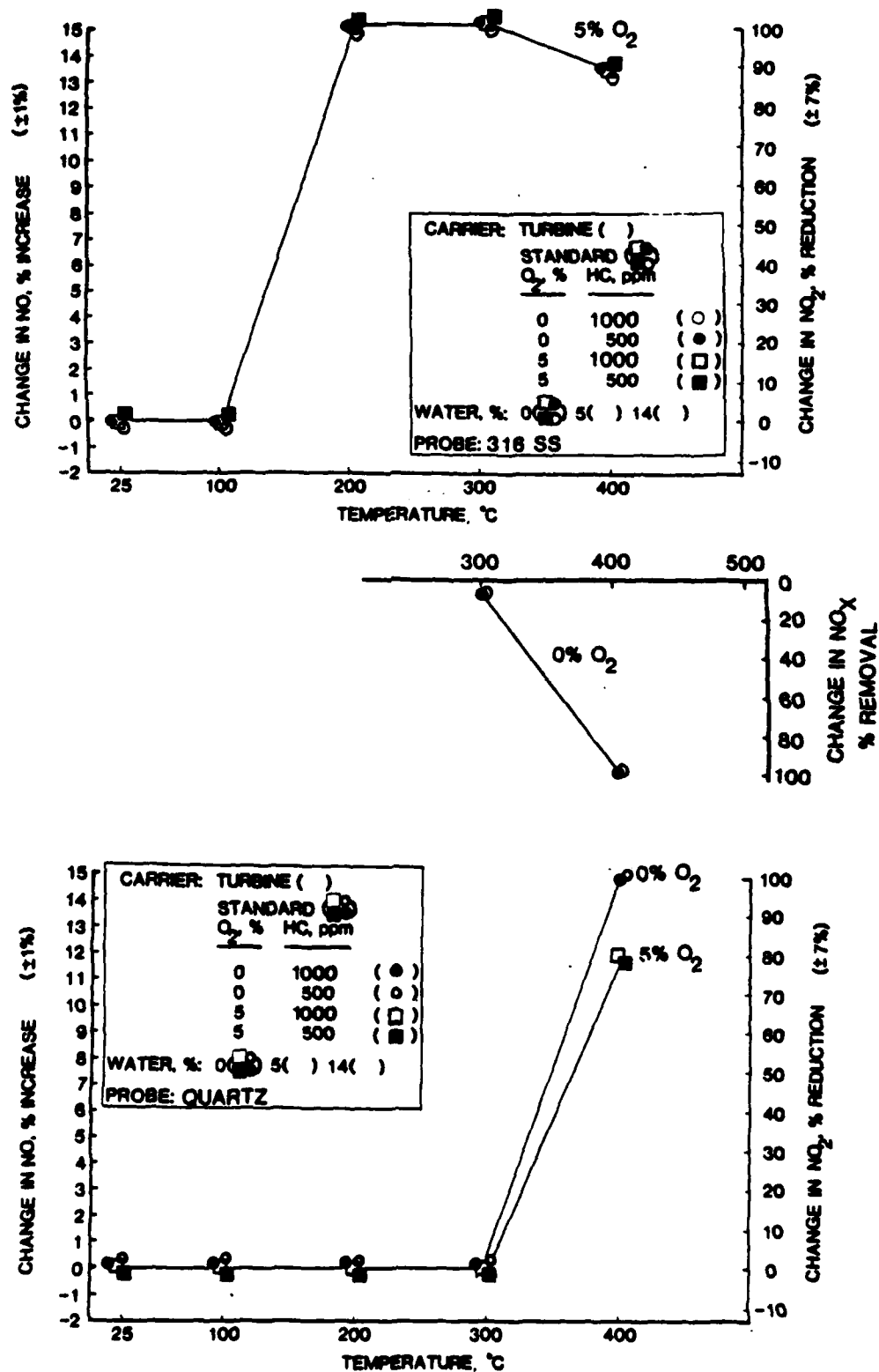
e)   TURBINE Carrier

Figure 21.   (continued)

117
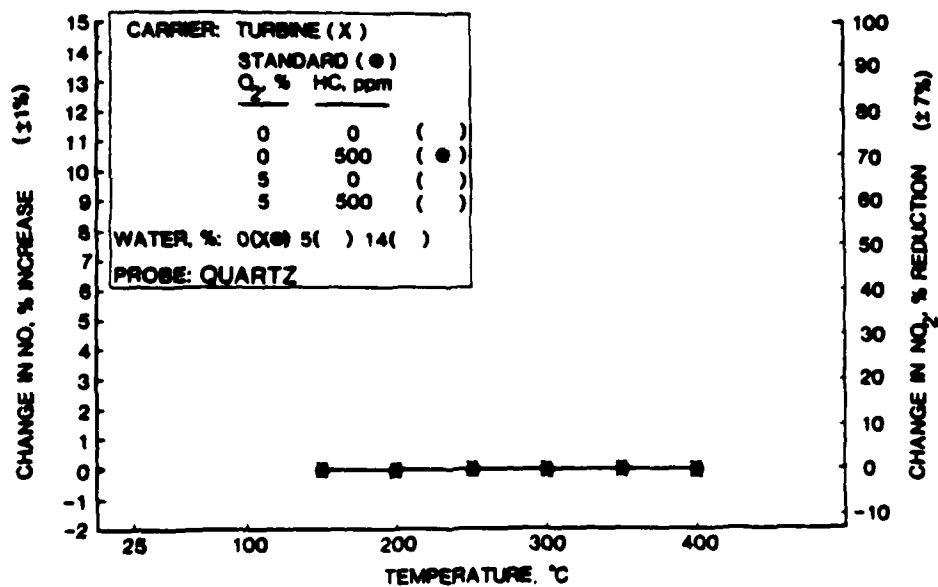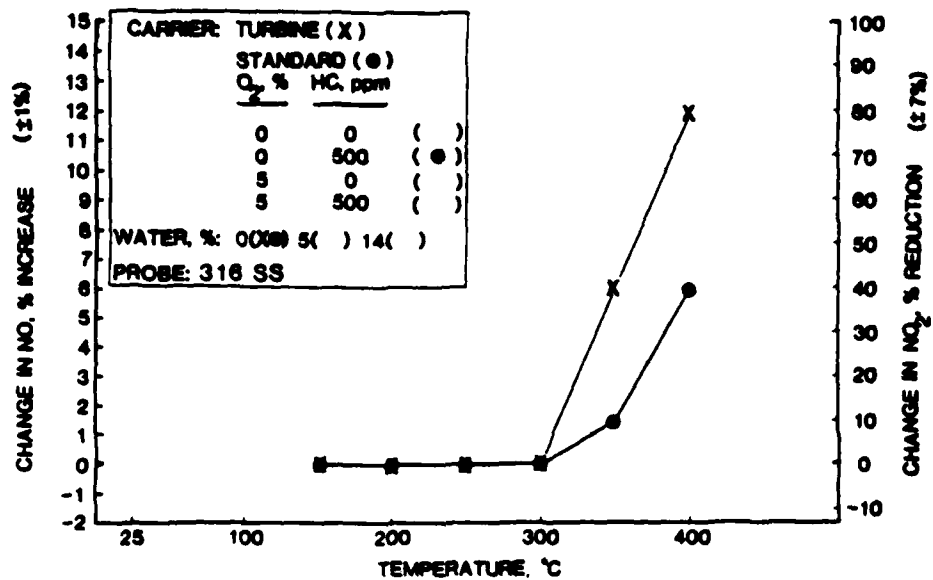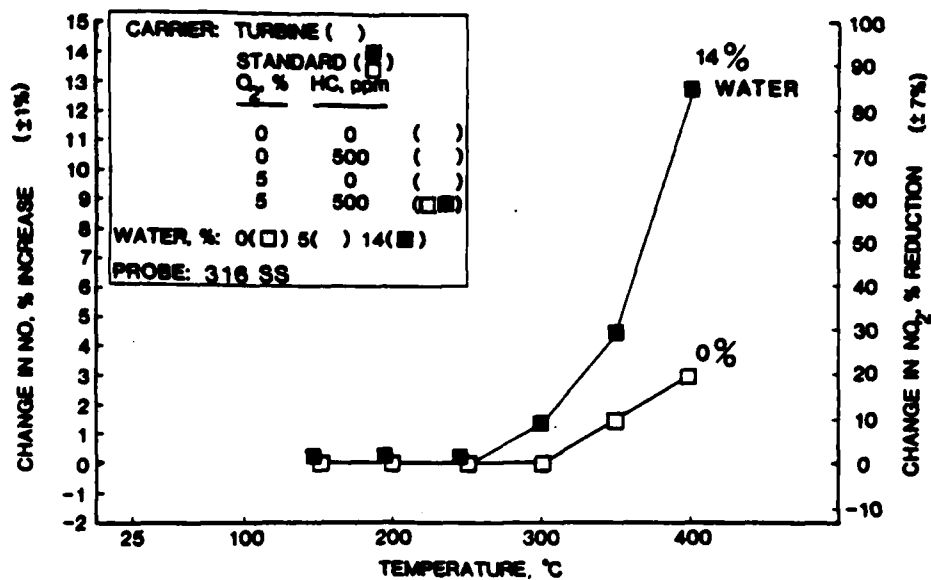
f) Effect of Water

g) Effect of Various Materials
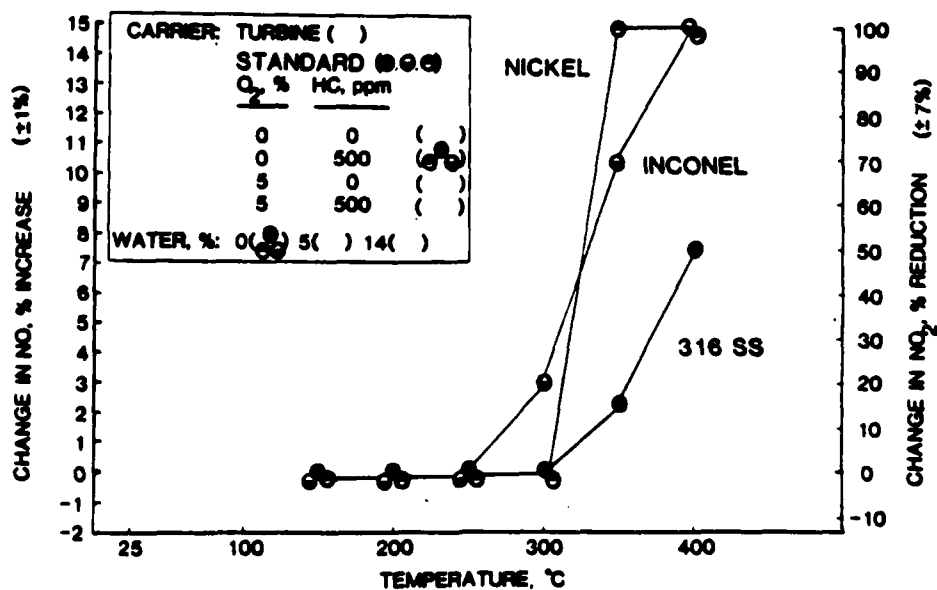
Figure 21. (concluded)

118

The samples from SP2 and SP3 are immediately cooled by water jackets in a specially designed water-cooled quartz extractor to 60°C and transported through the furnace wall and into a Blue M oven maintained at 60°C. The oven houses various solenoids as well as a carbon $NO_2 \longrightarrow NO$ converter. Monitored temperatures include that of the oven, the cooling water (at SP2, SP3, and the mixing venturi), and the converter. The NO_x converter jacket temperature is controlled by a constant input voltage from a variac, and the cooling water flow rate is monitored by a rotameter just upstream of the Blue M oven.

Instrumentation used to analyze the samples includes a TECO Model 10 AR Chemiluminescent $NO-NO_2-NO_x$ Analyzer, a Beckman Model 951 NO/NO_x Analyzer, and a Beckman Model 590 HC/CO Analyzer. From the control panel, the SP2 and SP3 samples can be routed, by means of a solenoid off-on switch, to the TECO or to the Beckman 951. In addition, the TECO sample can be routed through or around the converter. By the use of metering valves and rotameters (located on the control panel), as well as by vents, proper flows through the probe and to the instruments are maintained regardless of the sample path. For the trials in which propylene is introduced, a small portion of the Beckman 951 sample is extracted and routed to the Beckman 590. Water is condensed out of the samples before transportation to the analyzing instruments by means of ice baths.

The experiment is run in the following manner: with the appropriate carrier gas selected, the desired concenterations, if any, of water and methanol/propanol are added, and the NO, NO_2 and C_3H_6 (if selected) are introduced at 55°C to the carrier stream at the venturi port. The temperatures of the cooling water (at SP2, SP3, and at the mixing venturi), the oven, the converter, and the gas just downstream of the water towers are noted. The furnace is set at 150°C and, when this temperature is achieved,

119

the temperature of the furnace, and the temperatures and pressures of SP2 and SP3 are recorded. The following data are collected: a TECO analysis of the SP2 sample with the converter off, a TECO analysis of the SP3 sample with the converter off, a Beckman 951 analysis of the SP2 sample, a TECO analysis of the SP2 sample with the converter on, and a TECO analysis of the SP3 sample with the converter on. The furnace temperature is then incremented 50°C (up to 400°C) and the readings above are repeated. At least four successive probe trials are necessary for the probe response to stabilize.

Results. The combination of sample probe materials and carrier gas compositions are presented in Table VII. The parameters evaluated were probe exposure cycles, probe preconditioning, carrier composition, presence of water, and probe material.

The probes tested are repeatedly cycled through the temperature range described above until a steady-state response is achieved. The chemical transformation observed for all tests conducted is the reduction of NO_2 to NO. "Reactivity" is associated with the change of NO/NO_2 concentrations from the probe inlet (SP2) to the probe outlet (SP3). If NO_2 reduction is experienced in a particular trial, the probe is said to be reactive, with reactivity varying from low to high depending on the extent of NO_2 reduction and the temperature at which it first occurs. The concentration of NO_x (NO + NO_2) is also monitored and found to be conserved in all the tests reported here; although in previous work, as noted below, destruction of NO_x was observed at the elevated test temperatures.

An example of sequential exposure cycles of a 316 stainless steel probe is presented in Figure 21b for the baseline case in the STANDARD matrix. The initial reactivity of the probe is very high (cycle 1) with an 80% reduction of NO_2 to NO and the first evidence of change at 250°C. By the

TABLE VII PROBE TYPES AND CARRIER COMPOSITIONS TESTED

Probe Type	Case	Carrier							
		STANDARD						TURBINE	
		O_2, %		HC, ppm		Water, %		Water, %	
		0	5	0	500	0	14	0	5
316 SS, or	1	●		●		●			
Quartz	2	●		●			●		
	3		●	●		●			
	4		●	●			●		
	5	B[a]			B	B			
	6	●			●		●		
	7		●		●	●			
	8		●		●		●		
	9							●	
	10								●
Inconel-600, or Nickel-200	11	B			B	B			

[a] Baseline composition

fifth cycle, the NO_2 reduction stabilizes to approximately 40%, and the first evidence of change occurs at 350°C. This behavior is typical of all the metal probes tested. Generally, 3 to 5 cycles are required for a repeatable response to be achieved. In contrast, quartz exhibits no change from that measured for the first cycle.

For the results reported below, the probes were tested as received from the supplier. However, preliminary tests were conducted on 316 stainless steel to evaluate the effect of washing the probes prior to testing. The probes were washed with trichlorylethylene, rinsed with methanol, and dried at room temperature. Probes washed in this fashion proved to be more reactive. Extensive discussions with manufacturers of stainless steel tubes lead to the conclusion that this washing procedure removes residual dirt and grease from the inner tube surface, thereby exposing more sites to contribute to the initial reactivity. The decision to use probes as received (rather than washed) for the principal tests was predicated on the likelihood that those probes used in practical systems are installed as supplied.

The composition of the carrier gas was found to be a major factor in establishing the reactivity of the 316 stainless steel. The results for the STANDARD carrier (Table VI) are summarized in Figure 21c. The reactivity is highest for the baseline case, lower for the case where both oxygen and propylene are present, and inconsequential in the absence of the propylene (for both 0 or 5% oxygen). In contrast to the 316 stainless steel, the quartz tube is virtually nonreactive for all STANDARD carrier compositions. It is noteworthy that the 316 stainless steel and quartz reactivity is less than that observed and reported from the earlier experiment (Samuelsen and Benson, 1979), an example of which is presented in Figure 21d. Two factors lead to the higher reactivity in the previous work. First, the temperature was not

controlled as well as in the present experiment. The probe was heated in a Lindberg tube furnace rather than in the current box furnace. As a result, the probe experienced uneven heating. An investigation of the heating variation revealed that, at a 400°C set point, the probe could locally heat to 600°C at locations where the tube was in the vicinity of the heated filament. The design of the present experiment ensured that the temperature of the probe was maintained isothermal at the set point. Second, the sample extracted at SP2 and SP3 was not immediately cooled in the previous experiment and reaction could persist in the sampling tube. In the present experiment, the design of the sample ports included water-cooling to immediately quench the reaction.

The results for the TURBINE carrier are presented in Figure 21e. The results are similar to the STANDARD carrier where both oxygen and hydrocarbon are present albeit in differing amounts. The first transformation observed occurs at 300°C and reaches a 45% reduction of NO_2 at 400°C in 316 stainless steel.

The results reported above were obtained dry (i.e., 0% H_2O). To assess the effect of water, trials were also conducted with the water concentrations listed in Table VI, 14% H_2O for the STANDARD carriers, and 5% H_2O for the TURBINE carrier. The presence of water had no significant impact on reactivity for the STANDARD carriers in 316 stainless steel except for the case where both oxygen (5%) and hydrocarbons (500 ppm C_3H_6) are present. Here, the presence of water substantially increased the reactivity (Figure 21f), from 20% to 85% reduction of NO_2 at 400°C. The impact of water in the 316 stainless steel on the TURBINE carrier, which has a higher oxygen (14%) and lower hydrocarbon (~ 80 ppm), was not significant. In quartz, the water had no impact. The quartz is virtually passive for all carriers tested.

Various metallic materials were tested in addition to the 316 stainless steel to determine if available alternatives to quartz would suppress the reduction of NO_2 at elevated temperatures. Both nickel and inconel tubes were tested with negative results (Figure 21g). Both materials exhibited substantially higher reactivity than the 316 stainless steel.

Conclusions. NO_x is conserved in 316 stainless steel and quartz tubes up to 400°C. Above 400°C, NO_x can be destroyed.

The ratio of NO_2/NO is conserved up to 300°C in 316 stainless steel and 400°C in quartz. The present results were not changed appreciably by the presence or absence of water with one notable exception. In the stainless steel, the reactivity of the probe (reduction of NO_2 to NO) was significantly increased above 300°C (20-to 85-percent at 400°C) when both oxygen and hydrocarbons were present in the STANDARD CARRIER.

Stainless steel is more rugged than quartz and, as a result, more commonly used as a sampling probe material. The exploration of alternative metallic tube materials, such as nickel and inconel, was not successful in identifying a durable tube material that was less reactive than 316 SS. Both nickel and inconel were more reactive.

Based on the results of this study, quartz is the most desirable material to use for sampling at elevated temperatures. Quartz was inert to all the sample compositions and sample temperatures explored in the present experiment. The one practical exception to the use of quartz is the vulnerability to breakage. Stainless steel tubes with quartz glass linings, available commercially, represent a reasonable solution where sample integrity is a major objective and reasonable handling of the probe can be maintained.

Should quartz or quartz-lined stainless steel not be an option, then type 316 stainless steel is a reasonable alternative. However, if stainless steel

is used at temperatures exceeding 200°C, the tube should be water-cooled to ensure maintenance of sample integrity. Care must be excercised to cool the tube with hot water (> 60°C) to ensure that water in the combustion products does not condense.

SECTION 5

SUMMARY

The development of combustors that are both fuel efficient and fuel
flexible requires spatially resolved measurements of velocity, temperature,
and concentration in complex flows representative of both premixed and non-
premixed systems. Such data are needed to provide the physical insight
necessary to understand the basic processes of turbulent mixing and transport,
and support the evolution of modeling. The goal of the AFOSR program at the
UCI Combustion Laboratory was to develop laboratory model combustors and
experimental methodology suitable for the acquisition of the desired
information. The objectives of the program were:

(1)   To _establish_ and _evaluate_ laboratory model combustors for both
      premixed and non-premixed fuel/air injection suitable for studies
      of the complex flows,

(2)   To _acquire_ spatially resolved flowfield data using state-of-the-
      art diagnostics for the purposes of model verification and
      providing insight into the transport of mass, momentum, and energy
      in complex flows,

(3)   To conduct supplementary studies to support the development of
      methodologies required for measurements in complex flows.

Four combustion modules were considered: the Opposed Jet Combustor (OJC)
for premixed injection and, for non-premixed injection, the Centerbody
Combustor (CBC), the Centerbody Combustor with swirl, and the Dilute Swirl
Combustor (DSC). An evaluation of combustor performance and compatability
with a list of criteria for laboratory complex flow combustors established the
DSC as a viable configuration for non-premixed, complex flow combustor studies

in which swirl was a major aerodynamic feature.

Spatially resolved flowfield data were obtained in each of the premixed and non-premixed modules. Although laser anemometry and flow visualization were the principal diagnostic tools employed, flow mappings of species concentration and temperature were acquired in the OJC for a wide range of operating conditions. Studies in a hydrodynamic (water-channel) facility were also completed for both the OJC and CBC geometries. Extensive two-component laser anemometry data were obtained as well in the DSC including measurement of the Reynolds stress. In a complementary program with the National Science Foundation (NSF), the two-color measurements were combined with a fine-wire thermocouple probe to yield direct measurement of both axial and azimuthal heat flux in the DSC.

Three supplemental studies were completed: LA Seeder, Dump Combustor, and NO Sampling. The LA Seeder study addressed the development and evaluation of a seed generator for laser anemometer measurements in a reacting flow with two or more separate streams of fuel and air. Such flows require refractory particles injected uniformally in each of the individual streams to avoid biasing. The dump combustor study was an independent element to the AFOSR program provided by the Ramjet Division of the Air Force Wright Aeronautical Laboratories (AFWAL/PORT). Single component laser anemometry data were obtained in a dump combustor configuration with two area ratios for both non-reacting and reacting flows. The NO Sampling study, supported by the Environics Division of the Air Force Engineering and Services Center (AFESC/RDV), explored the chemical transformations of nitrogen oxides that can occur while sampling combustion products. The present effort expanded previous work conducted for AFOSR to (1) conduct experiments with more accurate temperature control, (2) consider the presence of water vapor in the

simulated combustion products as well as dry samples, and (3) evaluate

combustion product composition representative of gas turbine exhausts.

REFERENCES

Appleton, J.P., and Heywood, J.B. (1973). The Effects of Imperfect Fuel-Air Mixing in a Mixing in a Burner on NO Formation from Nitrogen in the Air and the Fuel, Fourteenth Symposium (International) on Combustion, The Combustion Institute.

Arcoumanis, D.C. (1980). Water Analog of the Opposed-Jet Combustor: Velocity Field Measurements and Flow Visualization, UCI Combustion Laboratory Report ARTR-80-5, Mechanical Engineering, University of California, Irvine, CA, 92717.

Benson, R.C., Samuelsen, G.S., and Peck, R.E. (1976). Oxides of Nitrogen Transformations While Sampling Combustion Products Containing Carbon Monoxide, WSS/CI 76-11, 1976 Spring Meeting of the Western States Section, The Combustion Institute, Salt Lake City.

Benson, R.C., and Samuelsen, G.S., (1977). Oxides of Nitrogen Transformation While Sampling Combustion Products Containing Carbon Monoxide, Hydrogen, and Hydrocarbons, WSS/CI 77-7, 1977 Spring Meeting of the Western States Section, The Combustion Institute, Seattle.

Brum, R.D. (1983). Evaluation of a Candidate Model Complex Flow Combustor Using Instantaneous Two-Color Laser Anemometry, Ph.D. dissertation, University of California, Irvine, UCI Combustion Laboratory Report ARTR-83-5, Mechanical Engineering, University of California, Irvine, Ca, 92717.

Brum, R.D., Ikioka, L.M., and Samuelsen, G.S. (1981). Axial Flowfield Characteristics of Reacting and Non-Reacting Flows in a Centerbody Configuration, WSS CI 81-34, presented at the Fall 1981 Meeting of the Western States Section, The Combustion Institute, Arizona State University, Tempe, October.

Brum, R.D., and Samuelsen, G.S. (1982a). Assessment of a Dilute Swirl Combustor as a Bench Scale, Complex Flow Test Bed for Modeling, Diagnostics, and Fuel Effects Studies, AIAA Paper 82-1263, Paper presented at AIAA/SAE/ASME Joint Propulsion Conference, Cleveland, Ohio, June.

Brum, R.D., and Samuelsen, G.S. (1982b). Two-Component Laser Anemometry Measurements in a Non-reacting and Reacting Complex Model Combustor, WSCI 82-53. Paper presented at the Fall Meeting of the Western States Section of The Combustion Institute, Livermore, Ca, October.

Brum, R.D., Ikioka, L.M., and Samuelsen, G.S. (1982). Assessment of Candidate Combustor configurations as Test Beds for Modeling Complex Flows, ASME-82-HT-36, Joint Fluids, Plasma, Thermophysics and Heat Transfer conference, AIAA/ASME, St. Louis, Missouri.

Brum, R.D., Seiler, E.T., LaRue, J.C., and Samuelsen, G.S. (1983). Instantaneous Two-Component Laser Anemometry and Temperature Measurements in a Complex Flow Model Combustor, AIAA-83-0334, presented at the AIAA 21st Aerospace Sciences Meeting, Reno, NV.

Brum, R.D., and Samuelsen, G.S. (1984a). Assessment of Candidate Configurations as Test Beds for Complex Flows, submitted to Experiments in Fluids.

Brum, R.D., and Samuelsen, G.S. (1984b). Two-Component Laser Anemometry Measurements of Non-Reacting and Reacting Complex Flows in a Swirl-Stabilized Model Combustor, presented at the Symposium on Experimental Measurements and Techniques in Turbulent Reactive and Non-Reactive Flows, ASME, Winter Annual Meeting, New Orleans, December.

Buckley, D.L., Craig, R.R., Davis, D.L., and Schwartzkopf, K.G. (1980). The Design and Combustion Performance of Practical Systems for Integral Rocket/Ramjets, AIAA 80-1119, AIAA/SAE/ASME 16th Joint Propulsion Conference, Hartford, Connecticut.

Chen, M.J., McLean, W.J., and Gouldin, F.C. (1979). The Oxidation of NO to NO_2 During Combustion Quenching Processes, WSS/CO 79-17, presented at the 1979 Spring meeting of the Western States Section/The Combustion Institute, Brigham Young University, Provo, Utah, April.

Cheng, R.K., Ng, T.T. (1981). Velocity Statistics in Premixed Turbulent Flame, Presented at the 1981 Fall Meeting, Western States Section/The Combustion Institute, Tempe, AZ.

Elghobashi, S.E., Samuelsen, G.S., Wuerer, J.E., and LaRue, J.C. (1981). Prediction and Measurement of Mass, Heat and Momentum Transport in a Non-Reacting Turbulent Flow of a Jet in An Opposing Stream, Journal of Fluids Engineering, 103, 127.

Elghobashi, S.E., W.M. Pun, and D.B. Spalding, (1977). Concentration Fluctuations in Isothermal Turbulent Confined Jets, Chem. Eng. Sci., Vol. 32, p. 161.

Fristrom, R.M., and Westenburg, A.A. (1965). Flame Structure, Mc-Graw Hill, New York, p. 26.

Fujii, S., Eguchi, K., and Gomi, M. (1981). Swirling Jets With and Without Combustion, AIAA Journal, Vol. 19, No. 11.

Gosman, A.D., and Pun, W.M. (1974). Lecture Notes for Course entitled, 'Calculation of Recirculating Flows', Report No. HTS/74/2, Mechanical Engineering Department, Imperial College of Science and Technology, London.

Grudovich, E. (1983). Experimental and Numerical Investigations of Two Water-Analog Combustor Models: The Opposed-Jet Combustor Analog, The Center Body Combustor Analog, UCI Combustion Laboratory Report ARTR-83-6, Mechanical Engineering, University of California, Irvine, CA, 92717.

Hanjalic, K., B.E. Launder, and R. Schiestel (1979). Multiple-Time-Scale Concepts in Turbulent Transport Modeling, Proceedings of Second Symposium on Turbulent Shear Flows, July, London.

Ikioka, L.M. (1982). Axial Velocity Measurements in Reacting and Non-Reacting Flows in a Centerbody Combustor, M.S. Thesis, UCI Combustion Laboratory Report ARTR-82-1, Mechanical Engineering, University of California, Irvine, CA, 92717.

Ikioka, L.M., Brum, R.D., and Samuelsen, G.S. (1983). Laser Anemometer Seeding Technique for Combustion Flows with Multiple Stream Injection, Combustion and Flame, Vol. 49, p. 155.

Janjua, S.I., McLaughlin, D.K., Jackson, T.W., and Lilley, D.G. (1982). Turbulence Measurements in a Confined Jet Using a Six-Orientation Hot-Wire Probe Technique. AIAA-82-1262.

Khalil, K.H., El-Mahallawy, F.M., and Moneib, H.A. (1976). Effect of Combustion Air Swirl on the Flow Pattern in a Cylindrical Oil Fired Furnace, Sixteenth Symposium (International) on Combustion, The Combustion Institute.

LaRue, J.C., Samuelsen, G.S., and Seiler, E.T. (1984). Momentum and Heat Flux in a Swirl-Stabilized Combustor, presented at the Twentieth Symposium (International) on Combustion, The Combustion Institute, University of Michigan, Ann Arbor, August.

LaRue, J.C., T. Deaton, and C.H. Gibson, (1975). Measurements of High Frequency Turbulent Temperature, Rev. Sci. Instrum., Vol. 46, No. 5, pp. 757-764.

Launder, B.E. (1978). "Measurements and Prediction of Complex Turbulent Flows," University of California, Davis.

Launder, B.E., and Morse, A. (1977). Numerical Prediction of Axisymmetric Free Shear Flows with a Second-Order Reynolds Stress Closure, Proceedings of the Symposium on Turbulent Shear flows, Pennsylvania State University.

Liepmann, H.W. (1979). The Rise and Fall of Ideas in Turbulence, The American Scientist, Volume 67.

Lilley, D.G., and Rhode, D.C. (1982). A Computer Code for Swirling Turbulent Axisymmetric Recirculating Flows in Practical Isothermal Combustor Geometries, Report Number NASA-3442, NASA-Lewis Research Center, Grant NAG 3-74.

Lockwood, F.C., and Moneib, H.A. (1981). Fluctuating Temperature Measurements in a Heated Round Free Jet. Combustion Science and Technology, Vol. 22, 63-81.

Lockwood, F.C., and A.S. Naguib (1975). The Prediction of the Fluctuations in the Properties of Free Round Jet, Turbulent Diffusion Flames, Combustion and Flame, Vol. 24, p. 109.

McDannel, M.D. (1979). An Experimental Study of Pollutant Formation in Premixed, Propane-Air Fired, Recirculating Flow Combustion, M.S. Thesis, UCI Combustion Laboratory Report UCI-ARTR-79-1, Mechanical Engineering, University of California, Irvine, CA, 92717.

McDannel, M.D., Peterson, P.R., and Samuelsen, G.S. (1982). Species Concentration and Temperature Measurements in a Lean, Premixed Flow Stabilized by a Reverse Jet, Combustion Science and Technology, Vol. 28, pp. 211-224.

Mellor, A.M. (1980). Semi-empirical Correlations for Gas Turbine Emissions, Ignition, and Flame Stabilization, Progress in Energy and Combustion Science, Vol. 6, No. 4, Pergamon Press.

Oven, M.J., Gouldin, F.C., and McLean, W.J. (1979). Temperature and Species Concentration Measurements in a Swirl Stabilized Combustor. Seventeenth Symposium (International) on Combustion, p. 363, The Combustion Institute.

Owen, F.K. (1976). Measurements and Observations of Turbulent Recirculating Jet Flows, AIAA Journal, Vol. 14, No. 11.

Peck, R.E., and Samuelsen, G.S. (1977). Eddy Viscosity Modeling in the Prediction of Turbulent, Backmixed Combustion Performance, Sixteenth Symposium (International) on Combustion, p. 1675, The Combustion Institute.

Peterson, P.R., and Hines, R.M. (1978). Opposed Jet Combustor Experimental Facility, UCI Combustion Laboratory Report ARTR-78-8, Mechanical Engineering, University of California, Irvine, CA, 92717.

Roman, V. (1984). Aerodynamic Structure of a Sudden Expansion Dump Combustor, M.S. Thesis, UCI Combustion Laboratory Report UCI-ARTR-84-9, Mechanical Engineering, University of California, Irvine, CA 92717.

Roman, V.P., and Samuelsen, G.S. (1982), Ramjet Combustor Studies, UCI Combustion Laboratory Report ARTR-82-08, Mechanical Engineering, University of California, Irvine, CA 92717.

Roquemore, W.M., Bradley, R.P., Stutrud, J.S., Reeves, C.M., and Krishnamurthy, L., (1980). Preliminary Evaluation of a Combustor for Use in Modeling and Diagnostics Development. ASME-80-GT-93, Twenty-fifth Annual International Gas Turbine Conference, The American Society of Mechanical Engineers, New Orleans, Louisiana.

Roquemore, W.M., Britton, R.L., and Sandhu, S.S. (1982). Investigation of the Dynamic Behavior of a Bluff Body Diffusion Flame Using Flame Emission, AIAA-82-0178, 20th Aerospace Sciences Meeting, Orlando, Florida.

Samuelsen, G.S., and Harman, J.N. (1977). Chemical Transformations of Nitrogen Oxides While Sampling Combustion Products, APCA Journal, Vol. 27, No. 7, July, p. 648.

Samuelsen, G.S., and Benson, R.C. (1979). "Chemical Transformations of Nitrogen Oxides While Sampling Combustion Products," Grosjean, D. (Ed.), Nitrogenous Air Pollutants — Chemical and Biological Implications, Ann Arbor Science Publishers, Inc., Ann Arbor, p. 65.

Samuelsen, G.S., Hamberg, R.M., and Osborn, J.K. (1978). Composition and Concentration of Hydrocarbon Species Emitted from Gas Turbine Combustors, UCI Combustion Laboratory Report ARTR 78-3, Mechanical Engineering, University of California, Irvine, CA 92717.

Samuelsen, G.S., LaRue, J.C., and Seiler, E.T. (1984). Instantaneous Two-Component Laser Anemometry and Temperature Measurements in a Complex Reacting Flow, presented at the Second International Symposium on Applications of Laser Anemometry to Fluid Mechanics, Lisbon, Portugal, July.

Seiler, E.T., LaRue, J.C., Sollberger, M.S., and Samuelsen, G.S.(1983). Heat and Momentum Fluxes in a Swirl-Stabilized Combustor, WSs/CO 83-51, presented at Fall Meeting of the Western States Section of the Combustion Institute, Los Angeles.

Seiler, E.T. (1983a). Compensated Thermocouple Measurements in a Complex, Reacting Flow, M.S. Thesis, UCI Combustion Laboratory Report ARTR-83-11, Mechanical Engineering, University of California, Irvine, CA, 92717.

Seiler, E.T. (1983b). Tabulated and Documented Data Base: Momentum and Heat Flux for a Propane-Fired, Swirl-Stabilized Complex Flow Combustor (15 mps, ϕ = 0.1), UCI Combustion Laboratory Report ARTR-83-13, Mechanical Engineering, University of California, Irvine, Ca, 92717.

Smith, G.D., and Giel, T.V. (1979). Two Component Laser Velocimetry Measurements in a Dump Combustor Flowfield, Stevenson, W. (Ed.), Laser Velocity and Particle Sizing, Hemisphere Publishing Corporation, Washington, p. 147.

Srinivasan, R., and Mongia, H.C. (1980). Numerical Computations of Swirling Recirculating Flow Final Report, AiResearch Report 21-3517, NASA-Lewis Research Center Report, NASA CR-165196.

Wuerer, J.E., and Samuelsen, G.S. (1979). Predictive Modeling of Backmixed Combustor Flows: Mass and Momentum Transport, 17th Aerospace Sciences Meeting, AIAA Paper 79-0215, New Orleans, LA, January.

Wuerer, J. (1978). Momentum and Mass Transport in Turbulent Flow with Recirculation, Ph.D. Dissertation, UCI Combustion Laboratory Report ARTR-78-5, Mechanical Engineering, University of California, Irvine CA 92717.

Yanagi, T., and Mimura, Y. (1981). Velocity-Temperature Correlations in a Premixed Flame, Eighteenth Symposium (International) on Combustion, The Combustion Institute, p. 1031.

END

FILMED

7-85

DTIC